Order Number 9131724

Aggregation of colloidal particles at the air-water interface

Williams, David Francis, Ph.D.

University of Washington, 1991

U·M·I
300 N. Zeeb Rd.
Ann Arbor, MI 48106

Aggregation of Colloidal Particles at the Air-Water Interface

by

David F. Williams

A dissertation submitted in partial fulfillment
of the requirements for the degree of

Doctor of Philosophy

University of Washington

1991

Approved by John Berg
(Chairperson of the Supervisory Committee)

Program Authorized
to Offer Degree Chemical Engineering

Date April 15, 1991

In presenting this dissertation in partial fulfillment of the requirements for the Doctoral degree at the University of Washington, I agree that the Library shall make its copies freely available for inspection. I further agree that extensive copying of this dissertation is allowable only for scholarly purposes, consistent with "fair use" as prescribed in the U.S. Copyright Law. Requests for copying or reproduction of this dissertation may be referred to University Microfilms, 300 North Zeeb Road, Ann Arbor, Michigan 48106, to whom the author has granted "the right to reproduce and sell (a) copies of the manuscript in microform and/or (b) printed copies of the manuscript made from microform."

Signature David H. Williams

Date April 18, 1991

University of Washington

Abstract

Aggregation of Colloidal Particles at the Air-Water Interface

by David F. Williams

Chairperson of the Supervisory Committee: Professor John C. Berg
Department of Chemical Engineering

Various investigators have noted that small particles at an interface exhibit a special tendency to aggregate. The most common manifestations of this phenomenon are the formation of an observable surface coagulum and the sensitivity of normally stable dispersions to flocculation induced by an agitation that renews the air-liquid interface. Aside from the obvious implications for dispersion stability, the "adsorption" and subsequent aggregation of colloids also modifies the interface and plays an important role in various separation processes (i.e. froth flotation, solvent extraction - emulsion stability) and in the adhesion between surfaces.

The underlying mechanism(s) responsible for the characterization of the interface as a critical locus of dispersion instability remain largely unknown and unexplored. The forces that exist between disperse colloids and the interface and between interfacial colloids are certainly key elements for understanding this phenomenon. We concentrate on those forces which govern the pair potential between adsorbed particles in order to explain the preferential aggregation at the surface. We propose modified van der Waals and electrostatic forces in addition to the capillary attraction intrinsic to the interface in order to explain this behavior. Additionally any special surface kinetics which influence the collision frequency between interfacial particles must also be included in the analysis. Interfacial pair potentials are used in conjunction with a two-dimensional model of surface flocculation kinetics to predict stability criteria and aggregation rates. Results from direct observation of surface flocculation by darkfield microscopy are presented and used to test model predictions.

Table of Contents

List of Figures

List of Tables

ACKNOWLEDGEMENTS

Above all I wish to thank my advisor, Professor John C. Berg, for his continuing support and timely advice during this research project. Professor Berg is an inspiring teacher and researcher and I consider myself fortunate to have had the opportunity to learn from him. I also wish to thank the members of my Ph.D. Supervisory Committee for their interest and guidance. The patient assistance of Professors E. James Davis, Bruce A. Finlayson, Christopher Viney, and Samuel Levine on technical matters is especially appreciated. A grant from the IBM Corporation for the Ceramic/Polymer Composites Program of the Washington Technology Center provided partial support for this project and is sincerely appreciated. Finally I would be quite remiss if I did not acknowledge the help of undergraduate research assistants in the completion of the experimental work. I owe a special debt of gratitude to Alex Shaffer in this regard.

1. Introduction

The interaction of colloids which are drawn to and trapped at the interface represents a special pathway for particle aggregation. The results of this aggregation pathway are most apparent for dispersions which, while stable in the bulk, exhibit substantial flocculation due to the presence or renewal of the fluid-fluid interface. During this process particles which migrate to the interface and are trapped experience a net attractive force with respect to other adsorbed particles, and therefore aggregate into flocs (Figure 1.).

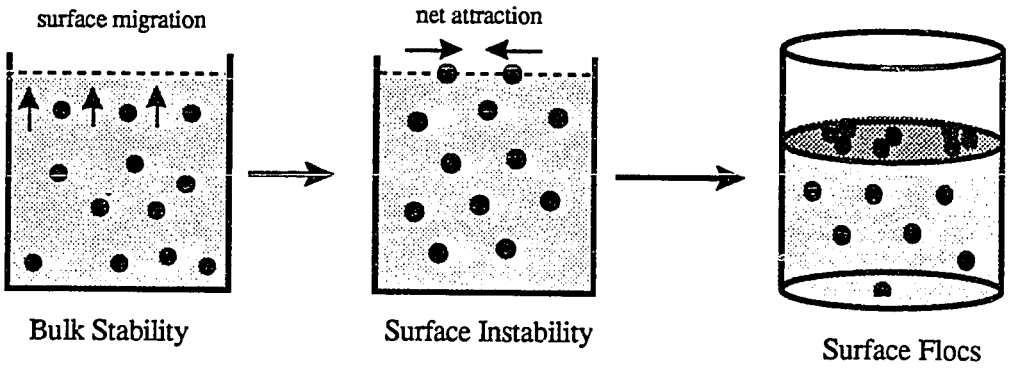

Figure 1. Schematic Illustration of the Surface Flocculation Process

While this surface flocculation phenomenon has been observed and recognized for many years; the underlying mechanisms which govern it remain largely unexplored.

The most obvious importance of surface flocculation is as a critical pathway for destabilization of a dispersion. Surface flocs which become redispersed can also serve as a critical locus for aggregation *in the bulk*; the redispersed flocs acting as "seeds" for further aggregation with dispersed primary particles. Thus the effects of surface flocculation often influence the progress of aggregation in the bulk. The importance of these effects has been observed in a number of commercial operations; most notably in the manufacture of emulsion polymers in stirred-tank reactors(1).

Surface flocculation also has a distinct significance that arises from the influence of adsorbed aggregates upon interfacial properties. Interfacial colloids have been used to

both enhance and diminish the bonding between two phases. Which role these additives play is largely determined by the adhesive properties of the native surfaces relative to those of the interfacial particles. The adhesion between phases is governed by both surface energy and contact area considerations. Low surface energy solids which act to separate high surface energy surfaces will diminish interphase bonding. During the manufacture of magnetic tape special colloids are added to the coating dispersions and act to diminish the bonding between successive layers on the spool by limiting the adhesive contact area for the native tape surfaces. These lubricating particles are referred to as "slip-agents" and must possess the ability to adsorb to the interface and remain evenly distributed (i.e. not aggregated) in order to function properly. The same process is involved in the production of some sandpapers; however in this case the goal is to distribute an abrasive rather than lubricating particle film. Alternatively one can imagine using colloidal particles to increase the bonding between surfaces or phases by providing increased contact area (particulate roughness) and enhanced contact energies.

The presence of colloids at the drop or bubble interface also plays a key role in separation processes such as froth flotation and solvent extraction. The beneficiation of mineral ore by selective attachment of low surface energy solids to bubbles (i.e. froth flotation) is contingent upon particle adsorption and the overall separation efficiency is dependent on the degree of surface aggregation(2). During solvent extraction operations both mass transfer and phase segregation are often hindered by the emulsifying action of microparticulate "interfacial scum" (3). In fact Pickering emulsions (4,5) are encountered in various resource recovery operations and owe their stability entirely to the action of colloids adsorbed at the droplet interface. One can also imagine that the elimination or enhancement of surface flocculation is necessary in certain ultra-clean thin film operations (6).

The motivation for studying surface flocculation also derives from the basic desire to understand this phenomenon on a scientific basis. The study of surface flocculation probes: (a) the fundamental nature of the interactions between colloids and the interface, and (b) the influence of the interfacial environment upon the interactions between colloids. To some degree one can draw upon experience in the areas of froth flotation and thin-film stability to help model the interaction between a dispersed colloid and the interface (adsorption step). The froth flotation literature provides a basic framework for

considering the separate interaction energies while the work on the stability (disjoining pressure) of thin liquid films on solid substrates (i.e. "wetting films") addresses the specific interactions more directly. Integrating the advances made in these areas permits the calculation of the energy of interaction as a colloid approaches the interface - the criterion for predicting the adsorption behavior of colloids.

Study of the interaction of colloidal spheres which reside at the interface is a new area. Besides the modern DLVO framework (7) for predicting colloidal stability in the bulk there is very little to draw upon. Van der Waals, electrostatic, and structural forces will all be modified by the interfacial environment, requiring new models for the pair potential energies. Additionally one must consider new elements, such as capillary forces, which are intrinsic to the interface and have no analog in the bulk. By modelling and examining the total pair potential between two adsorbed colloids we seek an understanding of the critical factors which lead to the enhancement of aggregation at the interface. The results of pair potential predictions provide both a means of explaining the qualitative stability behavior (i.e. "stability map") of surface colloids and a quantitative test of the influence of particle interactions upon flocculation kinetics.

We do not have a means of directly measuring the interparticle potential, rather our quantitative understanding of these interactions follows from the influence of the pair potential upon the observed flocculation kinetics. The study of surface flocculation requires a new approach for analyzing aggregation kinetics; one which accounts for the special two-dimensional nature of this process. By modelling the surface aggregation kinetics we seek to show the link between our model of particle interactions with that which is measurable: the evolving aggregate population at the interface. It is the comparison of the observed and predicted aggregate populations which provides the severest test of the proposed models.

2. Literature Review

The study of interfacial colloids has been approached from a variety of perspectives, and any discussion of the relevant literature must acknowledge this fact. Interest in this area originated with Freundlich's studies which identified the interface as a locus of colloidal instability. This observation led to a series of investigations(8) targeted at defining the role of surface flocculation in destabilizing dilute dispersions. More recently (9-12) researchers have focussed upon the behavior of special concentrated two-dimensional particulate films which do not arise from the simple interaction of disperse particles with the interface. These studies typically involve hydrophobic particles which are spread at the interface and remain trapped at the surface by capillary forces. The use of these films to investigate repulsive interparticle potentials is reviewed in Appendix B. It was found that under most conditions interfacial particles exhibit a net attraction and therefore aggregate at the surface. However at low salt conditions concentrated colloidal surface films have been observed to "crystallize" into an ordered pattern due to electrostatic repulsive interactions(13,14). This long range crystalline order has not been observed in dilute systems and is evidently a many body phenomenon. While this ordering phenomenon has been a useful proving ground for theories of two-dimensional phase transitions, the actual nature of the pair potential between two interfacial colloids remains in question.

A return to the class of studies inspired by Freundlich allows us to concentrate upon dilute systems which more directly reflect the influence of the interfacial pair potential. A number of fairly simple observations served to motivate this early work. Freundlich(15-18) was initially trying to explain why certain apparently stable sols coagulate under the influence of agitation. This mode of aggregation was referred to as "mechanical" coagulation even though subsequent observations(8) indicated the process is surface mediated rather than mechanically induced. The fact that the uncoagulated colloid concentration decreased linearly with time suggested that a zero-order surface reaction was occurring. Furthermore the high rate of flocculation and its dependence upon stirring velocity could not be reconciled with the existing bulk flocculation models. Additional credence was given to the surface flocculation hypothesis by the observation of Zsigmondy(19) that aqueous sols could be coagulated by shaking them in the presence of inert organic liquid droplets. Finally the most conclusive evidence was produced

when Freundlich conducted matched flocculation experiments for the cases of (a) an extensive air-liquid interface and (b) no air-liquid interface. In the absence of an air-liquid interface agitation did not induce flocculation.

The next significant investigation was conducted by Heller and co-workers in the 1970's(20-25). In the intervening years between Freundlich's and Heller's work there was an assortment of conflicting studies(8) that focussed on "mechanical" coagulation kinetics and speculated about different mechanisms. Heller's goal was to present a coherent view of what was still referred to as "mechanical" coagulation. The term "mechanical" coagulation is somewhat of a misnomer, since critically stable sols will exhibit a very slow rate of flocculation even at a quiescent air-liquid surface. The purpose of mechanical agitation is to continually renew the air-liquid interface so that a significant amount of aggregation can be observed in a reasonable time period. Heller induced flocculation in otherwise stable sols by: (a) vigorous agitation, (b) low shear renewal of the air-liquid interface, and (c) bubbling gas through the dispersion. All of the studies indicated that coagulation at the air-liquid interface was the prime cause of aggregation in these systems.

Again this conclusion was primarily based upon analyzing the kinetics of aggregation. The flocculation kinetics did not conform to simple second order(i.e. Smoluchowski) *or* zero- order models. Therefore Heller proposed a two-step process in order to explain the data: (a) adsorption to the interface and (b) subsequent flocculation at the interface. The adsorption was assumed to be Langmuirian with sufficient surface renewal to maintain equilibrium. Coagulation was modelled as a second-order bimolecular surface reaction of primary particles. The resulting rate equation has the form:

$$-dc/dt = (S/V)\cdot k_0 \cdot c^2/(k_1+k_2 \cdot c)^2 \qquad \{1\}$$

where:

S/V = surface area to volume ratio

c = bulk particle concentration

k_0 = bimolecular surface rate constant

k_1,k_2 are Langmuir constants[surface conc.= $c/(k_1+k_2.c)$]

For different values of $\{k_2 \cdot c/k_1\}$ the rate equation can "satisfy" kinetics ranging from zero order to second order. The flexibility of this model seemed to explain many of the apparent conflicts of previous studies. This model was also very successful in fitting the data for low-to-moderate degrees of aggregation. The neglect of the influence of large aggregates is probably responsible for the poor fit during the late stages of coagulation.

The importance of surface flocculation in the "mechanical coagulation" of sols was most recently affirmed by Lowry et al(1). This study was motivated by the problems experienced in the production of high-concentration polystyrene latex dispersions in stirred tanks. They studied both the effects of surface(air/liq.) to volume ratio and shear upon the rate of coagulation. The interfacial area was found to be the most important factor influencing the aggregation rate. By eliminating the air/liquid interface the coagulation rate was reduced by a factor of twenty-five. They also found that surface induced flocculation provided "seeds" of aggregates that promoted flocculation in the bulk.

One of the disadvantages of the previously described flocculation experiments is that models will inevitably require empirical constants (k_1,k_2 for Heller) in order to describe the aggregation data. It is highly unlikely that Heller's k_1 and k_2 actually pertain to an equilibrium(Langmuirian) adsorption process. Certainly one would be hesitant to ascribe fundamental significance to these parameters. It is the desire to probe the more fundamental aspects of this phenomenon that motivates the detailed microscopic examination of surface flocculation. Only a handful of microscopic studies have been performed to date, with Onoda's recent investigation(26) being the most noteworthy.

Onoda has studied the behavior of interfacial colloids derived from adsorption to the surface from the bulk. However Onoda's focus was on the clustering(floccing) of larger particles at the air/water interface. An inverted light microscope was used to examine the air/liquid interface. Instead of examining the "upper" interface Onoda constructed his cell to present the "lower" air/liquid interface directly to the inverted microscope objective. A small drop of 0.1 wt.% polystyrene latex suspension was placed over a hole in a thick aluminum foil and particle sizes ranging from 1 to 15μm were investigated by sequential trials with monodisperse sols. A somewhat flat meniscus

was formed at the lower foil surface and was examined with the inverted objective for periods of up to one hour.

By looking at a range of particle sizes Onoda hoped to observe reversible clustering that would correspond to a weak secondary minimum($E < 5$ kT) in the potential energy of particle-particle interactions. All of Onoda's results were reported as qualitative observations; no quantitative data were presented. Little clustering was observed for particles smaller than 2 μm. Particles of 2 μm diameter exhibited the dynamical clustering behavior sought by Onoda. Initially doublets were formed and separated on time scales ranging from 1 to 10 seconds. Eventually larger stable clusters formed which exhibited extensive particle rearrangement within the aggregate. Finally clusters grew large enough to maintain their structure except for some rearrangement at the edges. Particles with diameters of 5 μm or greater clustered very slowly (low mobility) and more irreversibly. Growth tended to be more dendritic.

3. Statement of Objectives

The focus of this investigation is a combined theoretical and experimental study of the fundamental aspects of the aggregation of hydrophobic colloids at the air-water interface. In support of this central theme the following aspects of the phenomenon are to be modelled:

(1.) the potential energy of interaction between a colloidal sphere and the interface ("adsorption" step),

(2.) the kinetics that govern the rate of adsorption of colloids to the interface,

(3.) the potential energy interactions between adsorbed colloids, and

(4.) the kinetics that govern the rate of aggregation between interfacial colloids in both: (a) diffusion-limited ("fast" flocculation) cases and, (b) cases of significant potential energy interactions.

The experimental portion of this study focuses upon the direct examination of surface adsorption and aggregation with the goal of quantitative measurement of surface aggregation rates for comparison with the model predictions. In particular, a suitable model system is chosen which permits determination of the important experimental parameters (i.e. monodisperse particle size, well defined surface chemistry, surface potential, Hamaker constant, contact angle. etc.). The experimental apparatus provides for the measurement of the evolving population of surface particles and aggregates for comparison with model predictions.

4. Theory and Modelling

4.1 Adsorption of Colloidal Particles to the Interface

The phenomenon of surface aggregation is preceded by the "adsorption" of colloids to the interface. Under the influence of diffusion or convection colloids are brought in the vicinity of the interface and undergo (Figure 2): (a) the "DLVO" class of interactions associated with the thinning of the intervening liquid between the particle surface and interface, and (b) the capillary interactions associated with the forces which act to establish the interfacial particle position once a three-phase contact line has been formed (i.e. "capillary trapping").

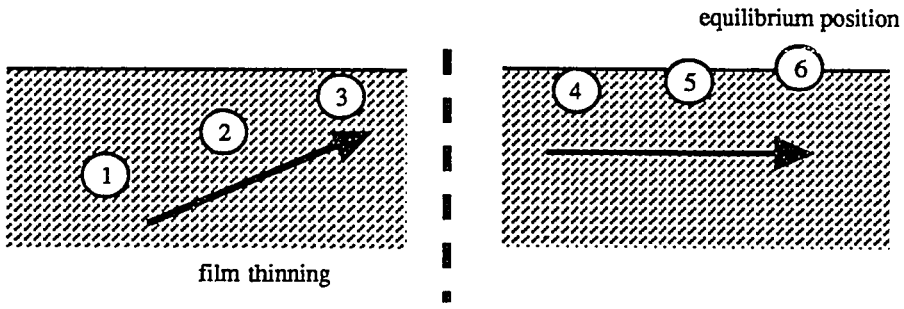

a: DLVO regime b: Capillary Regime

Figure 2. Adsorption Process: DLVO regime vs. Capillary regime

The following sections outline the models to be used in calculating the various interactions present in each regime, concluding with a discussion of the total interaction potential experienced by a colloidal particle upon approach to the interface.

4.1.1 van der Waals Interaction

While the physical picture of van der Waals forces as the universal attraction that exists between molecules due to dispersion (London), permanent dipole (Keesom), or induced dipole (Debye) interactions explains a wide variety of "condensation" phenomena; it belies a complexity that is inherent in its mathematical description. The

theoretical foundation for describing these forces between macrobodies is now quite advanced and has outpaced our ability to incorporate the newest developments into practical applications. So when one approaches the task of performing actual calculations some trade-offs must be made. The most rigorous treatment of van der Waals forces draws upon the modern macroscopic theory of Lifshitz (27), which automatically accounts for retardation effects and non pair-wise summation of molecular interactions in macrobodies. However this approach also requires extremely detailed information about the material polarizabilities, which are typically not available.

The primary deficiency of the classical microscopic theory of van der Waals interactions between macrobodies lies in the neglect of retardation effects which account for the finite time of propagation of electric fields. As the distance of separation (r) between molecules increases the dispersion energy decays with a r^{-7} rather than the unretarded r^{-6} (London) dependence. Therefore calculations which omit this retardation correction will tend to overestimate the van der Waals interaction at extended separations. The issue of non-pairwise additivity of molecular interactions is not as important, since van der Waals forces tend to be dominated by the dispersion terms which are amenable to pairwise summation (28). Therefore the most appropriate approach for calculating van der Waals forces between macrobodies utilizes the pairwise summation of the retarded dispersion interaction between individual molecules (29).

Some preliminary comments about the special nature of the van der Waals interaction between a colloid and the interface (planar half-space) are also in order. Note that this situation is fundamentally different from the universal attraction experienced between particles of identical polarizability (i.e. dielectric susceptibility or Hamaker constant). The interaction between dissimilar particles can be either attractive or repulsive depending upon the relative polarizabilities of each particle and the suspending medium. This is most easily illustrated by the simple (geometric mean) expression developed for the Hamaker constant (A) corresponding to the interaction of particle 1 ($A=A_{11}$) with particle 2 ($A=A_{22}$) in a suspending medium of material 3 ($A=A_{33}$):

$$A_{132} = (\sqrt{A_{11}} - \sqrt{A_{33}})(\sqrt{A_{22}} - \sqrt{A_{33}}) \qquad \{2\}$$

If the medium (3) exhibits a polarizability intermediate in value to that of the particles (1,2) the effective Hamaker constant is negative, resulting in a repulsion between the particles. Since water exhibits a Hamaker constant intermediate in value to that of air and most solids, a van der Waals repulsion of particles from the interface is the rule.

The expression for the retarded interaction potential between a sphere and half-space has the form (29):

$$V_{vdW} = \frac{-2\,A_{132}}{kT}\left(\frac{c_1}{x^2(x+2a)^2} - \frac{c_2(x+a))}{x^2(x+2a)^3}\right) \qquad \{3\}$$

where:

$$c_1 = \left(\frac{2.45}{2\pi}\lambda\right)\frac{a^3}{15}$$

$$c_2 = \left(\frac{2.04\lambda^2}{(2\pi)^2}\right)\frac{2a^3}{45}$$

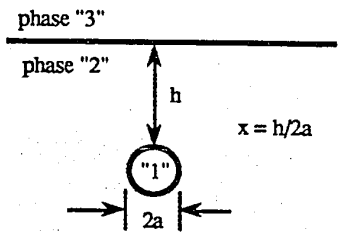

λ = dominant dispersion wavelength ≈ 100nm
kT = thermal energy

For small separations ($h < 3\lambda/2\pi \cong 50$ nm) a simpler formula is applicable(30):

$$V_{vdW}\left(h \le \frac{3\lambda}{2\pi}\right) = \frac{-A_{132}}{12\,x\,kT}\left(1 - c_3 x \ln\left(1 + (c_3 x)^{-1}\right)\right) \qquad \{4\}$$

and $c_3 = 5.32(2a)/\lambda$.

The magnitude of this interaction under typical experimental conditions is shown in Figure 3. Note that the potential displays the characteristic strong interaction at close approach ($\cong 1/x$) accompanied by the more rapid decay at extended separations ($\cong 1/x^4$).

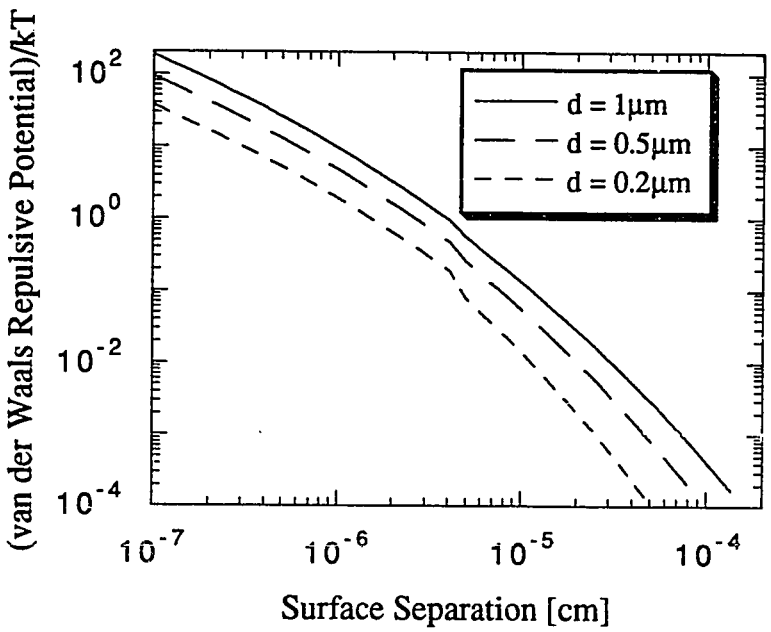

Figure 3. van der Waals Repulsion from the Air-Water Interface

4.1.2 Electrostatic Interaction

The existence of an electrostatic interaction associated with suspended colloids derives from the various charging mechanisms (adsorption, ionization, dissociation, ion-exchange) which operate at the particle surface. In ionizable media, such as water, this leads to a compact electric double-layer surrounding the charged particle surface. The considerable body of knowledge pertaining to the electric double-layer and double-layer interactions is based upon the defining differential equation: the Poisson-Boltzmann Equation, which combines the physics of Gauss' Law with Boltzmann statistics for the distribution of ion energies. The primary focus of previous work has been on the interaction of two bodies of identical surface charge or surface potential and identical geometry (i.e. two planar half-spaces, two spheres, etc.). The interaction of a charged colloid and the interface satisfies neither of these conditions, so some thought must be given to the relevance of literature solutions to this instance.

The electrostatic boundary condition at the interface plays a key role in the analysis. If you could measure a constant charge or constant potential boundary

condition at the interface it would be straightforward to perform the Deryaguin integration (Appendix A) necessary to convert the appropriate flat-plate potentials to account for the curvature associated with the particle. Unfortunately the electrostatic conditions at the interface are rarely known to any accuracy. The few studies(31) on the air-water interface that were devoid of surface active species indicate that a very weak potential is associated with the surface; consistent with the typical assumption(32) of the interface as a plane of zero charge. The stipulation of zero charge at the interface leads to considerable simplification (Figure 4), since image charge arguments can be used to cast the problem in more familiar terms.

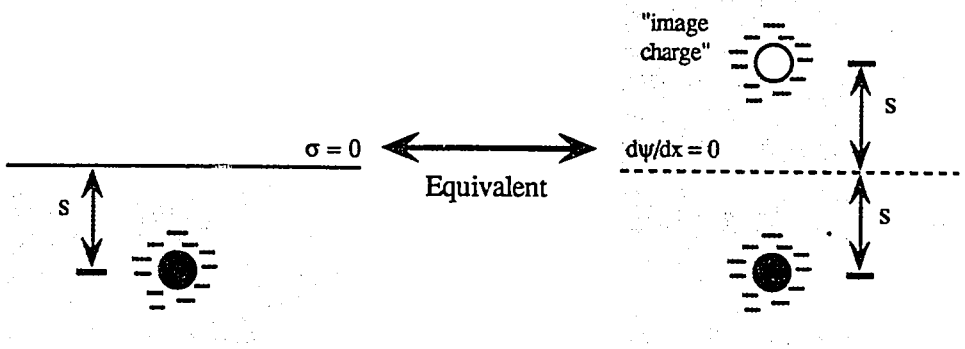

Figure 4. Image Charge Analogy

This view results in an interaction identical to that between two charged colloids in suspension, except that the hypothetical separation between the "particles" should correspond to twice the actual separation between the particle surface and the interface. Using the expression developed by Reerink and Overbeek(33) for the electrostatic interaction of two charged colloidal spheres we find:

$$V_{electrostatic} = \left(\frac{64\pi \, a \, n_0 \, kT \, \Psi_0^2}{\kappa^2} \right) e^{-2\kappa s} \qquad \{5\}$$

where:

$$\kappa = \text{Debye parameter} = \left(\frac{1000 \, e^2 \, N_{AV}}{\varepsilon (kT)} \sum_i (M_i \, z_i^2) \right)^{1/2}$$

$$V_0 = \frac{e^A - 1}{e^A + 1} \quad , \quad A = \frac{ze\varphi_d}{2kT}$$

and,

s = separation
a = particle radius
z_i = ionic charge on species i
n_0 = electrolyte conc.[1/m^3]
= 1000 M N_{AV}
M = electrolyte molar conc.
ε = dielectric constant [C^2/J m]
φ_d = Stern Potential [volts]
e= electronic charge

As shown in Figure 5 equation{5} always predicts a screened-coulomb repulsion of a charged colloid from a "clean" interface, analogous to the repulsion which stabilizes colloids in bulk .

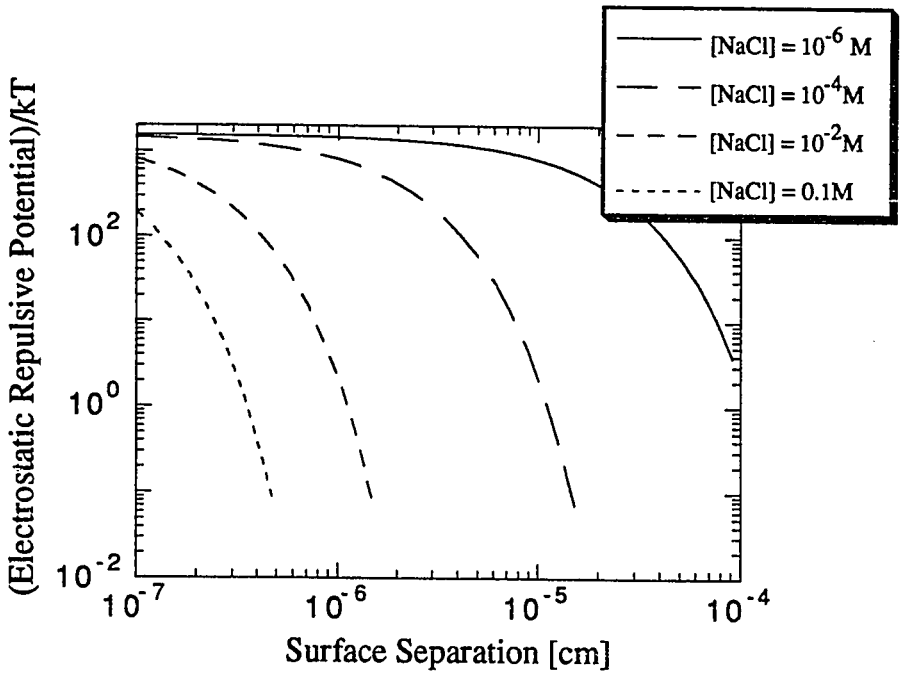

Figure 5. Typical Electrostatic Potential between Sphere and Half-Space, for the Case of a 1μm Particle (Standard Colloid) Approaching an Uncharged Air-Water Interface.

4.1.3 Structural Interaction

As the study of interparticle forces progressed it was clear that certain non-DLVO forces were exhibited upon the close approach of surfaces. Since treatment of electrostatic and dispersion forces in the DLVO theory is essentially a continuum approach that ignores any structural effects due to solvent orientation and interaction, this result is not too surprising. Depending on the nature of the solvent and the surface a wide variety of "non-DLVO" effects (attraction, repulsion, oscillatory, exponential decay) have been observed and assigned separate names, despite the fundamental basis shared by this family of forces. Structural forces is the most general description; as it refers to the free energy change, due to some unspecified solvent structuring, exhibited by the intervening liquid between approaching surfaces. The term solvation forces is also used for this purpose, but is typically limited to situations in which the free energy changes derive from the simple geometric packing constraints involving weakly interacting molecules. This type of interaction leads to a force that oscillates (sinusoidally) between attraction and repulsion as smooth surfaces approach one another at very small separations (1-20 solvent diameters). The terms hydration, hydrophilic, and hydrophobic forces all refer to the interaction of various classes of surfaces in aqueous environments. These forces are distinguished by their long-range exponentially decaying potentials, which can be either repulsive (hydration, hydrophilic) or attractive (hydrophobic). It is believed that roughness factors and the associative nature of the water molecule are responsible for the qualitative difference between this group of forces and the solvation forces. The focus here is on the attractive hydrophobic interaction displayed by the synthetic polystyrene latices used in this study.

Our understanding of the nature of hydrophobic surface forces is still in its infancy, being limited due to the lack of a mature theory for describing the basic phenomenon. Since predictive theories, as exist for van der Waals and electrostatic forces, have yet to be developed we must rely upon the most illuminating experimental studies. Disjoining pressure studies of thin liquid films(34) ("wetting films") and measurements using the surface forces apparatus(35) form the bulk of the data base for hydrophobic forces. Both classes of investigations find that the form of the structural potential between planar hydrophobic surfaces is a decaying exponential:

$$V_{Structural}(h) = K \exp(-h/\ell) \qquad \text{"planar geometry"} \qquad \{6\}$$

where:

h = surface separation

K = fitted pre-exponential factor (experimental), negative for hydrophobic

ℓ = fitted decay length (experimental)

The recent surface forces measurements of Christenson(36) provide the most accurate and reliable estimates (K = -0.366 erg/cm^2, ℓ = 13 nm) of the hydrophobic interaction applicable to the experimental conditions of this study. Conversion of the flat-plate potential of Christenson to a sphere/half-space potential can be accomplished by Deryaguin integration, since the decay length (13 nm) is much smaller than the particle diameter (typically 1μm), resulting in:

$$V_{Structural}(h) = 2\pi\, a\, K\ell \exp(-h/\ell) \qquad \text{"sphere/half-space geometry"} \qquad \{7\}$$

Note that (Figure 6) the hydrophobic potential displays a decaying attractive potential, in contrast to the previously discussed van der Waals and electrostatic repulsive interactions.

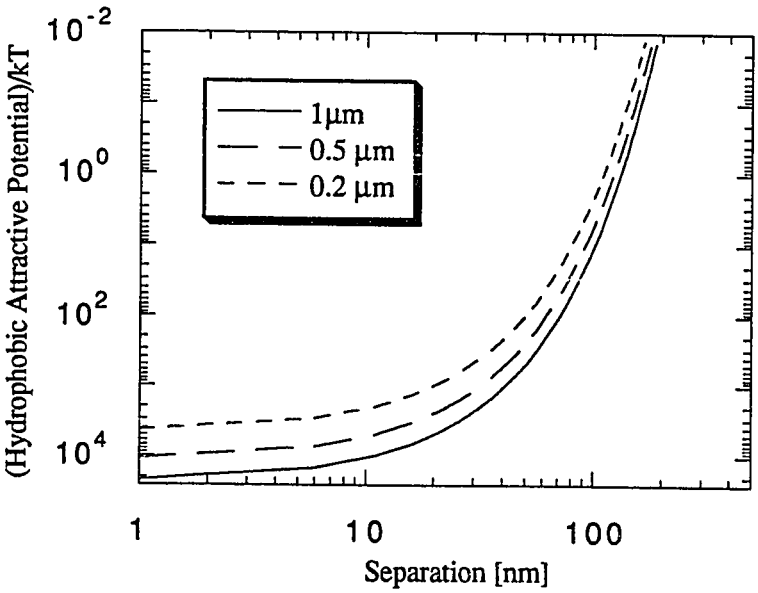

Figure 6. Typical Hydrophobic Interaction as a Sphere Approaches the Interface

In addition to the forces discussed in the previous sections there is a dissipative viscous force which resists the thinning of the liquid film between the particle and the interface. This subject had been treated in the flotation literature(37) in the context of an induction period associated with the time required to bring the particle in the range of the surface forces which act to rapidly rupture the film. Induction times are modelled using Reynolds' lubrication theory for the geometry of two parallel circular discs, one of whose surface is free and the other fixed (i.e. no-slip condition), yielding:

$$\tau_0 = \frac{3\eta\, r_0^2}{16\, t_i^2\, \Delta P} \qquad \text{where:} \qquad \{8\}$$

τ_0 = induction time for thinning to thickness t_i
ΔP = capillary pressure acting to thin film $\approx 2\sigma/r_0$
η = fluid viscosity
r_0=radius of film

For the typical experimental conditions of $\eta = 0.01$ poise (water), $r_0 = 0.5\mu m$, $t_i = 0.02\mu m$, and $\sigma = 72.8$ dynes/cm (water) we find $\tau_0 = 4 \times 10^{-7}$ seconds. This result indicates that the hydrodynamic resistance during the adsorption process is negligible, despite its importance in conventional flotation operations involving macroscopic (100-1000μm) particles. Another area that distinguishes conventional flotation processes from the adsorption of colloids is the importance of inertial terms in modelling the bubble-particle contact. These terms are also negligible for the interaction of colloids with the air-liquid interface(38,39).

4.1.5 Capillary Interactions

Under certain conditions the combined action of the van der Waals, electrostatic, and structural forces will permit the contact of the particle surface and the interface. Once the three-phase contact line has been established capillary forces act to fix the particle at its equilibrium interfacial position. It has been realized for many years that these capillary forces are responsible for the trapping of non-wetting(contact angle$\neq$0) particles at the interface. The rigorous treatment of the problem is complicated by the need to solve a

non-linear ordinary differential equation for the precise meniscus profile. A comprehensive treatment was finally provided by Rapacchietta and Neumann(40) in the framework of both a force and free energy analysis for the determination of the particle's equilibrium position. These calculations are quite complicated. Fortunately the capillary trapping of colloidal size particles corresponds to the limiting case of negligible gravitational forces compared to surface tension forces. Equivalently we may assert that the Bond number ($\Delta\rho\, g\, r^2/\sigma_{23}$) is effectively zero; corresponding to a flat meniscus. This asymptotic behavior permits significant simplification in the determination of the interfacial position. The validity of this assumption was checked by examining the James matched asymptotic expansion(41) for the meniscus profile about a small circular meniscus and using it to calculate the particle position with the model of Rapacchietta and Neumann. No significant deviation from the results of the following development was found.

For a particle, initially at its reference state (completely "wet", Figure 7), passing through the interface we have the following free energy changes:

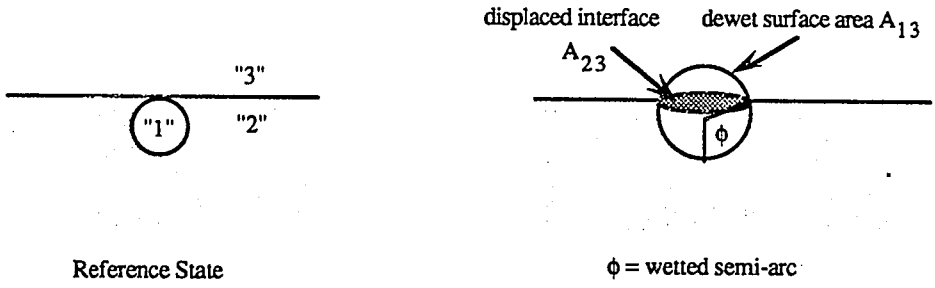

Figure 7. Convention for Calculating Capillary Free Energy Changes

ΔE_1 = work required to replace area A_{13} of surface energy σ_{12} with equivalent area of surface energy σ_{13}

$$= A_{13}(\sigma_{13}-\sigma_{12}) = A_1\,\sigma_{23}\cos\theta \qquad \text{(where } \theta = \text{contact angle)}$$
$$= 2\pi r^2 (1-\cos\phi)\,\sigma_{23}\cos\theta \qquad \{9\}$$

ΔE_2 = work done by eliminating 2-3 interface

$$= -A_{23}\,\sigma_{23} = -\pi r^2 \sin^2\phi\,\sigma_{23} \qquad \{10\}$$

$$\text{Total Free Energy Change} = \Delta E_1 + \Delta E_2 = V_{cap}(\phi)$$
$$V_{cap}(\phi) = \pi r^2 \sigma_{23} [2 \cos\theta (1-\cos\phi) - \sin^2\phi] \quad \{11\}$$

As expected the capillary potential exhibits a minimum at $\phi = (\pi-\theta)$, corresponding to an equilibrium position with a flat meniscus:

$$V_{cap}(\text{minimum}) = V_{cap}(\phi=\pi-\theta) = -\pi r^2 \sigma_{23} (1-\cos\theta)^2 \quad \{12\}$$

Often fractional immersion is a more convenient measure than wetted semi-arc:

$$\%\text{Immersion(linear or areal)} = L \times 100 = (1-\cos\theta)/2 \times 100 \quad \{13\}$$
$$\%\text{Immersion(by volume)} = (3L^2 - 2L^3) \times 100 \quad \{14\}$$

The following plots of $V_{cap}(\phi)$ vs ϕ (Figure 8) and $V_{cap}(\text{minimum})$ vs. θ (Figure 9) illustrate the depth of the capillary well and its relation to the contact angle for a 1μm particle at the air-water interface.

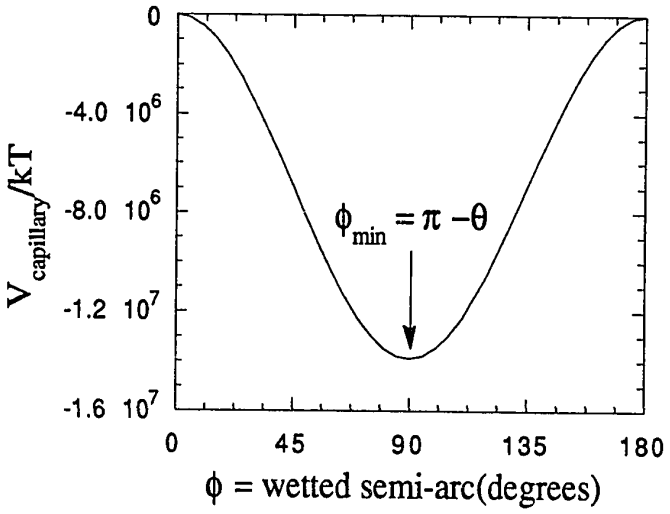

Figure 8. Capillary Potential Energy as a Function of Wetted Semi-arc

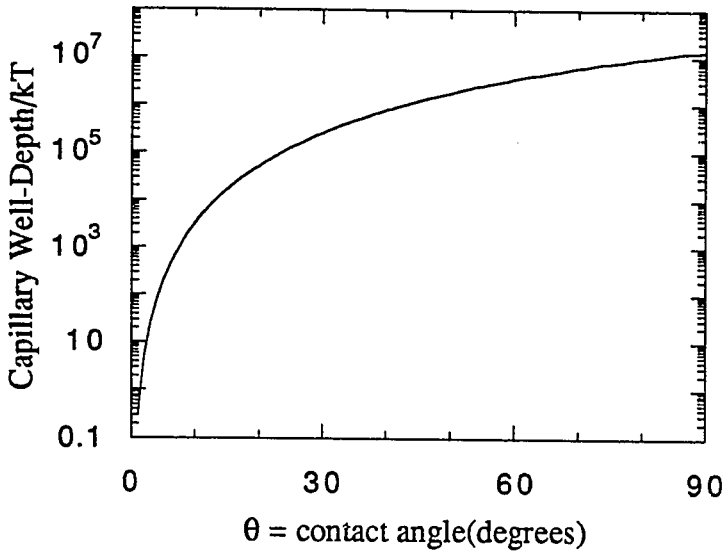

Figure 9. Capillary Well-depth as a Function of Contact Angle

4.1.6 Total Interaction Potential

The total potential of interaction of a spherical colloid with the interface serves as the criterion for determining the existence, strength, and rate of adsorption. The DLVO class of interactions (including structural forces) act to control the initial stage before a three-phase contact line is established, while the capillary forces govern the ultimate particle position at the interface. As a colloid approaches the interface (Figure 10) it first experiences the net potential resulting from the sum of the van der Waals (repulsive), electrostatic (repulsive), and structural(attractive) forces. It is apparent that the hydrophobic attraction serves as the ultimate driving force for adsorption and must counteract the barriers to adsorption imposed by the van der Waals and electrostatic repulsions. The interplay of the structural and electrostatic interactions, varied by changing the electrolyte concentration, determines the height of the potential barrier (if any) for adsorption to the interface. Any particle surmounting the potential barrier is drawn into a very deep capillary well and remains irreversibly adsorbed.

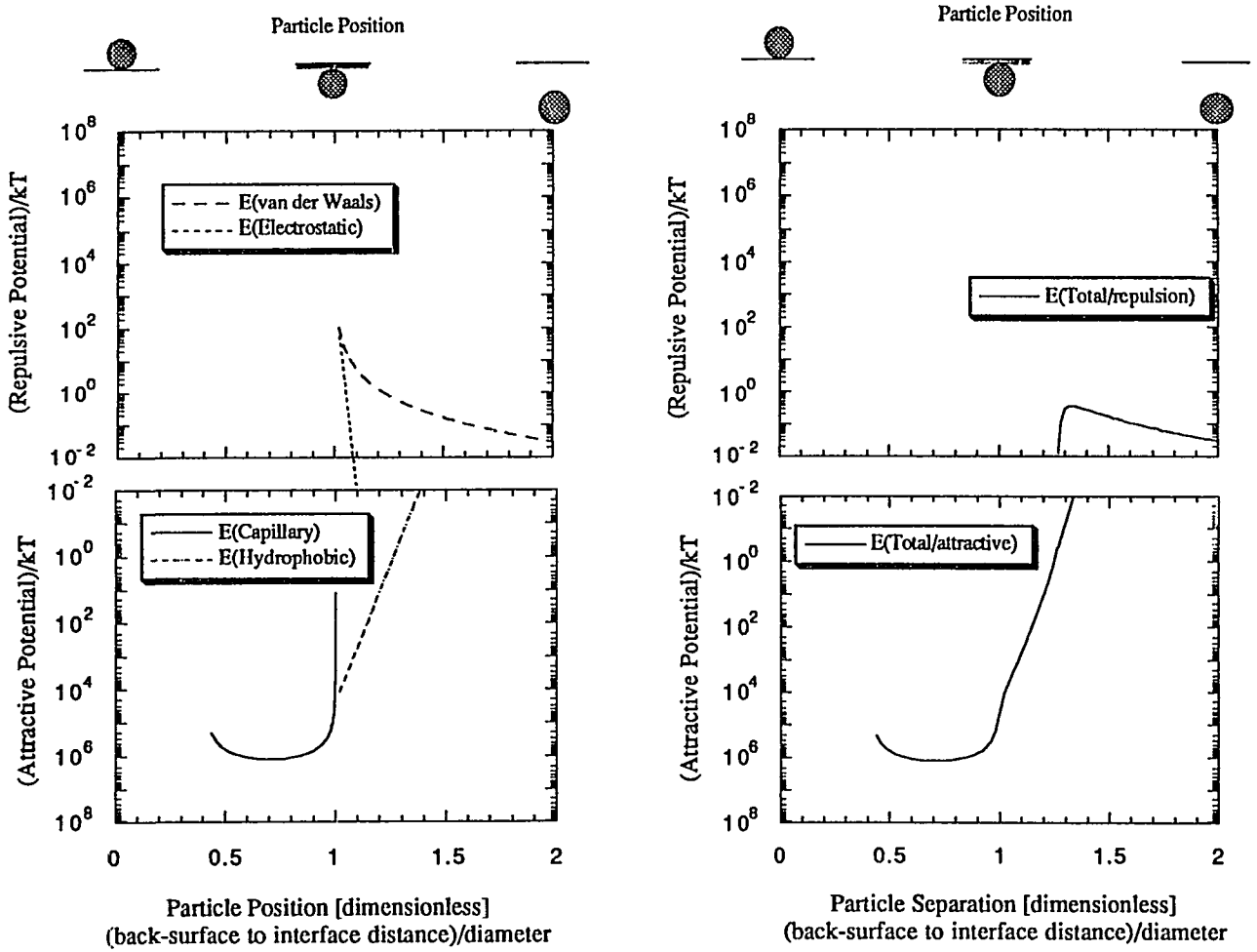

Figure 10. Total Interaction Potential between Sphere and Half-space for standard 1μm colloid, [NaCl] = 0.01 M, 45° contact angle (component parts, left, and net potential, right)

4.1.7 Adsorption Kinetics

While study of adsorption kinetics is not the major focus of this research; assessment of the adsorption data is necessary and requires some modelling. A useful base case to consider is that of a dispersion confined to a half-space whose interface serves as a perfectly absorbing wall. In a system devoid of convection and external forces the rate of adsorption is simply described by the one-dimensional diffusion equation(42) :

$$\frac{dc}{dt} = D\frac{d^2c}{d^2x} \qquad \{15\}$$

with boundary conditions:

$$c(0,t) = 0$$
$$c(x\rightarrow\infty,t) = c_0$$
$$c(x,0) = c_0$$

which results in a flux to the surface of:

$$J_{surface} = D\left(\frac{dc}{dx}\right)_{x=0} = \left(c_0\sqrt{\frac{D}{\pi}}\right)t^{-1/2} \qquad \{16\}$$

This equation serves as a limit to the rate at which particles whose mobility is purely diffusive can adsorb. Each collision is assumed to be 100% effective; corresponding to the absence of an energy barrier for adsorption. If each collision between particle and interface is only partially effective then we expect a proportionally lower adsorption flux. Conversely we may expect to observe fluxes in excess of the ideal diffusive flux due to either convection or attractive force fields (section 4.4). The influence of the pair potential in enhancing(attractive field) or diminishing(energy barrier) is readily modelled, however the degree of enhancement due to convection is more difficult to predict. It is expected that convection effects are relatively insensitive to changes in electrolyte concentration, while pair potential effects will show a marked change with salt concentration.

4.2 Pair Potential Interactions between Interfacial Colloids

4.2.1 van der Waals Interaction

The van der Waals interaction between partially immersed particles is considerably more complicated than that between dispersed colloids and does not lend itself to the rigorous macroscopic(Lifshitz) treatment. Rather than considering the complexity we start by making some simple observations. We expect the presence of a second fluid boundary provides for an attraction that is intermediate in value to that corresponding to each pure phase. For particles at the air-water interface the van der Waals interaction is enhanced due to the "dry" portion of the spheres which attract each other more strongly than the immersed portions.

The effect of the composite nature of the interface is most readily accounted for by extending the original arguments developed by Hamaker(43) for predicting the influence of an intervening medium upon the interaction between particles. Before this development the microscopic theory of dispersion forces was limited to the case of macrobodies interacting through a vacuum. Accounting for all of the dispersion energy changes as two colloids approach one another results in (Figure 11):

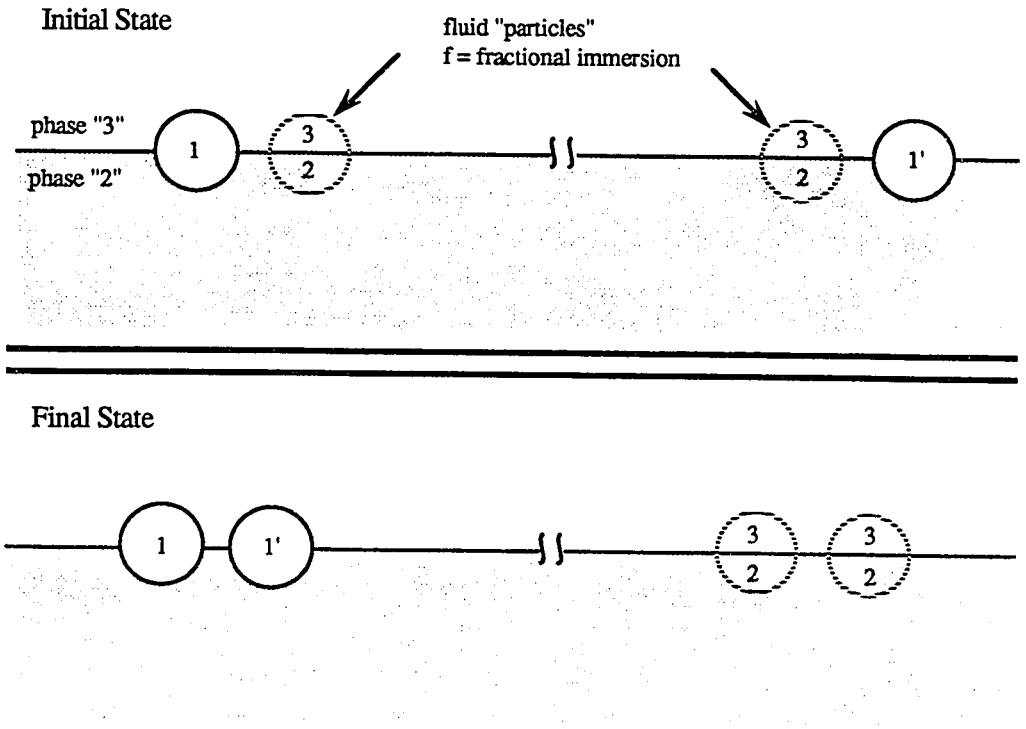

Figure 11. Use of Hamaker's Convention for Interfacial Geometry

$$\Delta E = \text{Final -Initial} = E_{11} - 2(f\,E_{13} + (1\text{-}f)\,E_{12}) + f\,E_{33} + (1\text{-}f)\,E_{22} \qquad \{17\}$$

or since E_{ij} is roughly proportional to A_{ij}

$$\begin{aligned} A_{1,23,1} &= \text{Interfacial Hamaker Constant} \\ &= A_{11} - 2(f\,A_{13} + (1\text{-}f)\,A_{12}) + f\,A_{33} + (1\text{-}f)\,A_{22} \end{aligned} \qquad \{18\}$$

Assuming the geometric mixing rule for dispersion interactions:

$$A_{1j} = \sqrt{A_{11}\,A_{jj}} \quad \rightarrow \quad A_{1j1} = \left(\sqrt{A_{11}} - \sqrt{A_{jj}}\right)^2 \qquad \{19\}$$

results in a simpler expression that requires only the Hamaker constants for the interaction in a vacuum (i.e. A_{jj}):

$$A_{1,23,1} = A_{131} + f\,(A_{121} - A_{131}) \qquad \{20\}$$

The variation of the Hamaker constant with particle immersion (Figure 12) is certainly significant; accounting for a seven-fold change for polystyrene particles at the air-water interface and substantially altering the pair potential predictions (Figure 13).

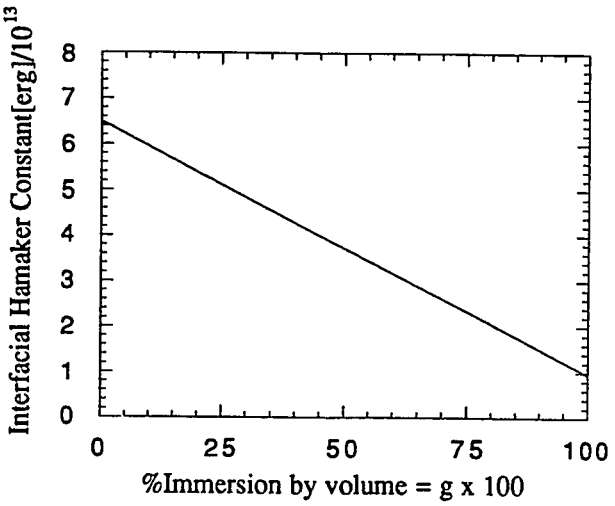

Figure 12. Variation of Interfacial Hamaker Constant with Immersion

The functional form of the dispersion interaction is again drawn from the work of Clayfield(44) and Gregory(30). The retarded dispersion interaction between two spheres at moderate separations ($h>3\lambda/2\pi$) is given by(44):

$$V_{vdW} = \frac{-A_{1,23,1}}{\rho\, kT} I_{s1}$$

$$I_{s1} = \sum_i a_i f_i(\rho)$$

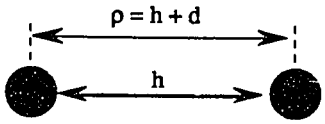

$x = h/d$

$$I_{s1} = a_1\rho^{-1} + a_2(\rho+d)^{-1}\, a_3(\rho-d)^{-1} + a_4\rho^{-2} + a_5(\rho+d)^{-2} + a_6(\rho-d)^{-2} + a_7\rho^{-3} + a_8(\rho+d)^{-3} + a_9(\rho-d)^{-3} + a_{10}\ln\left(\frac{\rho^2}{\rho^2 - d^2}\right) \quad \{21\}$$

with coefficients a_i :

$a_1 = D/90$ $\quad a_6 = Cd^2/120$

$a_2 = Cd/30 - D/180$ $\quad a_7 = Dd^2/180$

$a_3 = -(Cd/30 + D/180)$ $\quad a_8 = -Dd^2/360$

$a_4 = Cd^2/60 - Dd/180$ $\quad a_9 = -a_8$

$a_5 = Cd^2/120 - Dd/180$ $\quad a_{10} = C/30$

$C = 2.45/(2\pi/\lambda)$ $\quad \lambda$ = dominant dispersion wavelength (100nm)

$D = 2.04/(2\pi/\lambda)^2$

The interaction at closer approach ($h<3\lambda/2\pi$) reduces to the more manageable expression given by Gregory(30):

$$V_{vdW} = \frac{-A_{1,23,1}}{24\,kT}\frac{1}{x}\left(1 - c_3 \times \ln\left(1+(c_3x)^{-1}\right)\right) \qquad \{22\}$$

with $c_3 = 5.32(2a)/\lambda$ as before. Figure 13 displays the dispersion attraction predicted by equations {20}, {21} and {22} for varying degrees of immersion of 1μm polystyrene particles at the air-water interface.

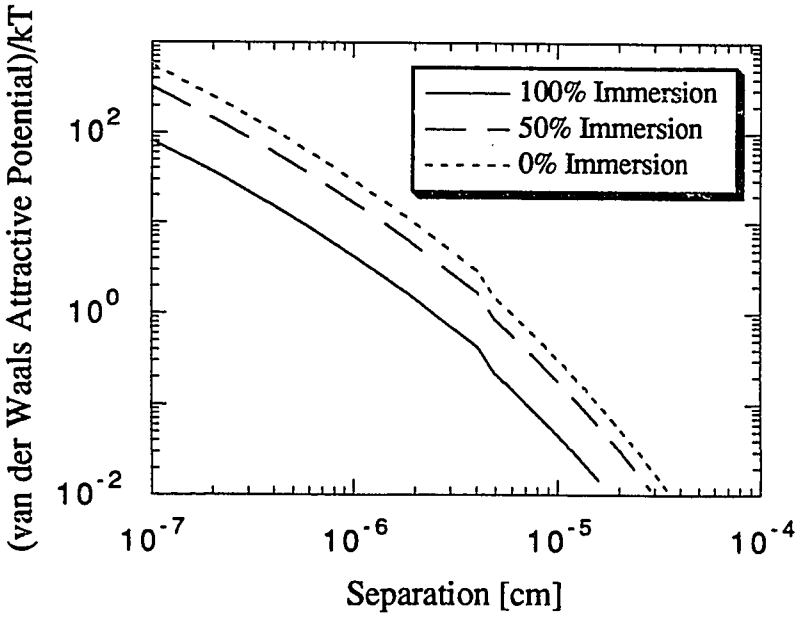

Figure 13. van der Waals Pair Potential at Various Immersions

4.2.2 Electrostatic Interaction

Recently Lyne and Levine(45) formulated the appropriate analog to the Poisson-Boltzmann Equation for the interaction of spheres which reside at the interface between an electrolyte phase (usually aqueous) and a dielectric phase (usually either air or an oil). Their approach, summarized schematically below (Figure 14.), focuses on solving the Poisson-Boltzmann Equation in the aqueous phase simultaneously with the Laplace Equation in the dielectric phase(s) for the global potential distribution; both equations being subject to the appropriate boundary conditions at the interfaces. Determination of the double-layer repulsion energy from the potential distribution is a significant task in itself and must be done carefully in order to achieve any numerical accuracy. It was found that direct calculation of the force between particles by integration of the electrostatic and osmotic stresses at the median plane provided the most accurate basis for potential energy estimates.

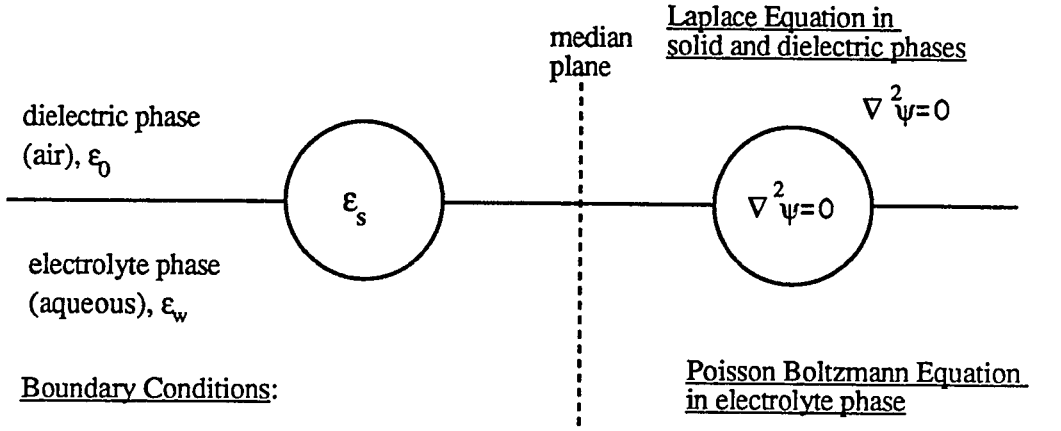

Figure 14. Lyne and Levine Formulation of the Interfacial Electrostatics Problem

Both the formulation and solution of the equations for the dual tasks of solving for the potential distribution and the resulting double-layer energy are quite involved; and actual solutions were limited to quasi-two-dimensional or axisymmetric geometries (i.e. infinite cylinders, isolated spheres embedded in a unit cell). A simpler approach is to model the interaction by appropriately weighting the interaction between the "dry"(uncharged) and "wet"(charged) surfaces using a modified Deryaguin integration. The details of this development are contained in Appendix A. As in the case of van der Waals forces we have two limiting cases corresponding to 0% immersion(no repulsion) and 100% immersion(dispersed particle repulsion). The analysis results in a family of curves (Figure 15) relating the diminished electrostatic repulsion as a function of particle immersion with the normalized particle radius(κa) serving as a double-layer thickness parameter.

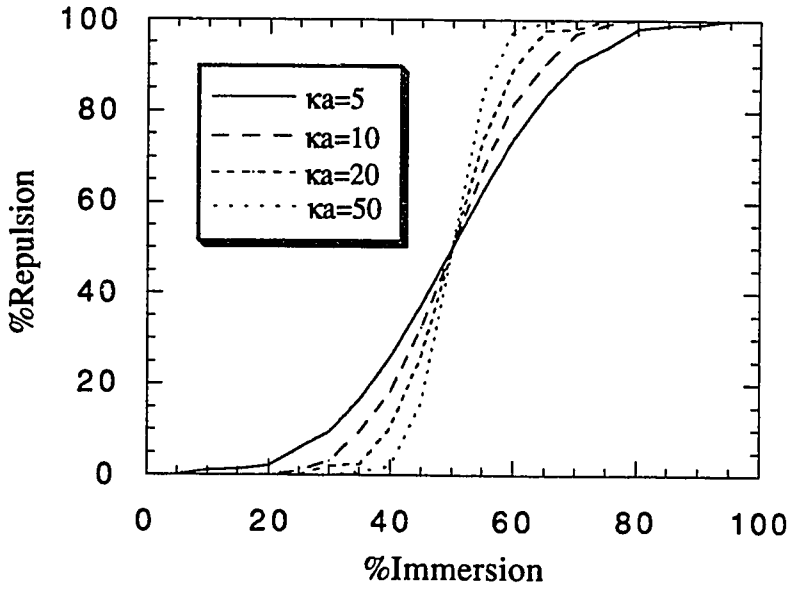

Figure 15. Diminished Electrostatic Repulsion vs. Immersion

The curves exhibits a sigmoidal character; becoming steeper about the 50% immersion condition as κa increases. The reference case of repulsion between two fully immersed spheres is calculated according to equation{5}; however in this case 2s represents the particle separation. Levine and Lyne(46,45) recently demonstrated (Figure

16.) the accuracy of this type of Deryaguin integration for the estimation of the electrostatic potential between partially immersed cylindrical particles. They found almost no difference between the repulsion predicted by the numerical solution to the "interfacial" Poisson-Boltzmann Equation and the approximate results of the Deryaguin analysis for the case of thin to moderate double layers ($\kappa a>5$). It is expected that Deryaguin approximation will also be accurate for spheres at the interface.

4.2.3 Structural Interaction

The attractive force that acts to draw a hydrophobic particle to the air-water interface (section 4.1.3) also exists during the approach of two hydrophobic particles. Since the de-wet portion of an interfacial particle does not contribute to the hydrophobic force partially immersed spheres experience only a fraction of the attraction that occurs between dispersed particles. In order to model this diminished attraction we again draw upon Christenson's measurements(36) of the hydrophobic potential between planar surfaces (equation{6}) and the Deryaguin approximation results outlined in the previous section. Since both the hydrophobic and electrostatic interactions are decaying exponentials the results of Appendix A(Figures 15,71-72) also serve to relate the diminished hydrophobic attraction to the degree of particle immersion.

In addition to the previous results the base case of the hydrophobic potential between two fully immersed spheres needs to be addressed. The sphere-sphere potential is also derived from the flat-plate potential by Deryaguin integration (Appendix A, equation{A5}) yielding:

$$V_{s\text{-}s}(100\% \text{ immersion}) = \pi a K \ell e^{-h/\ell} \qquad \{23\}$$

The fractional attraction ($V_{s\text{-}s}/V_{s\text{-}s}(100\%)$) is given by Figure 15 with a/ℓ standing in for κa. This analysis results in a family of curves very similar to those of the previous section, except that an attractive rather than a repulsive potential is seen to diminish progressively as a particle emerges from the bulk.

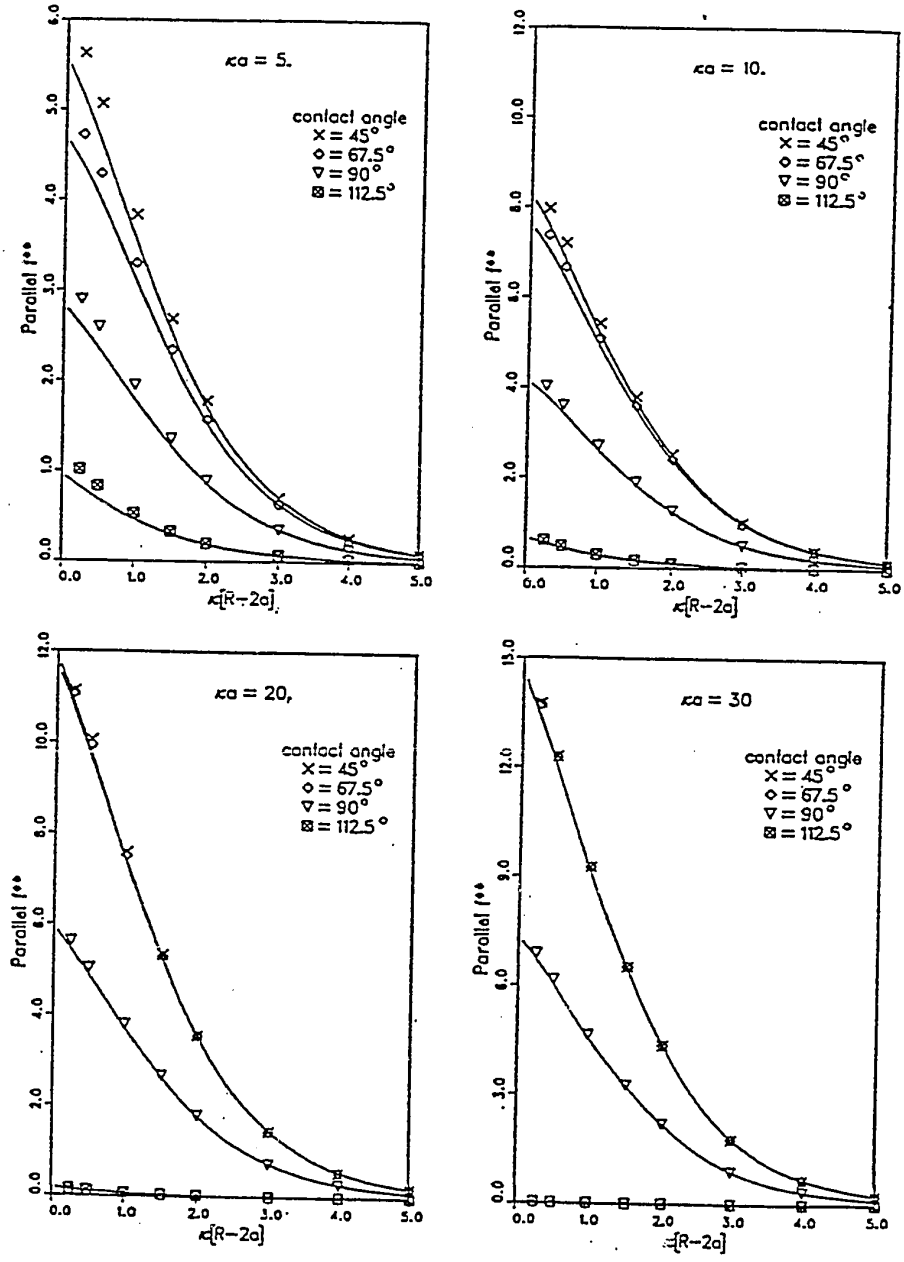

Figure 16. Lyne and Levine Results(45) Comparing Interfacial Deryaguin Approximation (solid lines) to the Solution of the Complete Interfacial Electrostatics Equations (Figure 14.) for the Lateral Repulsive Force Between Parallel Cylinders at an Uncharged Oil/Water Interface.

4.2.4 Capillary Effects (meniscus forces)

The capillary attraction of like wetting particles (i.e. "floating" waxed needles, cork, talc) is a common observation and is the most obvious explanation for enhanced aggregation at the interface. This attraction derives from the effect of a particle's buoyancy in producing a depressed (or elevated) meniscus which acts to attract other particles with similar menisci. The actual force on a particle is generated by the combination of the resolved surface tension force integrated about the contact line and the differential pressure developed on the wetted solid due to the unequally curved meniscus (Figure 17).

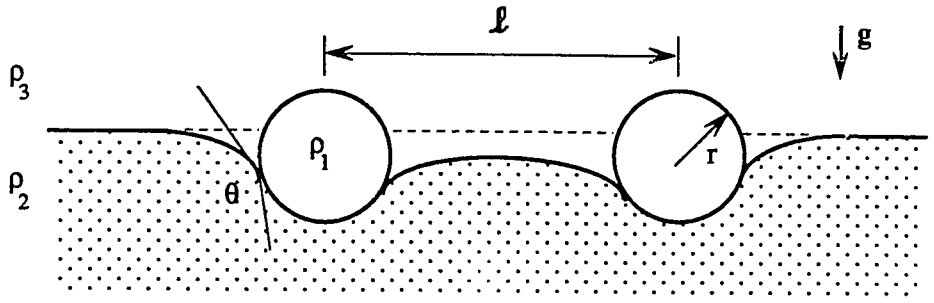

Figure 17. Typical Meniscus between Approaching Spheres

The reconciliation of the preceding figure and the previous assertion of a flat meniscus (section 4.1.5) lies in the relative significance of the meniscus forces. For the flat meniscus assumption to be valid only a negligible meniscus force(or energy < 1kT) should be predicted.

The precise calculation of these forces has only been carried out for the simplest of axisymmetric geometries (planar walls, parallel cylindrical particles of infinite extent)(47). However in the limit of small Bond numbers(Bond No. = $\Delta\rho gr^2/\sigma_{23}$ < 0.01) the approximate analysis of Chan(48) provides a good estimate of the capillary force between two partially immersed spheres. With the assumption of small Bond numbers Chan was able to linearize the Laplace equation for the meniscus profile and apply the superposition approximation for calculation of the interfacial profile between two approaching particles. He found the horizontal attractive force to be:

$$F(\ell) = \frac{-2\pi}{\sigma_{23}^{3/2}}((\rho_2-\rho_3)g)^{5/2}S^2 r^6 K_1(\lambda\ell) \qquad [24]$$

and the corresponding energy of interaction to be:

$$E(\ell) = \frac{-2\pi}{\sigma_{23}}((\rho_2-\rho_3)gS)^2 r^6 K_0(\lambda\ell) \qquad [25]$$

where:

$\lambda = \sqrt{(\rho_2-\rho_3)/\sigma_{23}}$ $\qquad$ $S = \frac{2}{3}D - \frac{1}{3} - \frac{1}{2}\cos\theta - \frac{1}{6}\cos^3\theta$

$D = (\rho_1-\rho_3)/(\rho_2-\rho_3)$ $\qquad$ $S_{max}(\theta=\pi)=2/3\ D$, θ=contact angle

K_0, K_1: modified Bessel Functions $\qquad$ $S_{min}(\theta=0) = 2/3\ (D-1)$

For colloidal particles $\lambda\ell \ll 1$ and the Bessel functions reduce to:

$K_0(\lambda\ell) = -\ln(\lambda\ell)$ $\qquad$ and $\qquad$ $K_1(\lambda\ell) = 1/(\lambda\ell)$

The most striking features of this prediction are the unusually long range of interaction and the dominating influence of particle size upon the strength of interaction. The extended range of action is in accord with our observations of the macroparticles at the surface. The fact that the magnitude of the force decreases dramatically with particle size explains why effects we observe with macroscopic particles are not as important for particles in the colloidal size range. Using the thermal energy associated with a colloid (kT) as a yardstick for assessing the significance of capillary interactions (Figure 18) we find a particle size of at least 10μm is required for the interaction to be judged appreciable.

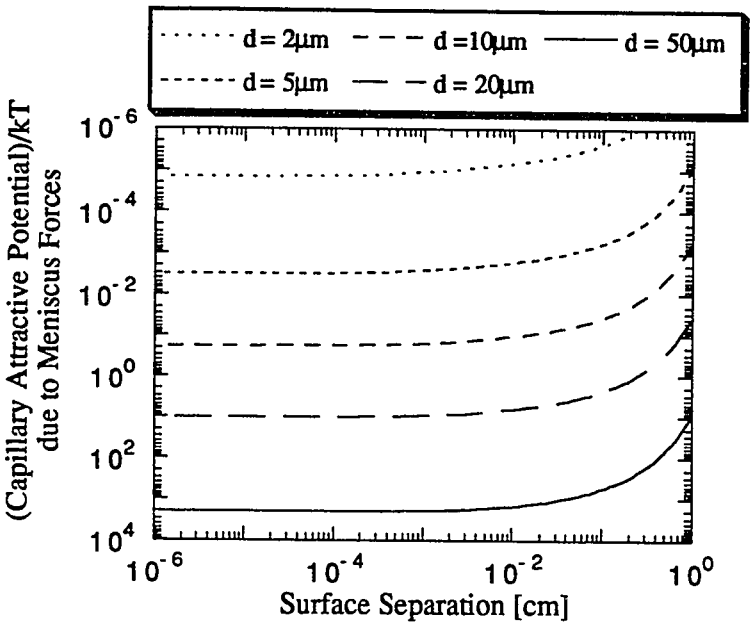

Figure 18. Capillary Potential due to Meniscus Forces between two Spheres (D=2)

The fact that meniscus forces are insignificant for the range of particle sizes within the scope of this study (0.1 to 3.0 μm) also justifies the assumption of a flat meniscus made in section 4.1.5. However it should be noted that as particles aggregate into clumps at the surface they will pass into the regime where meniscus forces will play an important part in determining floc structure.

4.2.5 Total Potential

As in section 4.1.6 the net pair potential is constructed by adding the component energy contributions in order to predict, in this case, the stability of interfacial colloids. For the moment I want to focus attention upon the combined effects of just the van der Waals and electrostatic components; leaving consideration of the structural (i.e. hydrophobic) contribution for separate consideration. The resulting curve (Figure 17) serves as a "DLVO" relationship at the interface and exhibits the same important features (potential barriers and wells) that exist for fully dispersed particles. Figure 19 clearly demonstrates the decreased stability of interfacial particles due to the increased van der Waals attraction and diminished electrostatic repulsion at the interface. For the case

displayed the potential barrier height is reduced from 500 to 100 kT and the potential well depth is increased from 0.3 to 2 kT for the transition from 100% immersion to 50% immersion.. This enhancement in the well depth is quite significant since it accounts for the transition from essential stability in the bulk to a situation of slow, reversible aggregation at the surface.

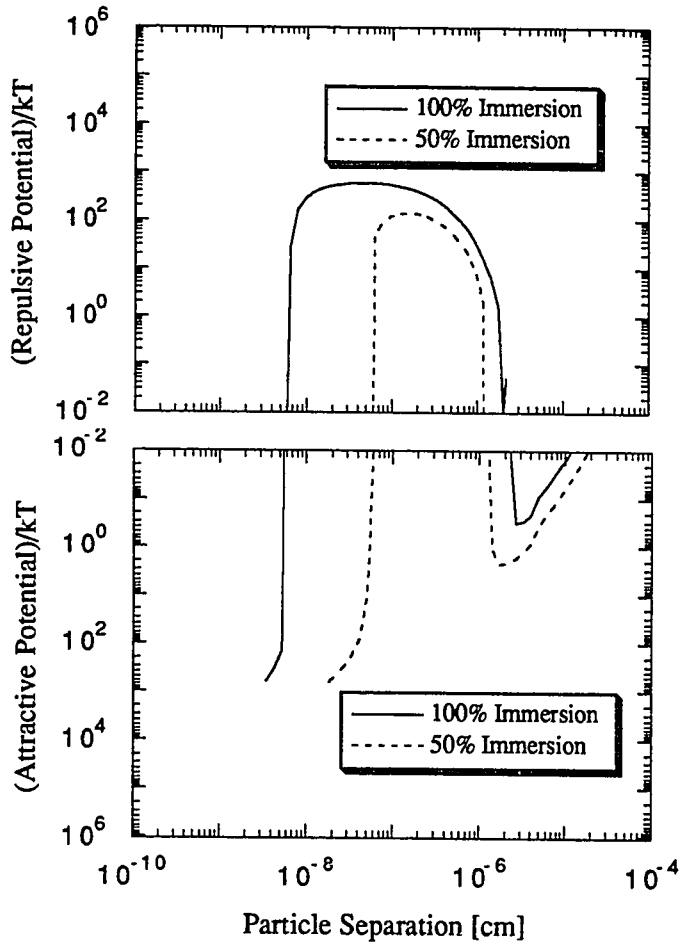

Figure 19. Typical Pair Potential for Standard 1μm Colloid, [NaCl] = 0.01M

It is also constructive to consider the evolution of these DLVO curves as a function of electrolyte concentration and particle immersion. Both of these parameters play an important role in determining both the stability and mode of stabilization or destabilization of surface colloids. In the previous example (Figure 19) it was apparent that the mode of destabilization was a reversible flocculation into a shallow secondary minimum. At a slightly lower degree of immersion(40%, Figure 20.) the mode of destabilization is primarily associated with the disappearance of the potential barrier and occurs over a narrow κa range (40<κa<50 or 0.006<[NaCl]<0.009).

One can also consider the evolution of the DLVO curves as a function of particle immersion at a fixed electrolyte concentration (Figure 21.). At degrees of immersion between 100% and 50% the secondary minimum is seen to increase in depth and attain significant values (>1kT). Greater degrees of de-wetting (Immersion < 50%) results in the disappearance of the primary maximum altogether and leads to fast, irreversible aggregation.

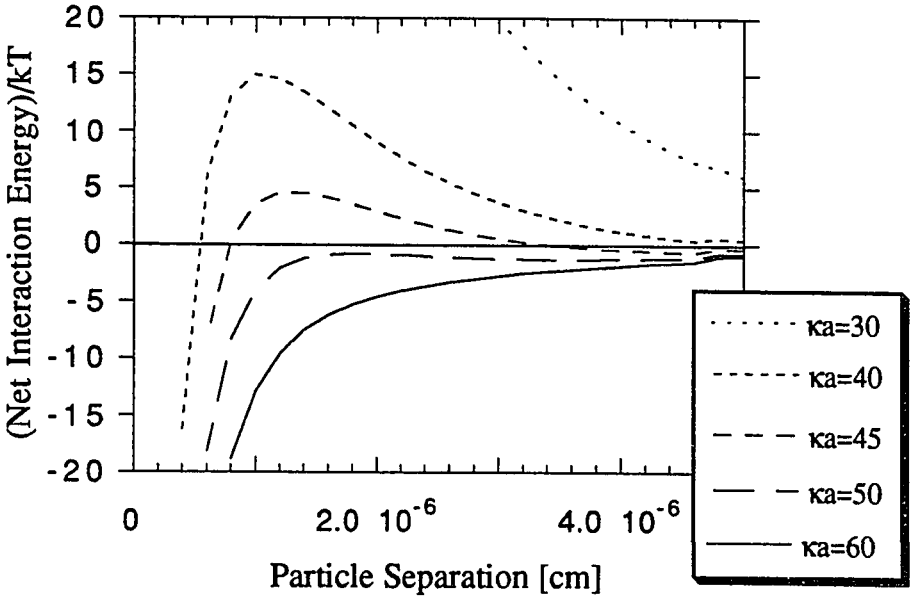

Figure 20. Variation of Interfacial Pair Potential with Double-Layer Thickness for Standard 1μm Colloid, %Immersion =40%

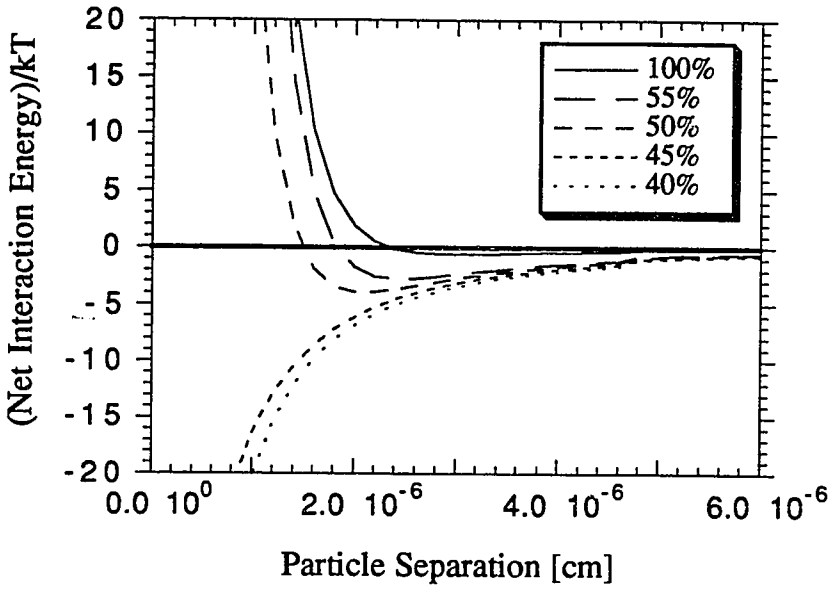

Figure 21. Variation of Interfacial Pair Potential with %Immersion for Standard 1μm Colloid, [NaCl] = 0.01M, κa =150

The preceding picture is in agreement with our observations of aggregation in the bulk and at the surface and supports the assertion of the interface as a critical locus of instability. A somewhat different picture emerges when the hydrophobic interaction is included. Hydrophobic attraction can only act to destabilize surface particles even more completely than the preceding predictions. However, in contrast to the van der Waals attraction, the hydrophobic force is a decreasing function of the degree to which a particle is de-wet (section 4.2.3). This behavior is in opposition to the action of electrostatic and dispersion forces, which tend to magnify the differences between stability in the bulk and that at the surface.

The basic nature of the net potential energy curve is fundamentally changed by the addition of the exponentially decaying hydrophobic potential. By this addition the augmented "DLVO" curve loses some of the complex character that derives from the competition between exponential ($\exp(-\kappa r)$, electrostatic) and algebraic (r^{-n}, dispersion) functions, and is dominated by the competition between two exponentially decaying

functions of opposite sign (i.e. electrostatic(+) .vs. hydrophobic(-)). The consequences of this new character are: (a) the disappearance of the secondary minimum potential well, and (b) the existence of a single "universal" salt concentration at which particles are destabilized; regardless of size, surface charge, or degree of immersion. At first glance Figure 22 is quite similar to previous "DLVO" curves which omitted hydrophobic attraction. Despite the diminished hydrophobic attraction at 50% immersion a reduced barrier height is still exhibited for the interfacial particle. However, notice the complete absence of any significant potential well at extended separations (Figures 22 and 23). A further reflection of the dominance of the interplay of electrostatic and hydrophobic forces is the fact that particles are predicted to pass from stability to fast aggregation over a very narrow range of salt concentrations (Figure 23). This narrow range, or "universal" salt concentration, is relatively insensitive to particle surface charge or particle immersion and is primarily determined by the salt concentration which produces a Debye length ($1/\kappa$) equal to the 13nm hydrophobic decay length. Note also that this "universal" concentration is an order of magnitude lower than the typically observed critical coagulation concentrations of polystyrene latices (0.01 to 0.2M, 1-1 electrolyte).

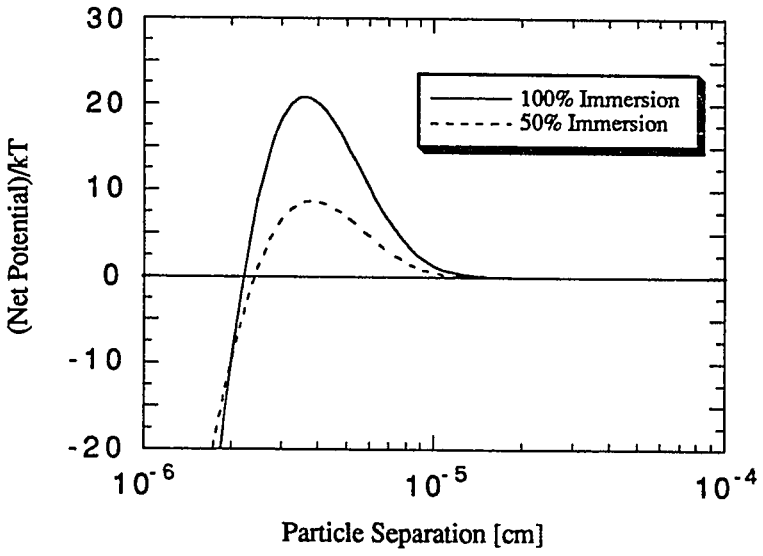

Figure 22. Net Pair Potential Curves Including Hydrophobic Attraction for Standard 1μm Colloid at [NaCl]=0.004 M

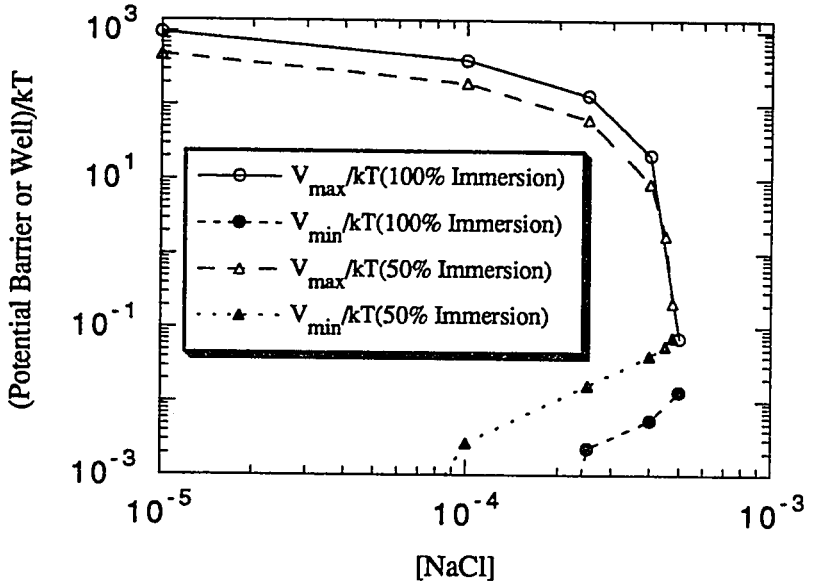

Figure 23. Summary of Maxima and Minima for Net Pair Potential Curves, Including Hydrophobic Attraction, for Standard 1μm Colloid

The unrealistic predictions that follow from inclusion of the hydrophobic potential reflect issues that remain unresolved in the theory of stability of disperse colloids. Most of the uncertainty derives from our lack of fundamental understanding of the nature of hydrophobic forces between particles. All of our measures of hydrophobic forces are essentially flat-plate measurements and the degree to which curvature plays a role is unknown. There certainly remains an attractive element between particles, but the form which it takes is uncertain due to our lack of a supporting theory. The Deryaguin integration approach taken in this study is at least unbiased and has proven quite accurate for estimating van der Waals and electrostatic potentials between curved surfaces. It should also be pointed out that the data-base for interactions between hydrophobic surfaces is quite limited and the use of the most reliable estimates of recent work is provisional. Because of these uncertainties the hydrophobic force between surface particles can only play a "wild-card" role in the modelling of the interfacial pair potential and will be omitted from the detailed predictions for comparison with experimental data.

4.3 Flocculation Kinetics

The measurement and modelling of flocculation kinetics has been the primary means of quantitatively investigating the stability of colloids in the bulk. Models that relate the rate of flocculation to the influence of an energy barrier (i.e. "primary maximum") or a potential well (i.e. "secondary minimum", Figure 28) have successfully predicted the aggregation kinetics of dispersed colloids. The basis for all of these models is Smoluchowski's theory of fast flocculation, which establishes the reference condition of diffusion-limited aggregation (i.e. collision efficiency=100%, frequency factor determined solely by Brownian diffusion). The fast flocculation flux usually serves as an upper limit; since an energy barrier or shallow potential well will impede the process of diffusion-limited aggregation. The ratio of the fast flocculation rate and the actual diminished flux is known as the stability ratio (W=1/{collision efficiency}) and is the quantity which "slow" flocculation models must predict based upon the pair potential. The last step in modelling integrates the results from the fast flocculation analysis and the stability ratio estimates into a population balance that predicts the evolution of the aggregate size distribution. The same basic strategy outlined above can be applied to the aggregation of colloids at the surface. However the situation is somewhat more complex due to the distinct character of the two-dimensional equations. The specific differences in the fast flocculation analysis, slow flocculation analysis, and the population balance equations are addressed in the following sections.

4.3.1 Fast-Flocculation at the Surface

The starting point for modelling aggregation kinetics is the analysis of the flocculation of mobile surface colloids with a stationary central particle (Figure 24):

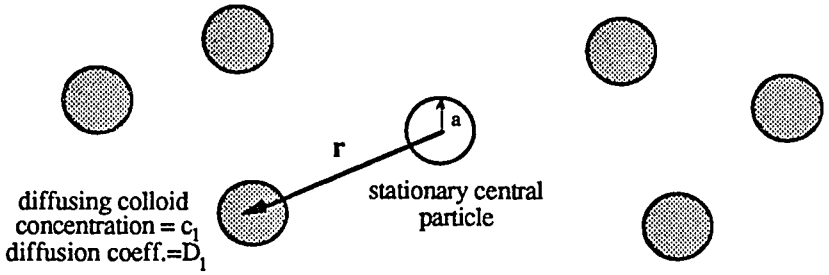

Figure 24. Geometry for Surface Aggregation with a Central Particle

The governing equation and boundary conditions in cylindrical coordinates are:

$$\frac{\partial C}{\partial \theta} = \nabla^2 C = \frac{1}{R}\frac{\partial C}{\partial R} + \frac{\partial^2 C}{\partial R^2} \qquad \text{(Diffusion equation)} \tag{26}$$

boundary conditions:

$C(R>1, \theta=0) = 1$
$C(R=1, \theta>0) = 0$
$C(R\text{-->}\infty, \theta>0) = 1$

dimensionless variables:

$C = C_1/C_1(t=0)$
$\theta = D_1 t/(2a)^2$ (t=time)
$R = r/2a$

Crank(49) reports the resulting dimensionless flux as:

$$\overline{F} = \frac{F_{11}(2a)}{D_1 C_1} = \left(\frac{dC}{dR}\right)_{R=1} = \frac{-4}{\pi^2}\int_0^{\infty} \frac{e^{-u^2\theta}\, du}{u\left(J_0^2(u) + Y_0^2(u)\right)} \tag{27}$$

This result, along with the corresponding expression for fast flocculation in the bulk(50), is plotted below:

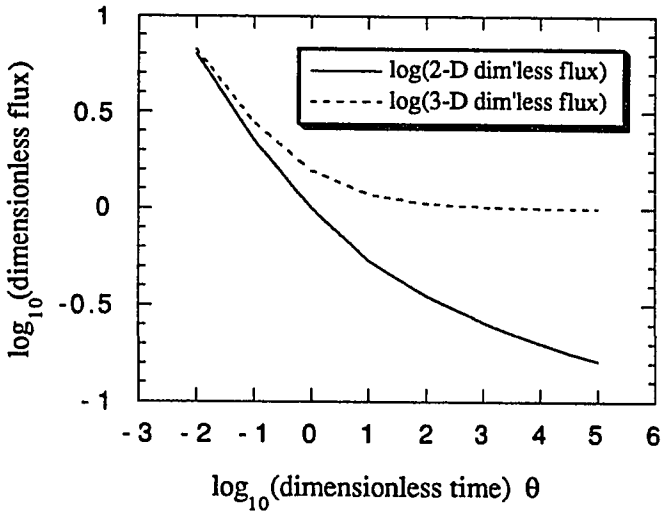

Figure 25. Two-Dimensional and Three-Dimensional Fast Flocculation Results

Note that the fundamental difference between the two results is that a constant (pseudo steady-state) flocculation flux is never established for the case of surface aggregation. The simple expressions developed for flocculation in the bulk are contingent upon this steady-state assumption, so we expect the analogous expressions for surface aggregation to be somewhat more complicated.

While this stationary central particle result forms the kernel of the analysis it does not account for the fact that each particle acts as a mobile "reaction" center. Correcting for the mutual diffusion of the multiple "reaction" centers we find the rate of singlet consumption to be:

$$\begin{aligned} J_{11}(\theta) &= \text{rate at which species 1(singlets) are lost due to 1-1 collisions} \\ &= \left(\text{stationary particle flux}\cdot\text{"reaction perimeter"}\right) C_1 \frac{D_1 + D_1}{D_1} \\ &= \left(\bar{F}\frac{D_1 C_1}{2a} 2\pi(2a)\right) 2C_1 = \left(2\pi D_1 \bar{F}\right) C_1^2 \\ &= k_{11}(\theta)\, C_1^2 \end{aligned} \qquad \{28\}$$

where $k_{11}(\theta)$ serves as a time dependent rate coefficient for the second order rate process of singlet-singlet interactions. In addition to the singlet-singlet interactions the interaction of higher order aggregates need to be accounted for. Modelling of the aggregation of higher order species with the standard assumptions(50)

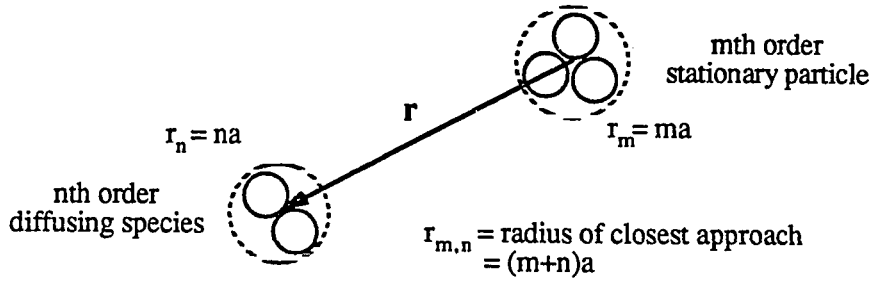

Figure 26. Geometry for Interaction with Higher Order Aggregates

results in a diffusion equation of the form:

$$\frac{\partial C}{\partial \theta_{m,n}} = \nabla^2 C = \frac{1}{R}\frac{\partial C}{\partial R} + \frac{\partial^2 C}{\partial R^2} \qquad \{29\}$$

boundary conditions:

$C(R>1, \theta=0) = 1$
$C(R=1, \theta>0) = 0$
$C(R\text{-->}\infty, \theta>0) = 1$

dimensionless variables:

$C = C_n/C_n(t=0)$
$\theta_{m,n} = D_n t/(r_{m,n})^2 = 4\theta/[(m+n)^2 n]$
$R = r/r_{m,n} \quad D_n = D_n/n$

which is identical to equation{28} except for the time scale ($\theta_{m,n}$). Obviously the dimensionless diffusion fluxes are also identical except that they are mapped to smaller values of time by $\theta_{m,n}$. The formulation of rate coefficients from these fluxes requires some care since $F_{m,n} \neq F_{n,m}$ (i.e. $\theta_{m,n} \neq \theta_{n,m}$). The appropriate accounting for each species (m and n) as a reaction center requires we define:

$$\begin{aligned} J_{n,m} &= \text{rate at which species m and n are lost due to n-m collisions} \\ &= 2\pi D_1 \left(\frac{1}{n} + \frac{1}{m}\right) \cdot \frac{1}{2}\left(\overline{F}(\theta_{m,n}) + \overline{F}(\theta_{n,m})\right) C_m C_n \\ &= k_{m,n}(\theta)\, C_m C_n \end{aligned} \qquad \{30\}$$

As the order of species (m,n) vary there are two counterbalancing factors which act to keep $k_{m,n}$ relatively invariant. The effect of decreased mobility of higher order species is offset by the influence of the increased radius of larger aggregates. This tradeoff is displayed in Figure 27 and was also evident in the simpler formulas developed for flocculation in the bulk.

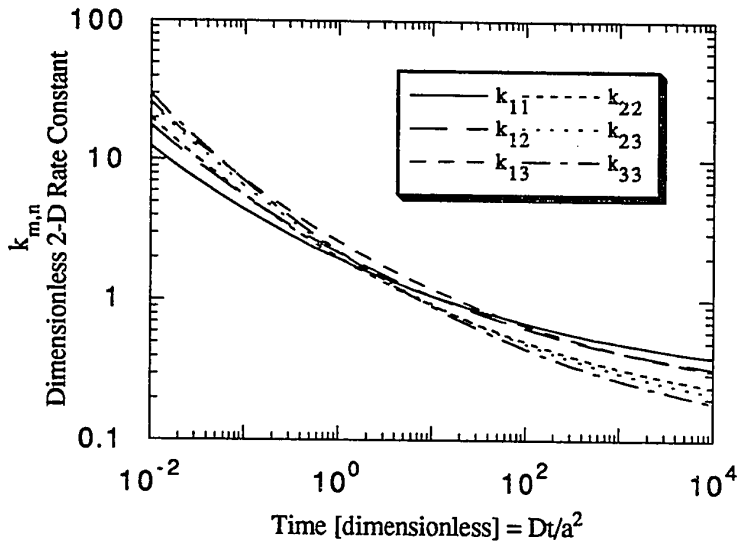

Figure 27. $k_{m,n}$ .vs.θ

4.3.2 Two-Dimensional Slow Flocculation

Models for slow flocculation seek to relate the characteristics of the interparticle potential with the stability ratio (W) or equivalently with the effectiveness factor (α=1/W) associated with particle-particle collisions. The most prominent of the bulk flocculation models is due to Fuchs(51), who applied steady-state constraints to the Smoluchowski equation (diffusion in a field of force, section 4.4.) and arrived at (50):

$$W = 2a\int_{2a}^{\infty} \frac{e^{V/kT}}{r^2}\,dr \qquad \{31\}$$

where a is the particle radius, V is the net pair potential and r is the center-center separation.

There are a number of drawbacks to this approach for modelling slow flocculation at the surface. The most obvious is the necessity of assuming steady-state conditions which, as demonstrated in Figure 25, do not exist at the surface. Another flaw in this approach is that it only deals with irreversible flocculation into the primary minimum. Reversible flocculation into a weak or secondary minimum cannot be handled within the Fuchs' framework.

Recent kinetic models for analyzing slow flocculation in the bulk incur none of the limitations associated with the Fuchs analysis. Colloidal particles are assumed to exhibit a Maxwellian distribution of kinetic energies and the flocculation efficiency (α) is determined by classical treatment of the escape of particles over a potential barrier (primary minimum aggregation) or the trapping of particles in a shallow potential well (secondary or weak flocculation). The development that follows is analogous to the kinetic model of Marmur(52) for flocculation in the bulk.

Start by modelling the velocity distribution of surface colloids as that of a 2-D gas(53):

$$dp(v) = (m/kT)\, v\, e^{-(m/2kT)v^2}\, dv \qquad \{32\}$$

= probability of finding a particle with speed between v and v+dv

For convenience we also define:

$$x^2 = \frac{mv^2}{2kT} = \text{dimensionless kinetic energy} \qquad \{33\}$$

and find that the velocity distribution can be cast:

$$dp(x) = 2xe^{-x^2}dx \qquad \{34\}$$

For aggregation into the primary minimum particles must overcome potential barrier $\Delta\Phi$ (Figure 28),

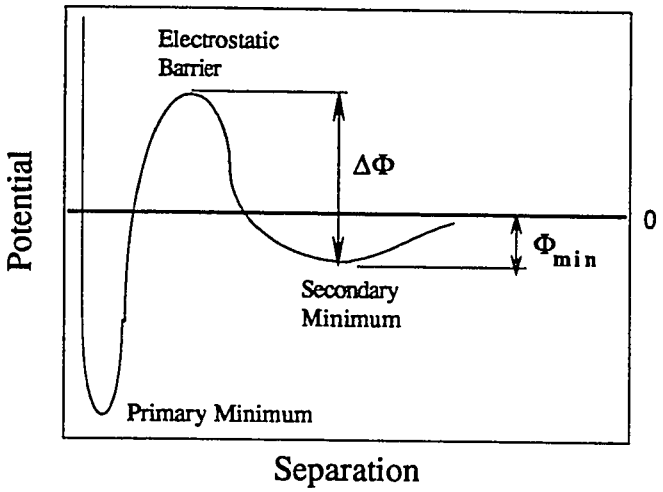

Figure 28. Idealized Pair Potential and Important Features

or $x_1^2 + x_2^2 > \Delta\Phi$. Given kinetic energy $x_1^2 < \Delta\Phi$ the probability of finding a second particle with sufficient energy to overcome $\Delta\Phi$ is:

$$p(x_p) = \int_{x_p}^{\infty} dp(x) = \int_{x_p}^{\infty} 2xe^{-x^2}dx = e^{-x_p^2} \qquad \{35\}$$

with $$x_p = \sqrt{(\Delta\Phi - x_1^2)}$$

To obtain the entire fraction of particles capable of overcoming $\Delta\Phi$, f_p, we must multiply $p(x_p)$ by the distribution function dp(x) for the first particle and integrate over the appropriate ranges:

$$f_p = \int_0^{\sqrt{\Delta\Phi}} p(x_p)\, dp(x) + \int_{\sqrt{\Delta\Phi}}^{\infty} dp(x) = e^{-\Delta\Phi}(1 + \Delta\Phi) \qquad \{36\}$$

For particles which coagulate in the secondary minimum (Figure 28) $x_1^2 + x_2^2 < \Phi_{min}$. Given kinetic energy $x_1^2 < \Phi_{min}$ the probability of finding a second particle with sufficiently small kinetic energy is:

$$p(x_s) = \int_0^{x_s} dp(x) = 1 - e^{-x_s^2} \quad , \qquad \text{with} \quad x_s = \sqrt{\Phi_{min} - x_1^2} \tag{37}$$

As before summing over all x_1 gives f_s, the fraction of particles capable of being trapped in potential well Φ_{min}:

$$f_s = \int_0^{\sqrt{\Phi_{min}}} p(x_s)\, dp(x) = 1 - e^{-\Phi_{min}}\left(1 + \Phi_{min}\right) \tag{38}$$

The total effectiveness of collisions is the sum of the fractions for the two aggregation modes:

$$\alpha = f_p + f_s \qquad \text{and} \qquad W = \text{Stability Ratio} = (f_p + f_s)^{-1} \tag{39}$$

The relationship between aggregation efficiencies, f_p and f_s, and the barrier height ($\Delta\Phi$) and well depth (Φ_{min}) is displayed in Figure 29.

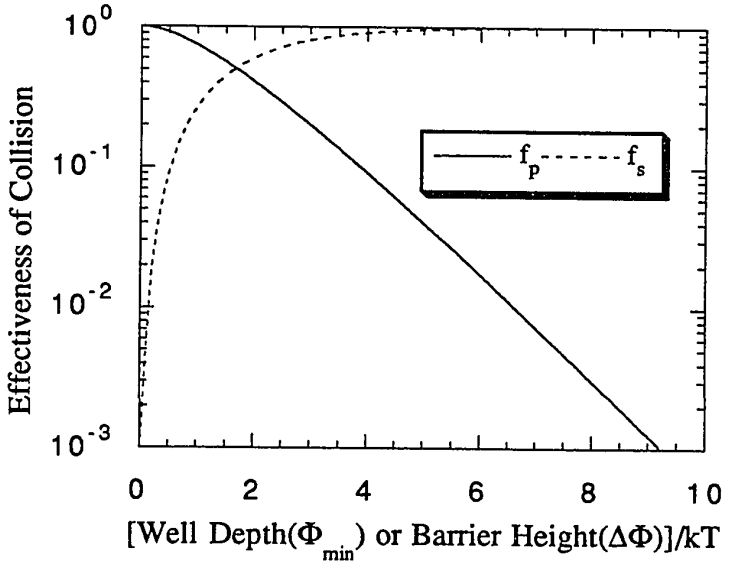

Figure 29. Aggregation Efficiencies from Kinetic Theory

Note that these curves also obey the empirical rule for assessing the significance of potential barriers and wells for flocculation in the bulk (i.e. wells less than 1 kT in depth and barriers greater than 10 kT in height correspond to situations of essential stability with respect to flocculation).

4.3.3 Accounting for Higher Order Aggregates (Population Balance Equations)

The model of singlet-singlet interactions in section 4.3.1 can only predict the doublet formation rate at the very beginning of the coagulation process. As aggregation proceeds collisions with higher order species become significant and must be accounted for. Additionally adjustment of the diffusion-limited rate coefficients to include the effects of "slow" flocculation ($\alpha \neq 1$) is necessary. Both of these issues can be addressed within the framework of the set of hierarchical population balances developed by Smoluchowski(50):

$$\frac{dc_k}{dt} = \frac{1}{2} \sum_{\substack{i=1 \\ i+j=k}}^{i=k-1} k_{ij} c_i c_j - \sum_{i=1}^{\infty} k_{ik} c_i c_k \qquad \{40\}$$

This set of balance equations can be applied to the case of surface flocculation with the proviso that the k_{ik} rate coefficients be normalized according to equation{30} (since $k_{ik} \neq k_{ki}$). Accounting for slow flocculation is, at least in theory, straightforward:

$$k_{ij}(\text{slow flocc.}) = \alpha_{ij}\, k_{ij}(\text{fast flocc.}) \qquad \{41\}$$

While α_{11} is readily calculated based upon pair potential predictions, the estimation of α for higher order species is much more complex. In general we expect the attraction between higher order species to be stronger and result in α's that approach unity. So the two limiting cases entail either setting all the higher order α's to 1 or setting them equal to α_{11}.

The actual population balances used in this study differ from equation{40} by the addition of a singlet adsorption source term ($\phi(t)$) and the truncation of calculations to species of order 4 or less. This results in the following system of equations:

$$\frac{dc_1}{dt} = \phi(t) - k_{11}c_1^2 - k_{12}c_1c_2 - k_{13}c_1c_3 - k_{14}c_1c_4$$

$$\frac{dc_2}{dt} = \frac{1}{2}k_{11}c_1^2 - k_{12}c_1c_2 - k_{22}c_2^2 - k_{23}c_2c_3 - k_{24}c_2c_4 \qquad \{42\}$$

$$\frac{dc_3}{dt} = k_{12}c_1c_2 - k_{13}c_1c_3 - k_{23}c_2c_3 - k_{33}c_3^2 - k_{34}c_3c_4$$

$$\frac{dc_4}{dt} = k_{13}c_1c_3 + \frac{1}{2}k_{22}c_2^2 - k_{14}c_1c_4 - k_{24}c_2c_4 - k_{34}c_3c_4 - k_{44}c_4^2$$

The solution of this set of simultaneous non-linear ordinary differential equations was carried out using a Runge-Kutta algorithm in the standard LSODE package(54). The adsorption source term was drawn from the experimental data. The typical form of the predicted evolution of aggregate species is shown below (Figure 30) for the case of ideal adsorption(equation{16}) and fast flocculation of 1μm diameter particles (c_0(bulk) = 1.9 x 10^7 particles/cc).

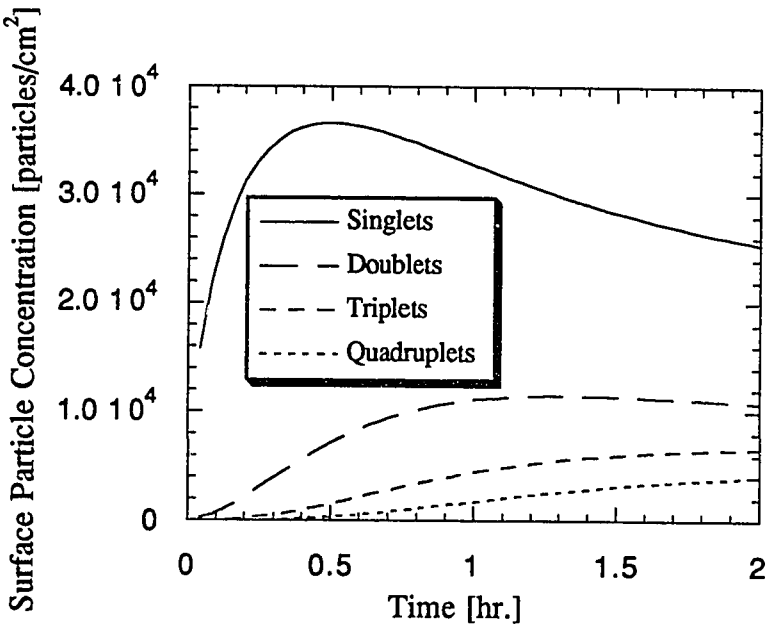

Figure 30. Typical Form of Aggregate Evolution at the Interface

4.4 Secondary Influence of the Pair Potential upon Flocculation and Adsorption Rates: - Diffusion in a Field of Force

The pair potential is typically viewed as influencing only the effectiveness of collisions and not their frequency. Most discussions assume that colloids diffuse with an unperturbed Brownian motion. However it is apparent that the same attractive forces which act to coagulate colloids have the potential to enhance the frequency of collisions such that a rate in excess of fast flocculation is achieved. The same situation and arguments also apply to the adsorption of colloids to the interface.

Smoluchowski(50) made an attempt to account for this "secondary" effect by defining an equivalent radius of interaction. This extended radius was chosen to correspond to the equivalent square-well potential that produces the same effect as the actual potential (Figure 31). The particle mobility is still assumed to remain unchanged.

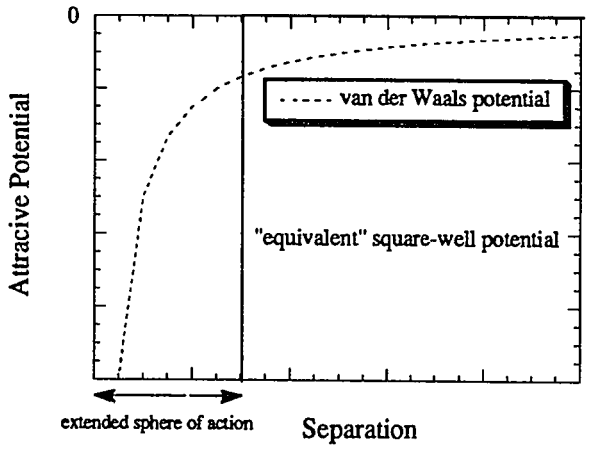

Figure 31. Smoluchowski's Equivalent Radius of Interaction

While this artifice permits recognition of the accelerated motion during aggregation, it does so only in an ad hoc manner (i.e. the effective radius cannot be independently determined). However the concept of an equivalent radius of interaction is useful in putting this secondary enhancement in perspective. It is clear that potentials whose range is much smaller than the particle radius will produce little enhancement in flocculation rates.

Smoluchowski(55) also treated the secondary effect of the pair potential formally by deriving the equation for the diffusion of a particle in a field of force, now known as the Smoluchowski equation. The basis for the Smoluchowski equation is the partition of the material flux into a diffusive and external component:

$$\mathbf{J} = -D\nabla c + c\mathbf{v}_{external} = \mathbf{J}_{diffusive} + \mathbf{J}_{external}$$

$$\mathbf{J} = -D\nabla c + c\frac{\mathbf{F}}{f} \qquad \{43\}$$

where $\mathbf{v}_{external}$ = velocity induced by external force $\mathbf{F}$ and impeded by friction coefficient f. Application of the divergence theorem results in a continuity equation that governs the diffusion in a field of force:

$$\frac{\partial c}{\partial t} = -\nabla\cdot\mathbf{J} = D\nabla^2 c - \frac{1}{f}\nabla\cdot(c\mathbf{F}) \qquad \{44\}$$

The following sections outline the solution of the preceding equations using forces derived from our pair potential predictions for the adsorption (1-D planar geometry) and surface flocculation (2-D cylindrical geometry) cases. Solutions are examined with the primary goal of assessing the significance of the pair potential in producing fluxes in excess of the ideal adsorption or fast flocculation values.

4.4.1 "Enhanced" Adsorption

Consider a particle diffusing in the vicinity of the air-liquid interface:

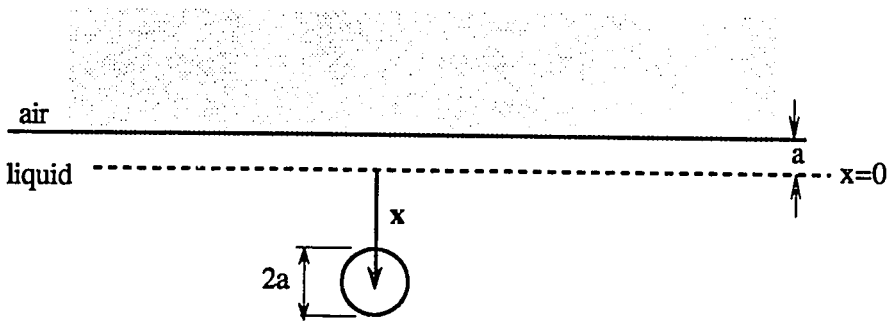

Figure 32. Geometry for 1-D Diffusion Equation

In one dimension equations{43} and {44} become:

$$J = J_x = -D\frac{dc}{dx} + \frac{F_x}{f}c \qquad \{45\}$$

$$\frac{\partial c}{\partial t} = D\frac{\partial^2 c}{\partial x^2} - \frac{1}{f}\left(F_x\frac{\partial c}{\partial x} + c\frac{\partial F_x}{\partial x}\right) \qquad \{46\}$$

with boundary conditions:

$$c(x=0,\ t>0) = 0$$
$$c(x>0,\ t=0) = c_0$$
$$c(x\text{-->}\infty,\ t>0) = c_0$$

The form of F_x, typically a complicated non-linear function, usually precludes a direct analytical solution of equation{46}. The following transformations are appropriate for the numerical solution of this equation. Non-dimensionalizing and introducing the pair potential gives:

$C = c/c_0$ $\qquad$ $\theta = Dt/(2a)^2$

$z = x/2a$ $\qquad$ $D = kT/f$

P =pair potential(sphere/half-space) $\qquad$ $\overline{P} = P/kT$

$F_x = \frac{dP}{dx} = \frac{-1}{2a}\frac{dP}{dz}$ $\qquad$ $\overline{J} = \frac{J(2a)}{Dc_0}$

and transforming from a semi-infinite domain, z(0,∞), to a finite domain, y(0,1) by y=z/(z+1) yields:

$$\frac{\partial C}{\partial \theta} = (1-y)^4\left(\frac{\partial^2 C}{\partial y^2} + \frac{\partial \bar{P}}{\partial y}\frac{\partial C}{\partial y} + C\frac{\partial^2 \bar{P}}{\partial y^2}\right) - 2(1-y)^3\left(\frac{\partial C}{\partial y} + C\frac{\partial \bar{P}}{\partial y}\right) \qquad \{47\}$$

with transformed boundary conditions:

$$c(y=0,\ \theta>0) = 0$$
$$c(y>0,\ \theta=0) = 1$$
$$c(y=1,\ \theta>0) = 1$$

For the case of no external force ("free diffusion", section 4.1.7) the solution in dimensionless form is:

$$C = \mathrm{erf}\left(\frac{z\theta^{-1/2}}{2}\right) \qquad \text{and} \qquad \bar{J}_{x=0} = \frac{1}{\sqrt{\pi}}\theta^{-1/2} \qquad \{48\}$$

The maximum effect of forced diffusion can be assessed by considering the limiting case of attraction to the surface only under the influence of the hydrophobic potential (equation{7}). The solution of equation{47} was accomplished using a modified version of Professor B.A. Finlayson's program PDE.FOR(56) to set up the spatial finite difference equations and the GEARB routine DRIVEB(54) to solve the resulting set of simultaneous ODE's(i.e. initial value problems) using implicit difference formulas. Since the gradients are steepest at the surface a geometric step spacing was used to concentrate grid points near the origin.

The results of these calculations are displayed in Figure 33 and show the degree of adsorption enhancement for various particle sizes.The adsorption flux is only enhanced for particles of a size comparable to the decay length (13nm) of the hydrophobic force. For the range of particle sizes used in this study (0.5 to 3.0μm) no significant enhancement is predicted.

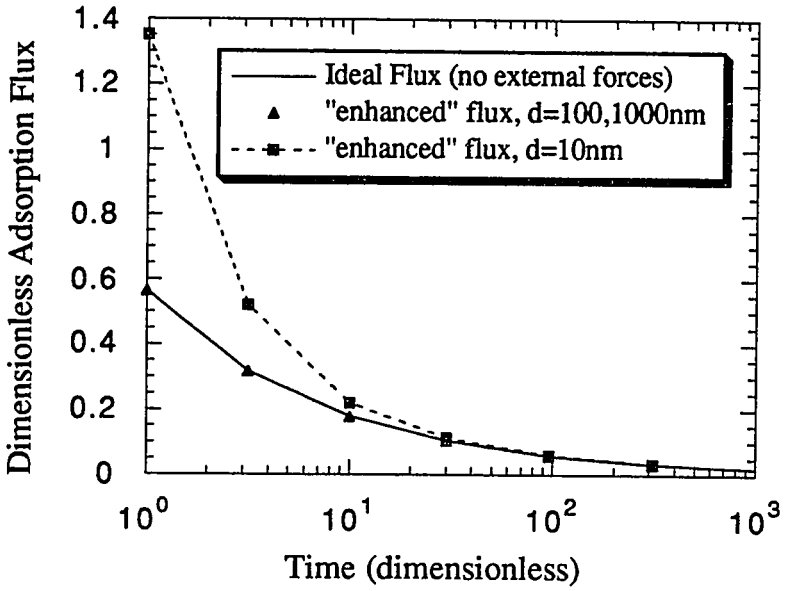

Figure 33. Enhanced Adsorption Rates for Hydrophobic Particles

An additional influence upon the ideal adsorption flux predicted by equation {48} is just the force of gravity. Since the standard 1μm colloid of this study is almost neutrally buoyant in water (specific gravity = 1.055) the Stokes settling velocity is quite low (2.93×10^{-6} cm/s or 1.8 diameters/minute). Even though the buoyancy force is quite small in this case the consequences of its long range requires that we consider the impact of sedimentation at extended times. Chandresekhar(57) considered this problem in the context of equation {48} with reflection rather than adsorption at the interface and arrived at the law of isothermal atmospheres for the equilibrium vertical distribution of colloids. The case of an absorbing surface does not lend itself to solution by the sort of transformations used by Chandresekhar.

For the system as shown in Figure 32, and as it exists during the experiments, gravity acts to diminish the transport of particles to the interface. The solution for the adsorption flux, as accomplished by the numerical solution of equation {47} with the simple sedimentation potential, is displayed in Figure 34. Note that only after an extended period of time ($\theta = 1000$, or t = 30 minutes) is the effect of gravity significant.

The importance of this effect must also be judged in the light of any convective flows, which may (Chapter 6) have much greater influence.

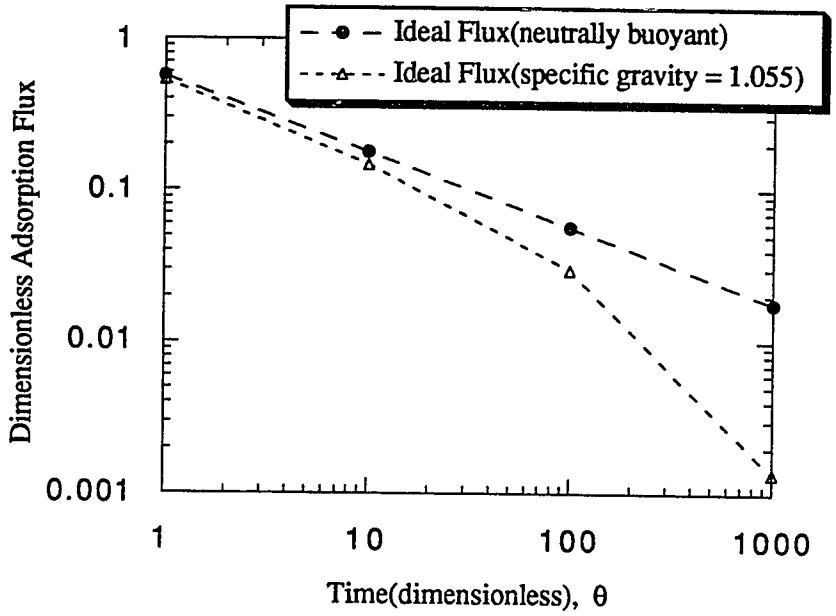

Figure 34. Diminished Adsorption Rate due to Sedimentation of the Standard 1μm Colloid.

4.4.2 "Enhanced" Surface Flocculation

Recalling the picture of surface flocculation developed in section 4.3.1 (Figure 24) and applying equations {43} and {44} in the 2-D cylindrical coordinate system we find:

$$J = J_r = -D\frac{dc}{dr} + \frac{F_r}{f}c \qquad \{49\}$$

$$\frac{\partial c}{\partial t} = D\left(\frac{1}{r}\frac{\partial c}{\partial r} + \frac{\partial^2 c}{\partial r^2}\right) - \frac{1}{f}\left(c\left(\frac{F_r}{r} + \frac{\partial F_r}{\partial r}\right) + \frac{\partial c}{\partial r}F_r\right) \qquad \{50\}$$

with boundary conditions:

$$c(r=2a,\ t>0) = 0$$
$$c(r>2a,\ t=0) = c_0$$
$$c(r\text{-->}\infty,\ t>0) = c_0$$

Again non-dimensionalizing and introducing the pair potential, P:

$$C = c/c_0 \qquad \theta = Dt/(2a)^2$$
$$\rho = r/2a \qquad D = kT/f$$
$$\bar{J} = \frac{J(2a)}{Dc_0} \qquad F_r = \frac{dP}{dr} = \frac{-1}{2a}\frac{dP}{d\rho}$$
$$\bar{P} = P/kT$$

and transforming from a semi-infinite domain, $\rho(1,\infty)$, to closed domain $z(0,1)$ with $z=1-1/\rho$ yields:

$$\frac{\partial C}{\partial \theta} = (1-z)^4\left(\frac{\partial^2 C}{\partial z^2} + \frac{\partial \bar{P}}{\partial z}\frac{\partial C}{\partial z} + C\frac{\partial^2 \bar{P}}{\partial z^2}\right) - (1-z)^3\left(\frac{\partial C}{\partial z} + C\frac{\partial \bar{P}}{\partial z}\right) \qquad \{51\}$$

with transformed boundary conditions:

$$c(z=0,\ \theta>0) = 0$$
$$c(z>0,\ \theta=0) = 1$$
$$c(z=1,\ \theta>0) = 1$$

The flux result for free diffusion (F_r=0) was presented in section 4.3.1(Figure 25). The numerical solution of equation{51} was accomplished using the same methods as described in the previous section, however the potential terms took a different form. In this case we have the possibility of two different attractive terms, one due to van der Waals forces and the other due to hydrophobic forces.These cases were considered separately, since the van der Waals force and hydrophobic force exhibit an opposite dependence on the immersion of a particle. The maximum van der Waals attraction exists for a completely de-wet particle while the maximum hydrophobic force is exhibited between fully immersed particles.

Calculations using the maximum hydrophobic potential between two spheres (equation{23}) are displayed below in Figure 35.

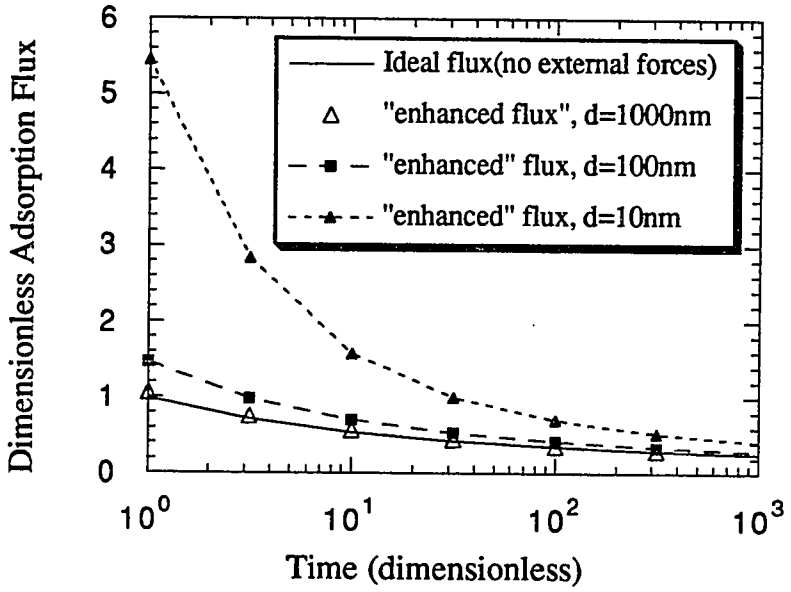

Figure 35. Enhanced Flocculation Rates for Hydrophobic Attraction

The trends are similar to those seen in the previous section and the same conclusion can be reached: enhanced surface flocculation is not an important factor for the conditions of this study. Calculations using the maximum van der Waals potential between two spheres (equations{20-22}, f=0) are displayed in Figure 36 below.

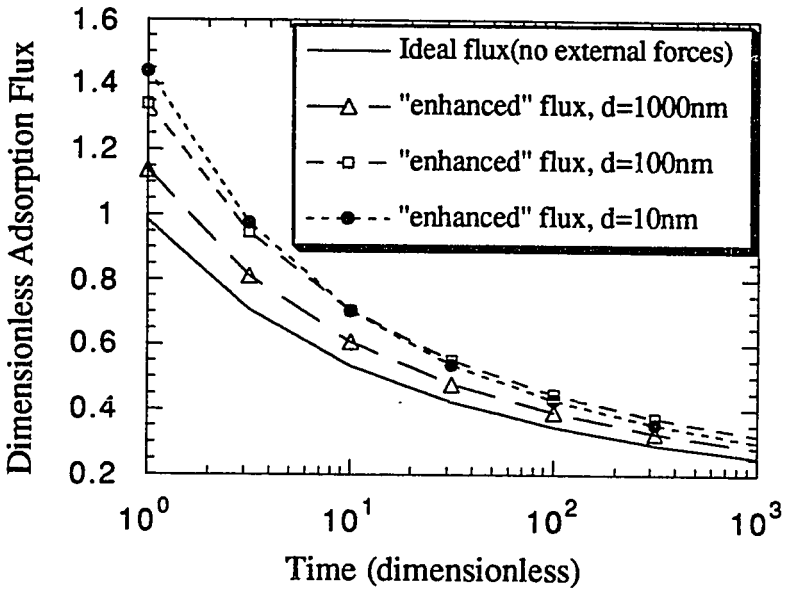

Figure 36. Enhanced Flocculation Rates for van der Waals Attraction

In contrast to the previous cases flocculation is somewhat enhanced for a variety of particle sizes. The enhancement predicted for the 1μm diameter colloid used in most of this study is quite minor. The fact that an increased enhancement is experienced for smaller particles, with an asymptotic limit reached at a diameter of about 10nm, also deserves some comment. One normally considers van der Waals forces to scale with the dimensionless separation(x=r/2a) so that particles always exhibit a van der Waals sphere of action in proportion to their size. This scaling is only exact for the unretarded formulas. The variation exhibited for the 1000nm and 100,10nm cases is a direct reflection of the influence of retardation in decreasing the proportional van der Waals attraction associated with the 1000nm particles.

4.5 Summary

In this chapter I have sought to develop a coherent model for understanding the aggregation of colloids which reside at the fluid-fluid interface. The controlling factors have been dealt with in detail in the preceding sections and it is useful to put them in perspective by summarizing the major points. It is also worthwhile to draw distinctions between developments that are: (a) applications of well established models, (b) significant extensions of previous models, and (c) developments which represent new and original contributions to the field. Summarizing and characterizing the major conclusions from preceding modelling sections we find:

(1.) The "adsorption" step precedes surface aggregation and is initially controlled by a "DLVO" class of interactions associated with the thinning of the intervening liquid film and is finally dominated by the capillary forces which act to trap particles at the interface. This view is an extension of flotation theory and contains fewer ambiguities than the traditional models because of the ability to neglect inertial effects for colloidal particles.

(2.) For the simple model system of this study it is the hydrophobic attraction to the interface which provides the ultimate driving force for adsorption. While potential energy curves have been used to explain capture efficiencies in flotation operations, an integrated approach combining potential energy predictions and diffusion equation models (i.e. Smoluchowski Equation) for estimation of the adsorption flux to the air-liquid interface is a new development. Previous work has focussed upon deposition studies of flowing particles at the solid-liquid interface under quasi-steady-state conditions. For the conditions of this study enhancement of the adsorption flux over the diffusion-limited value is not expected due to the relatively short range of the potential energy interactions. Only the electrostatic barrier imposed at low salt concentrations is expected to diminish the diffusion-limited flux.

(3.) The diminished stability of interfacial colloids is most readily accounted for by models which demonstrate an increased van der Waals attraction and a diminished electrostatic repulsion for partially immersed particles. The individual models for the interfacial interactions represent a significant extension of the present "DLVO"

framework and their integration constitutes a new and original basis for understanding the fundamentals of surface flocculation[1].

(4.) The detailed treatment of the aggregation kinetics of colloids in two dimensions is an original contribution and is a necessary element in any study which seeks to compare theory and experiment. While the problem, as posed within the diffusion equation framework, has a fundamentally unsteady-state character; it remains amenable to modelling as a second order rate process if the rate coefficients are recognized as time dependent quantities. The impact of the pair potential in diminishing the diffusion-limited flocculation rates is derived from an extension of Marmur's theory of aggregation kinetics to two dimensions. The 1kT and 10kT rules for assessing the significance of potential barriers and wells in the stability of dispersed particles were seen to hold at the surface.

The role of the attractive force field in enhancing the frequency of particle collisions was seen to play a minor role for the conditions of this investigation. However the concept of an equivalent radius of interaction was shown to be useful in assessing the significance of various potential fields and was supported by the numerical solutions of the Smoluchowski Equation. The actual solution of the equations for diffusion in a field of force in both one and two dimensions represents an original contribution, since the literature is dominated by analyses based upon the quasi-steady-state approach of Fuchs(51).

---

[1]Some of the developments, especially the electrostatic modelling, were derived independently by Levine et al (45, 46, 58, 59) and reported simultaneously with this author at the 1989 American Chemical Society Surface and Colloids Conference.

5. Experimental Methods and Materials

Microscopic examination of interfacial colloids provides the most direct means of studying the phenomenon of surface flocculation. The rates of particle "adsorption" and surface aggregation are derived from these basic observations and are used to test pair potential models. In order to carry out these measurements an appropriate microscope system must be used in conjunction with a carefully constructed sample cell. The preparation of the dispersion for examination is also an important step because of the possible effects of surface active contaminants. The microscope system, sample cell, and typical experimental procedure is documented in the following paragraphs.

Viewing interfacial colloids requires an optical system that has excellent resolution, high contrast capabilities, and very narrow depth of field. High resolution (down to 0.3μm) and narrow depth of field (about 0.4μm) is achieved by using a high magnification objective lens (Nikon CF BD Plan Achromat 60x/0.8NA) in conjunction with a 2.5x projection lens for relay of the image to the film plane of a 35mm camera. All of the optical components are mounted on a standard upright metallurgical microscope (Nikon Optiphot-M). High contrast is provided by integral darkfield illumination (epi-style, 100 watt).

The sample cell must provide for a flat and stable meniscus for photomicrography. The influence of both vibrations and convection will tend to perturb the interface, resulting in poor pictures and biased results. Care was taken to isolate the microscope from room vibrations and the sample cell from the shutter (Nikon PFX) motion. A number of different cell designs were tested before it was realized that convection was the primary problem. The arrangement suggested by Onoda was found to be the least susceptible to convective flows and was used in most of the experiments (Figure 37). In some experiments a humidifying chamber was added to the microscope stage in order to suppress evaporation from the sample.

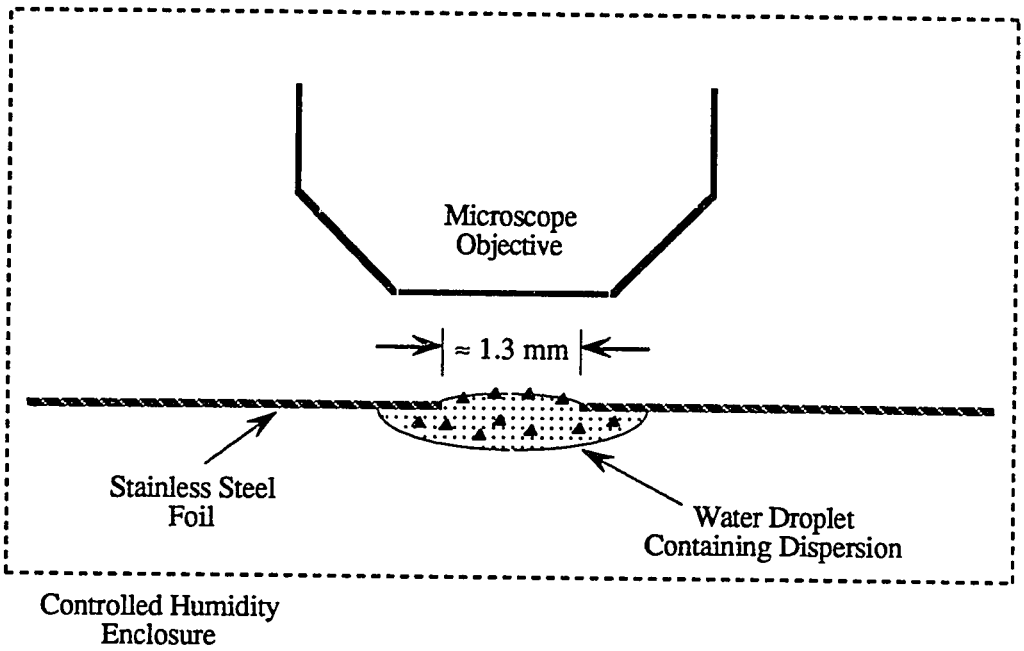

Figure 37. Sample Cell for microscopic observations

The first step in sample preparation is the cleaning of the stock dispersion to remove any contaminants from the suspending liquid. The standard colloid of this study is a 0.989μm diameter surfactant-free polystyrene latex made by Interfacial Dynamics Corporation. These monodisperse, spherical particles are stabilized by surface sulfate groups (215 Ångstrom^2/$SO_4^=$), resulting in a zeta potential that ranges from -50mV to -80mV for NaCl concentrations between 0.1 and 0.002M. Any residual contaminants are removed by three sequential centrifugation/decantation washings with ultra-pure distilled water.

Preparation of a dispersion for surface flocculation tests consists of mixing an aliquot of the cleaned dispersion, stock electrolyte solution (reagent grade NaCl), and ultra-pure water to arrive at the target salt and particle concentrations (Table 1).

Table 1. Experimental Conditions for Surface Flocculation Runs

Interfacial Dynamics Corporation latex 10-110-13
0.989μm diameter, Temperature = 22 C
[latex in sample] = 10ppm = 1.9×10^7 particles/cc

[NaCl] M	number of trials (ambient)	number of trials (humidified)	number of trials (total)
0	1	1	2
0.01	8	3	11
0.02	7	1	8
0.05	7	1	8
0.1	6	1	7
0.2	2	2	4

The salt solution and water are mixed first to avoid any local "hot" spots of concentrated electrolyte. Immediately after addition of the stock latex the sample is gently mixed and a drop is placed on the sample cell and loaded onto the microscope stage for observation. Elapsed time, or "interface age", is measured after the instant the drop is placed on the cell. Photographs are taken of the interface at regular intervals, usually about every five minutes. Once the surface becomes dominated by higher order aggregates (n>3) the situation is difficult to analyze and the experiment is terminated. This occurs fairly rapidly at high salt conditions (about 30 minutes), while for low salt conditions two hours is a more typical experiment duration.

In order to capture the faint darkfield images a special high-speed black and white film (TMAX 3200) is push processed to ASA 25,000. After development the negatives are loaded into a projector and the number of singlets, doublets, triplets, and other higher order aggregates are counted manually. In this manner a record of the aggregate evolution at the interface is obtained. A typical sequence of photomicrographs is presented in Figures 38-41 for the adsorption and flocculation of the standard 1μm colloid from.a 10ppm suspension in 0.05M NaCl.

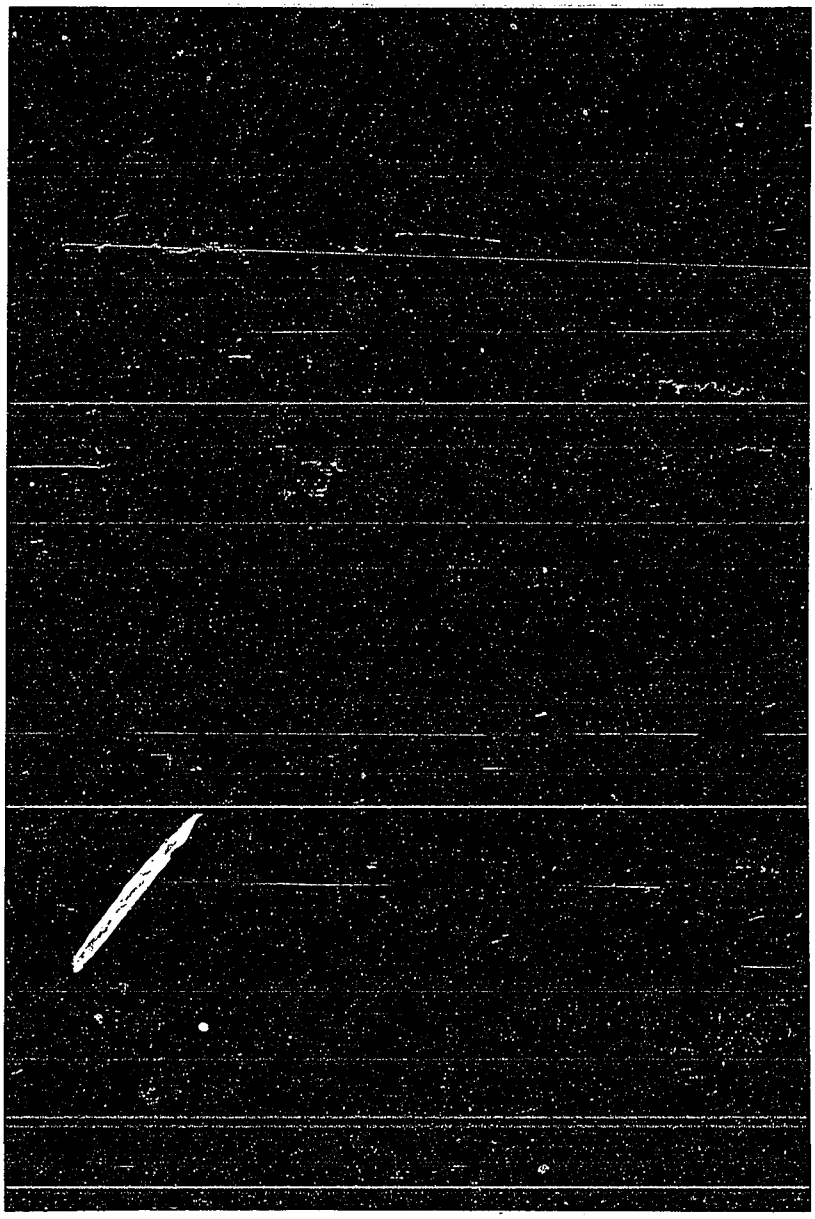

Figure 38. Evolution of Surface Aggregates, Interface Age = 0.22 hr.
700X linear magnification (1cm ≈ 14μm)

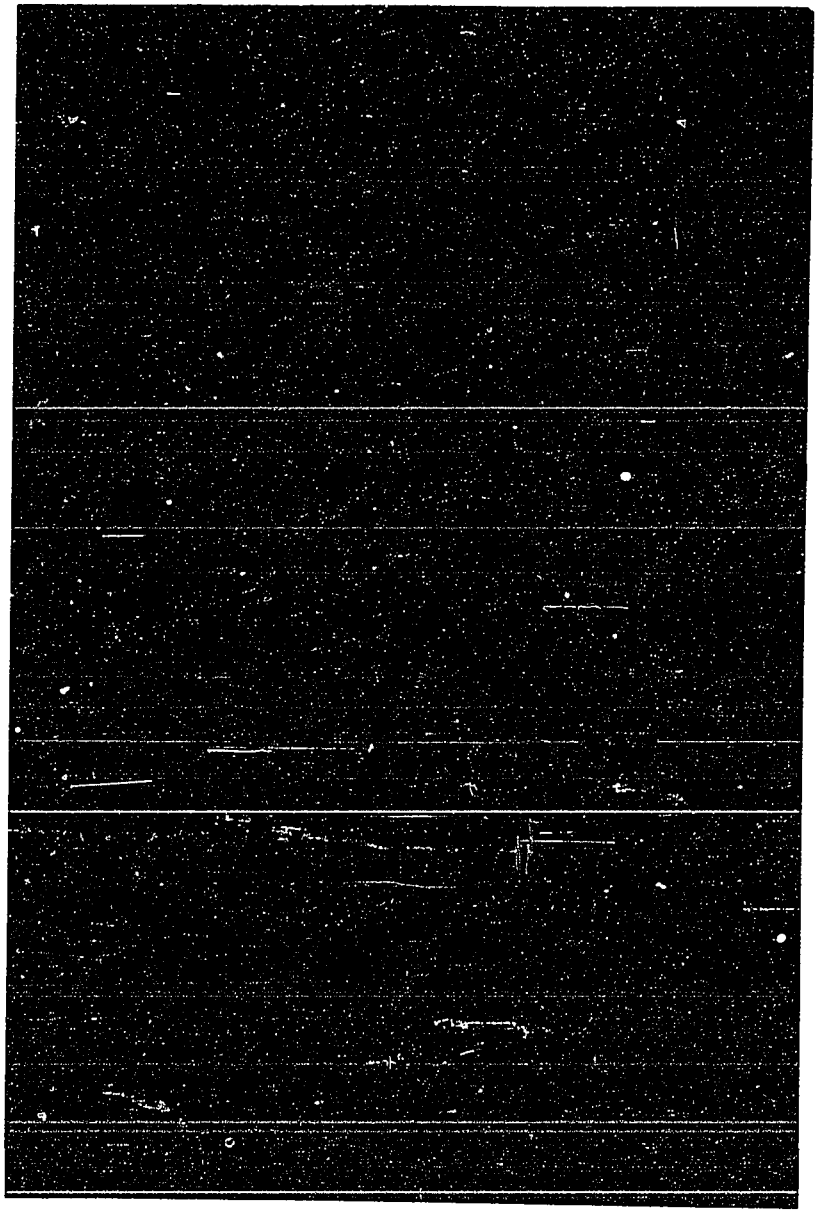

Figure 39. Evolution of Surface Aggregates, Interface Age = 0.58 hr.
700X linear magnification (1cm ≈ 14μm)

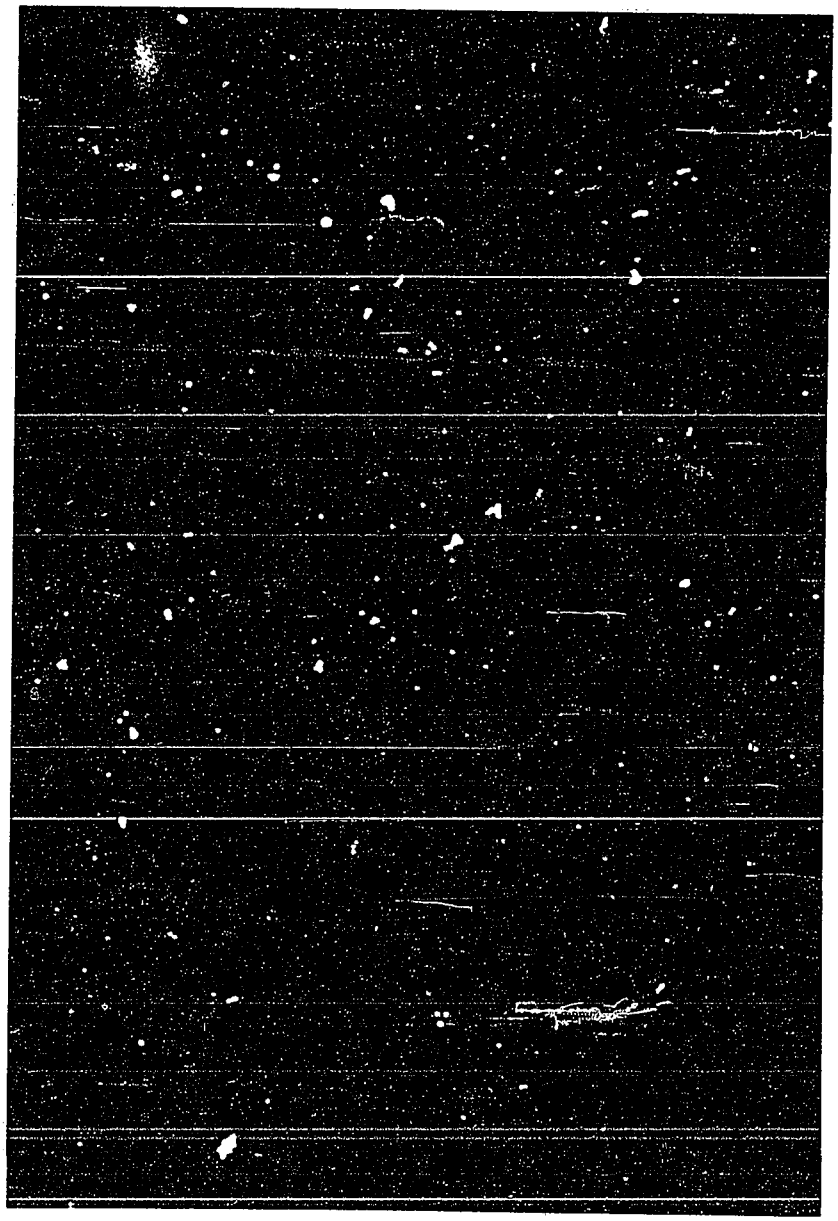

Figure 40. Evolution of Surface Aggregates, Interface Age = 1.6 hr.
700X linear magnification (1cm ≈ 14μm)

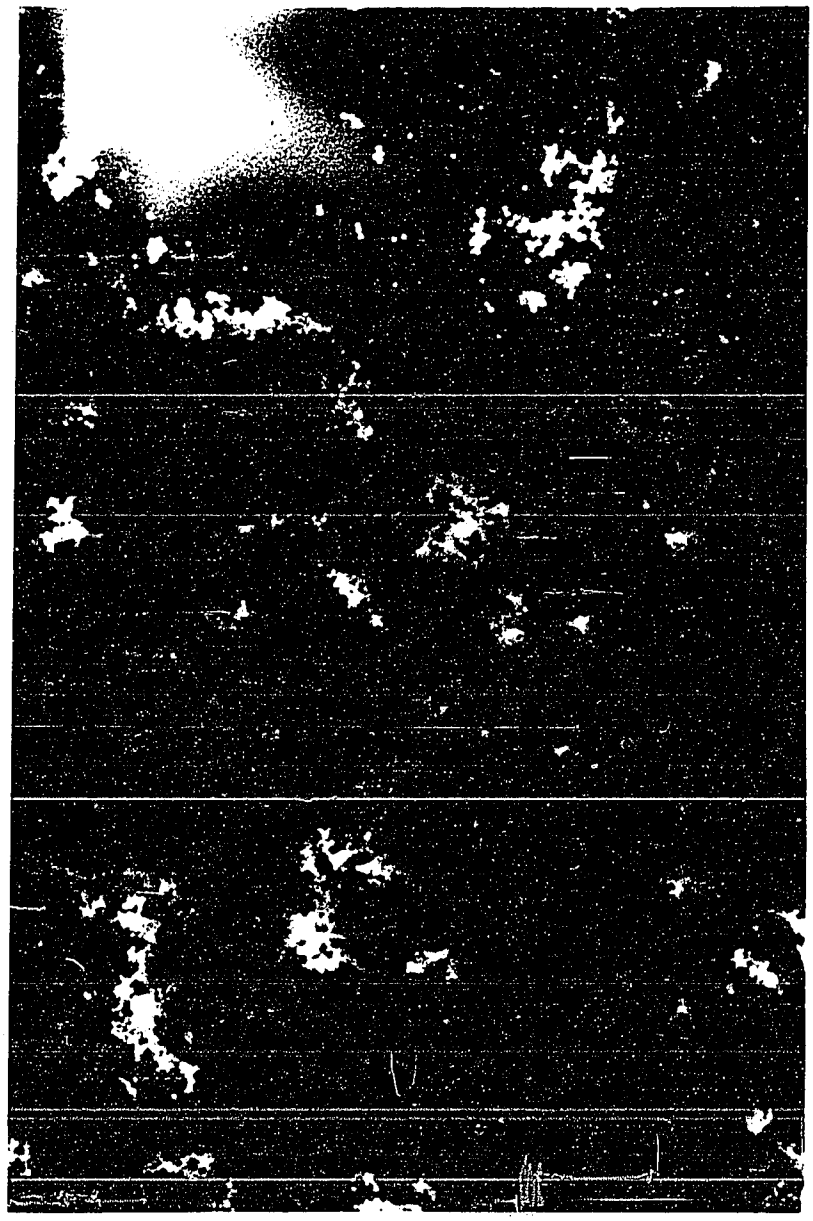

Figure 41. Evolution of Surface Aggregates, Interface Age = 18 hr.
700X linear magnification (1cm ≈ 14μm)

6. Experimental Results and Discussion

Both the experimental measurements and the models developed in Chapter 4 are concerned with the process of adsorption of colloids to the interface and the subsequent surface interaction that produces aggregates. The basic experimental results describe the evolution of the population of surface particles and surface aggregates. In order to apply the models of Chapter 4 an additional piece of information is needed: the interfacial particle position (i.e. %Immersion). This will be discussed in the context of contact angle measurements made on films derived from the experimental latex particles. The logical progression of subjects starts with (a) consideration of the adsorption of particles to the interface, followed by (b) estimation of the interfacial particle position based upon contact angle measurements, and concludes with (c) comparison of the actual flocculation rate data with our models of fast and slow flocculation.

6.1 Adsorption of Colloids to the Interface

The adsorption of particles to the interface serves as the source term for the subsequent surface aggregation events and is the natural starting point for the discussion. In Chapter 4 we considered the modelling of "ideal" diffusion-limited adsorption and the effect of potential energy interactions upon adsorption rates. Before comparing the experimental data to these models the basic nature of the experimentally determined adsorption flux needs to be examined. One of the primary goals of this examination is the identification of some regular adsorption behavior which can be used in the subsequent population balance modelling (i.e. source term identification).

The first impression that one gets from examining the experimental data is that there is a great deal of variability. This is emphasized in summary plots Figure 42 and Figure 43 and will be discussed in greater detail later.

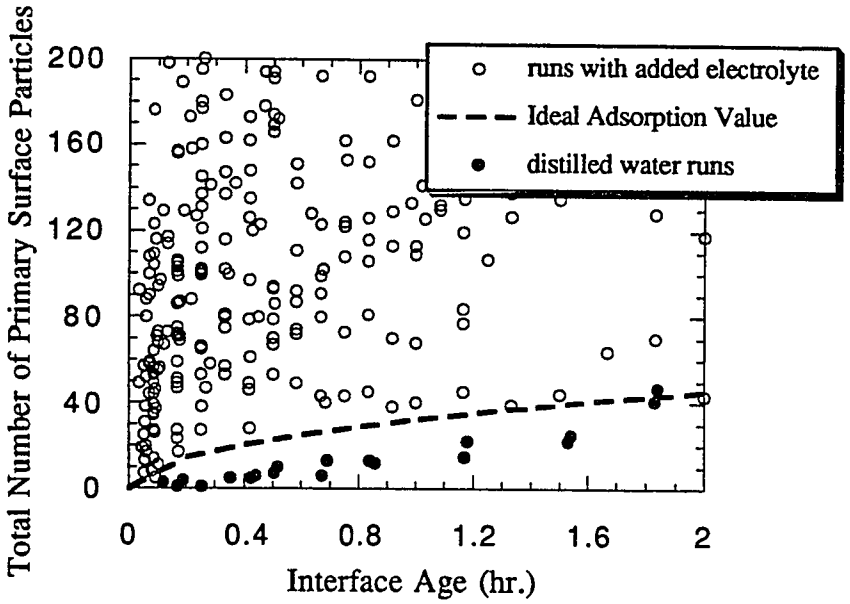

Figure 42. Evolution of Primary Particles at the Interface (Summary)

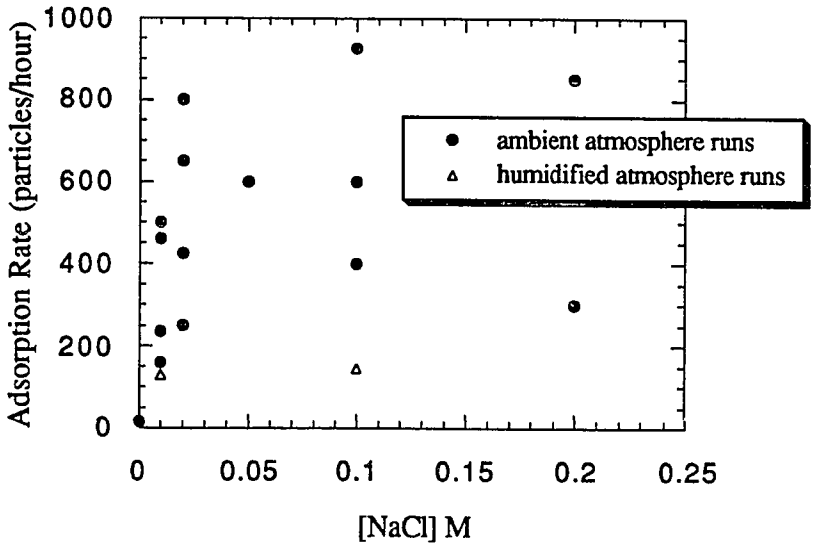

Figure 43. Summary of Initial Linear Adsorption Rates

However if one examines each trial independently it is usually possible to identify a nearly linear ("constant rate") adsorption regime. The period of this linear regime varies with both electrolyte concentration and adsorption rate as shown in the following figures:

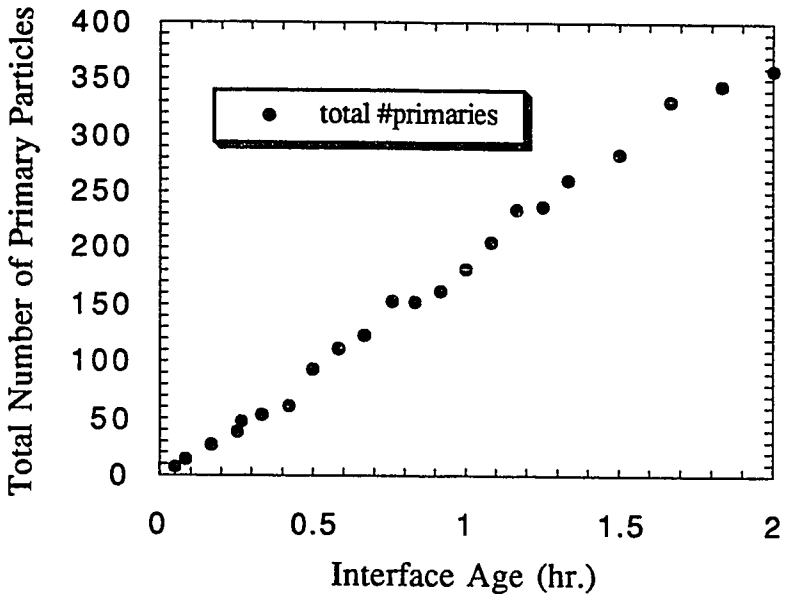

Figure 44. Primary Particle Evolution at the Interface, low salt (0.01M)

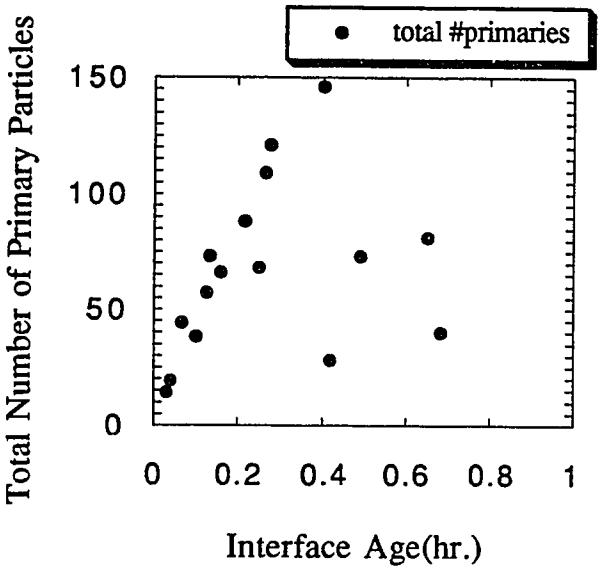

Figure 45. Primary Particle Evolution at the Interface, high salt (0.2M)

At low salt concentrations this linear regime is very extended, especially for runs which exhibit a low adsorption rate, while for high salt conditions the linear period is quite short. In both situations adsorption beyond the linear regime is quite irregular and is not amenable to accurate modelling.

Having accomplished the primary goal of identifying the source term for a particular run, we turn to consideration of the variability we see from run to run. Some variability is to be expected, being due to either the random effects associated with sampling a small field of view or the systematic effects associated with different electrolyte concentrations. However the variation in the linear adsorption rates displayed in Figure 43 is far beyond that expected from sampling effects and is exhibited even at identical salt concentrations. It is also evident from Figure 42 that except for the case of distilled water runs the adsorption of particles is far in excess of the ideal diffusion-limited calculation. Additionally the form of the adsorption data is linear with time in accordance with a constant rate convection model rather than being proportional to the

square root of time as predicted by the diffusion calculations. Another piece of evidence can be derived from the comparison of runs with ambient atmosphere and those with a humidified atmosphere (Figure 43). The suppressed rate of adsorption associated with a more saturated atmosphere is likely due to the reduced evaporation from the sample and further supports the role of convection in transport of particles to the surface. It should also be noted that these suppressed rates are still far in excess of the diffusion-limited predictions.

A final point for discussion with respect to adsorption concerns to the effect of added electrolyte. Because of the obscuring nature of variable convection influences it is difficult to make quantitative comparisons at each salt concentration. However the distinct nature of the distilled water runs (Figure 42) suggests that there is a significant energy barrier associated with adsorption to the interface at very low electrolyte concentrations. The electrolyte concentration in distilled water is at least 10^{-7}M due to the dissociation of water and is probably closer to 10^{-6}M due to the dissociation of dissolved CO_2 as carbonic acid. The fact that only distilled water runs clearly demonstrate an energy barrier to adsorption is in agreement with the potential energy predictions of Chapter 4, as displayed in Figure 46.

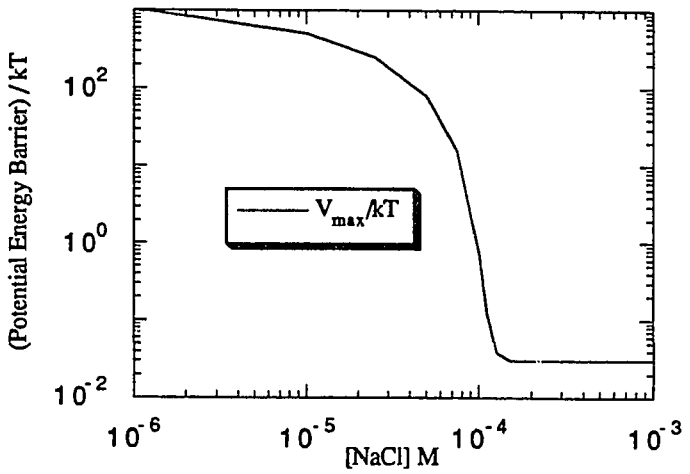

Figure 46. Potential Barrier to Adsorption vs. Electrolyte Concentration for standard 1μm colloid of this study.

6.2 Interfacial Particle Position

The models which predict the interfacial pair potential also govern our estimates of the collision efficiency, α, used in the population balance equations. The developments of Chapter 4 also demonstrated that the interfacial pair potential is primarily dependent upon the degree of particle immersion. In fact it is this dependence that is responsible for the phenomenon of surface flocculation at conditions of stability for particles dispersed in the bulk. It was also shown that the equilibrium position of the interfacial particles should be a simple function of the contact angle established at the air-water-particle contact line.

Some preliminary comments about the interpretation of contact angle measurements will help to clarify the meaning of the wetting measurements. While the equilibrium contact angle has a precise and unambiguous meaning; the actual contact angles we measure do not necessarily access this quantity. The advancing and receding contact angles are usually more readily measured and are reproducible for carefully prepared surfaces and liquids. The advancing contact angle is determined from measurements upon surfaces in which the liquid is advanced over a clean "dry" solid surface. The maximum angle observed before interline displacement corresponds to the advancing contact angle. As a liquid is withdrawn and the interline recedes a corresponding minimum angle is observed and identified as the receding contact angle. The equilibrium value lies somewhere between the two extremes. Note that the static contact angle often measured is generally not precisely reproducible and does not correspond to the equilibrium value because of potential energy wells and barriers associated with interline displacement on physically and chemically heterogeneous solid surfaces.

Results from goniometric measurements of contact angles (Rame-Hart Contact Angle Goniometer model no. 100-00-115) on dried films of standard latex particles are summarized in Table 2. It is clear from these values that the equilibrium particle position is in the neighborhood of 40% linear immersion in the water phase. The actual distribution of particle positions may exhibit more variation due to particle heterogeneity and the fact that the equilibrium particle position may take a considerable time to

establish. Therefore it seems reasonable to consider 40% linear immersion as the upper limit on the degree to which particles are de-wet.

Table 2. Measured Contact Angles on Latex Films and Corresponding Particle Positions

	Advancing	Receding	Static	Equilibrium (estimated)
θ, contact angle	120	85	100 - 108	102.5
ϕ, wetted semi-arc	80	95	80 - 72	77.5
%Immersion (linear)	23%	54%	41.3 - 34.5%	40%
%Immersion (volume)	15.6%	56%	37.1 - 27.5%	34%

6.3 Surface Flocculation Kinetics

For a variety of reasons the primary focus of this discussion will be on doublet formation rates during the early period of surface flocculation. The most obvious reasons for narrowing our focus to this area derives from the modelling work. In theory the population balance equations allow calculation of the complete evolution of aggregates at the surface; however the truncation of the rigorous equations to a manageable number of terms limits the accuracy of the solution to some initial period of time. One measure of this accuracy is the degree to which the inventory of primary particles at the surface, as calculated by the population balance equations, agrees with the inventory based upon the flux to the surface given by the adsorption term (Figure 47).

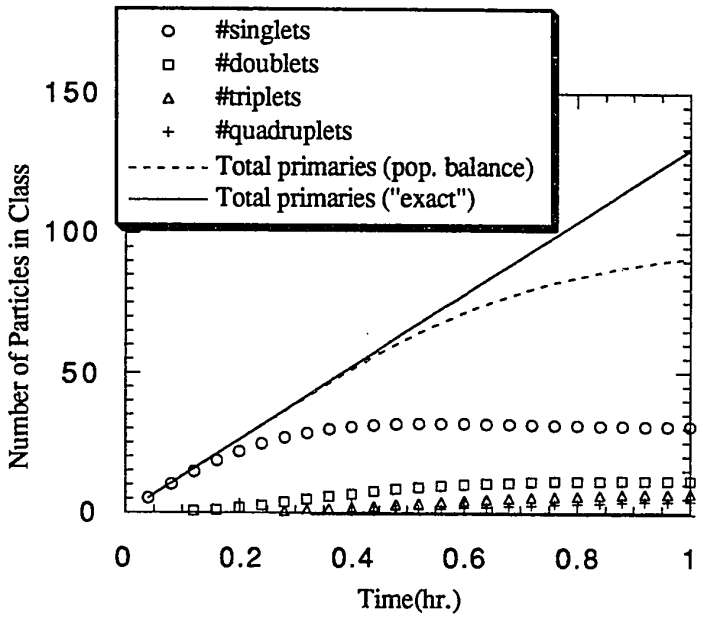

Figure 47. Comparison of Surface Particle Inventory as a Measure of Population Balance Equation Accuracy (equation{42}),Fast Flocculation, Adsorption Rate = 130/hr.

Another modelling factor which contributes to the difficulty of predicting the formation of higher order surface aggregates (n>2) is the uncertainty associated with modelling the collision efficiencies (i.e. pair potentials) between larger surface flocs. Modelling the interaction between aggregates is much more complex than that between singlets. For the case of fast flocculation we can assume $a_{ij} = 1$, but for slow flocculation we can only bracket the situation by assuming: $1 \geq a_{ij} \geq a_{11}$ (i.e. we assume greater net attraction between larger floccs). Throughout this study it was found that the form of the aggregate evolution was more consistent with setting the higher order collision efficiencies equal to unity.

Experimental factors also suggest that we concentrate upon the doublet formation at early times. Earlier it was demonstrated that the adsorption flux could be accurately estimated only during an initial period. During this initial period only the doublet

concentration grows to the statistically significant numbers that justify comparison with model calculations.

The following examination of doublet formation rates will be considered with respect to: (a) fast surface flocculation calculations, (b) slow surface flocculation calculations, and (c) the transitions from stability to slow flocculation and from slow flocculation to fast flocculation. Since both the electrolyte and the adsorption rate vary for any given run every trial must be considered independently and compared with the appropriate model calculation. Doublet evolution and model calculations are displayed in ascending salt concentration and in increasing adsorption rate for a particular salt concentration in the following figures (Figures 48 to 64).

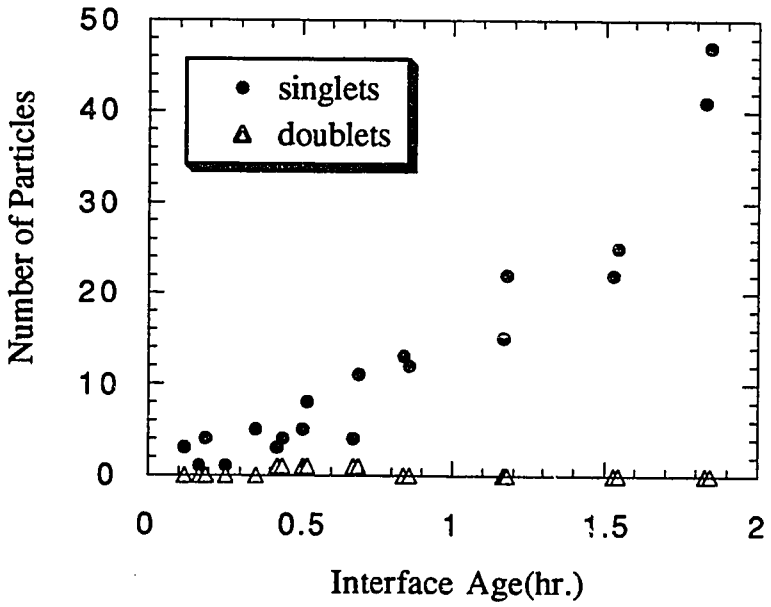

Figure 48. Experimental Particle Evolution distilled water, 16 particles/hr.adsorption rate

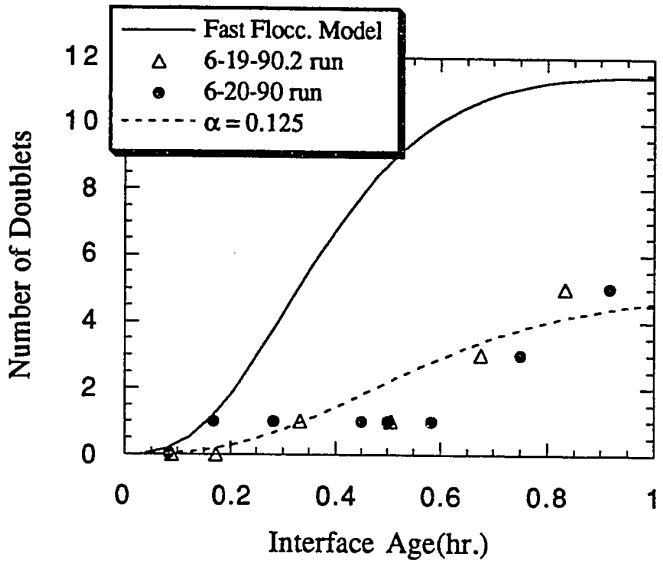

Figure 49. Doublet Evolution (0.01M NaCl, 130 particles/hr.)

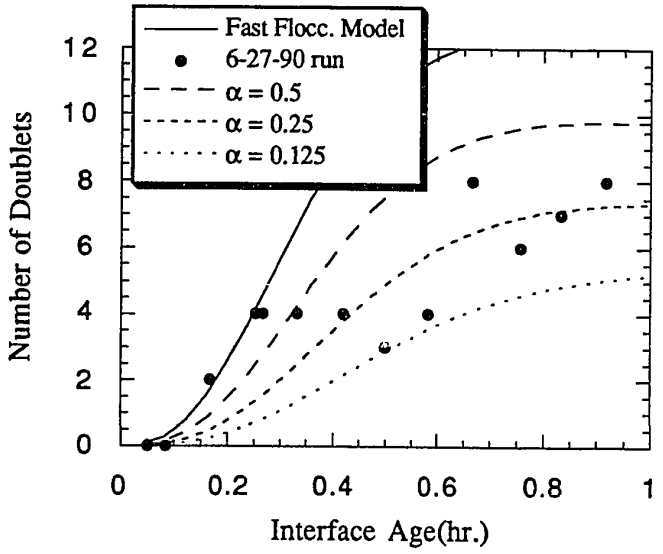

Figure 50. Doublet Evolution (0.01M NaCl, 160 particles/hr.)

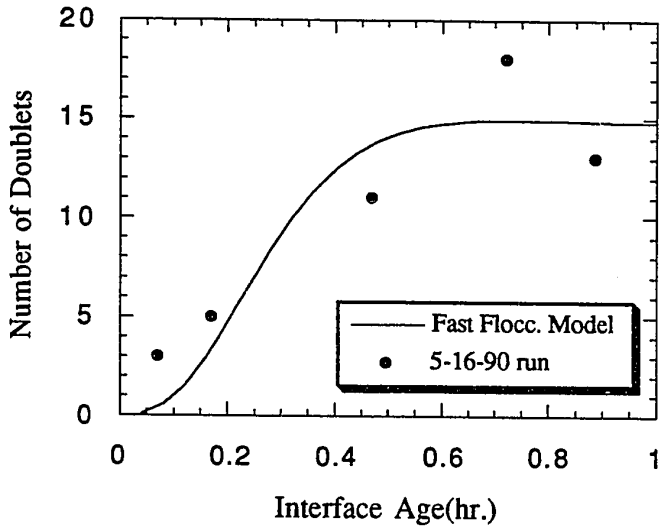

Figure 51. Doublet Evclution (0.01M NaCl, 235 particles/hr.)

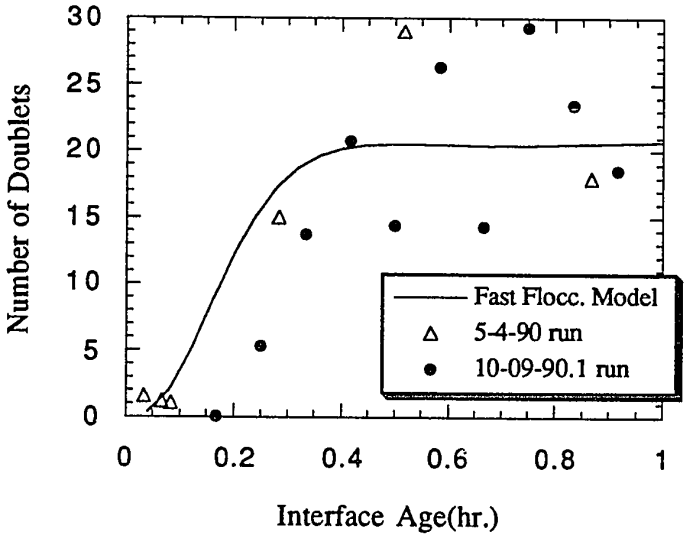

Figure 52. Doublet Evolution (0.01M NaCl, 475 particles/hr.)

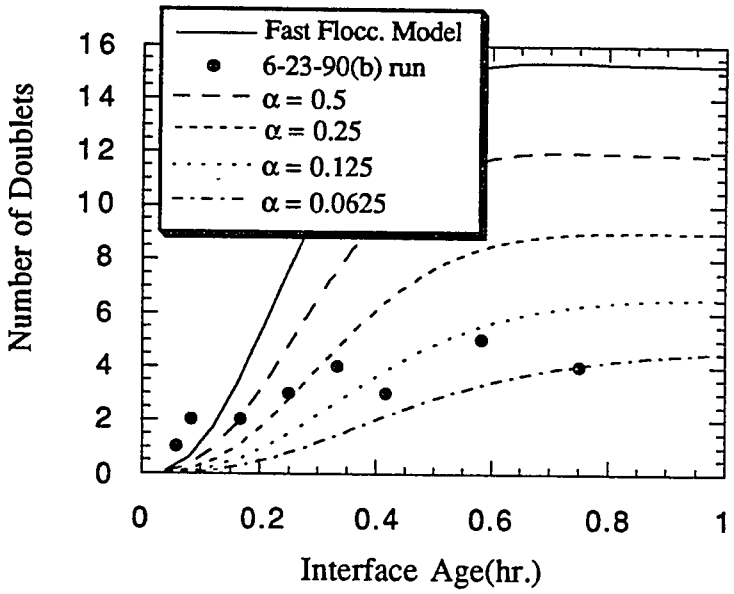

Figure 53. Doublet Evolution (0.02M NaCl, 250 particles/hr.)

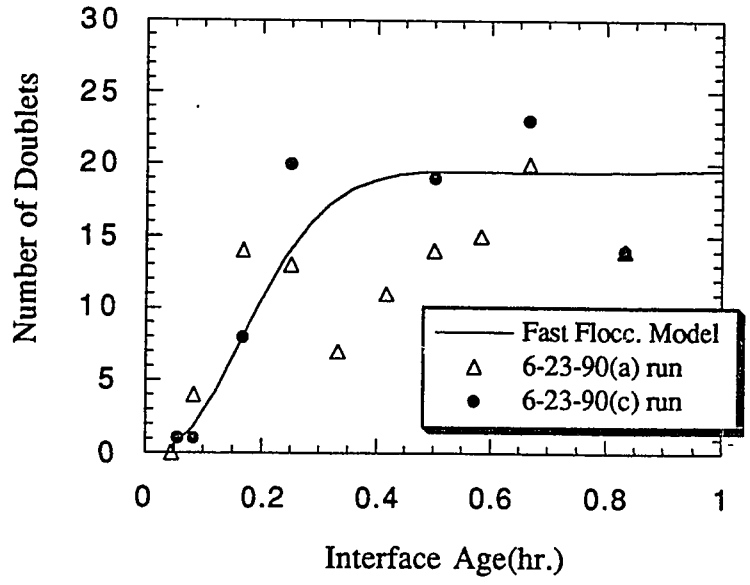

Figure 54. Doublet Evolution (0.02M NaCl, 425 particles/hr.)

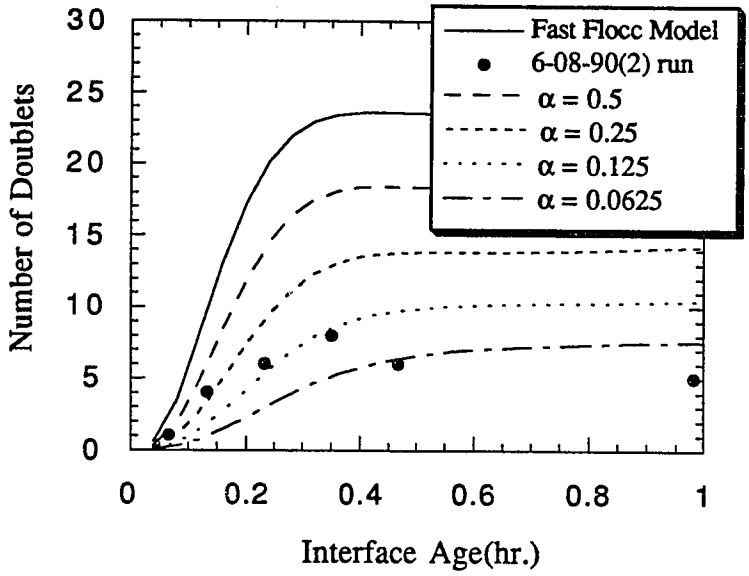

Figure 55. Doublet Evolution (0.02M NaCl, 650 particles/hr.)

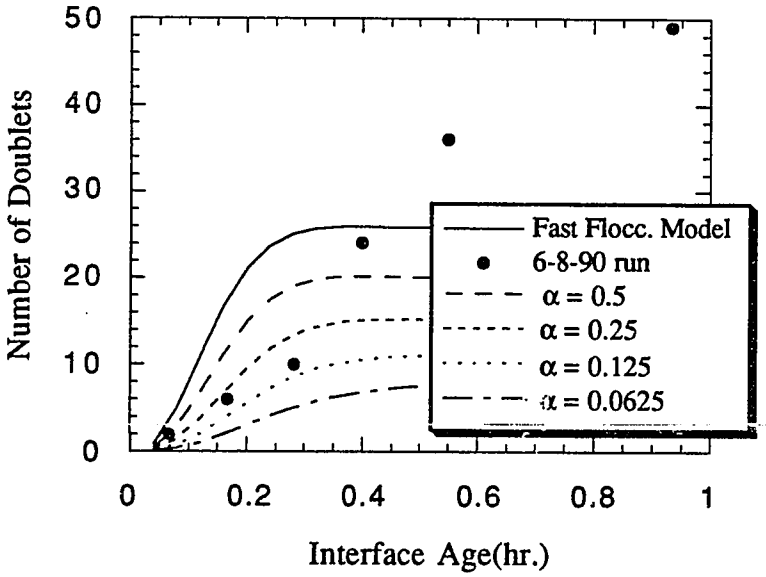

Figure 56. Doublet Evolution(0.02M NaCl, 800 particles/hr.)

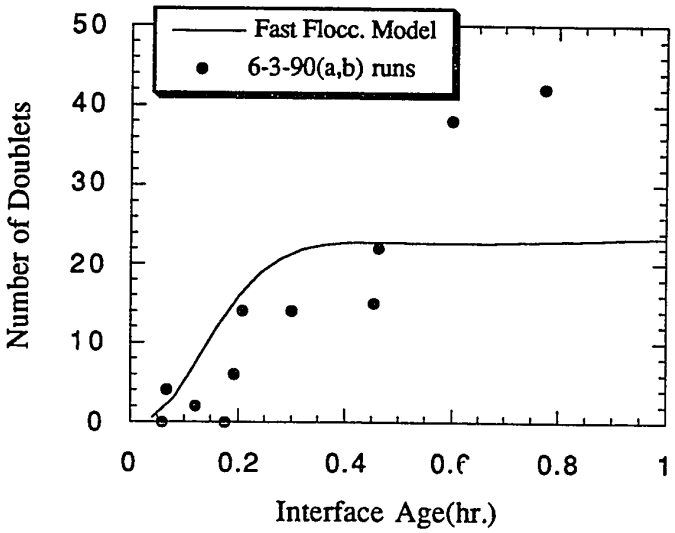

Figure 57. Doublet Evolution (0.05M NaCl, 600 particles/hr.)

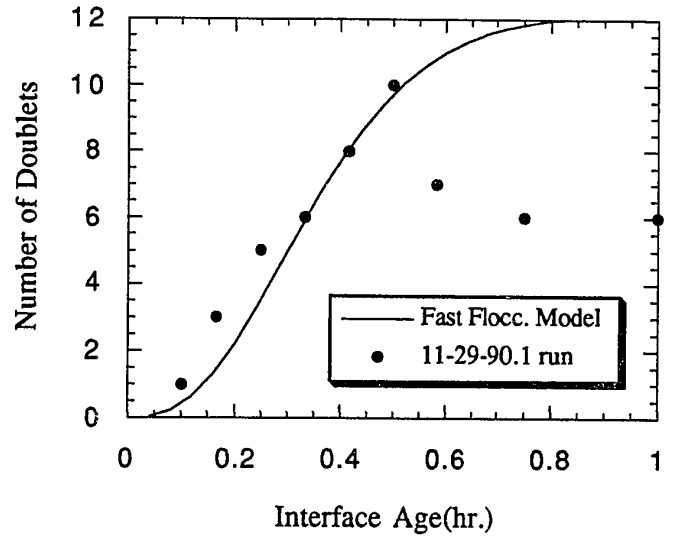

Figure 58. Doublet Evolution (0.1M NaCl, 146 particles/hr.)

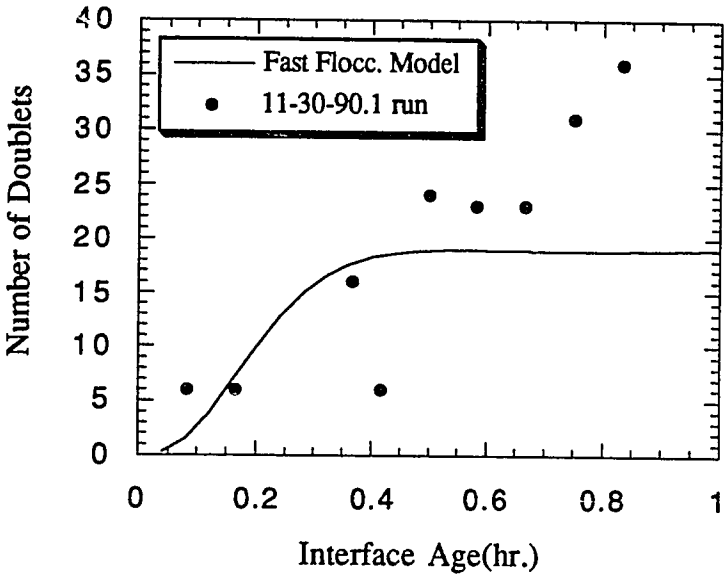

Figure 59. Doublet Evolution (0.1M NaCl, 400 particles/hr.)

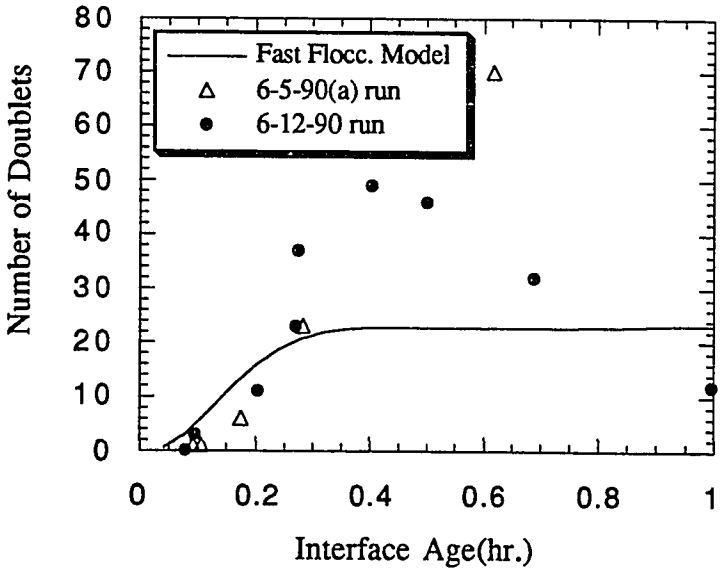

Figure 60. Doublet Evolution (0.1M NaCl, 600 particles/hr.)

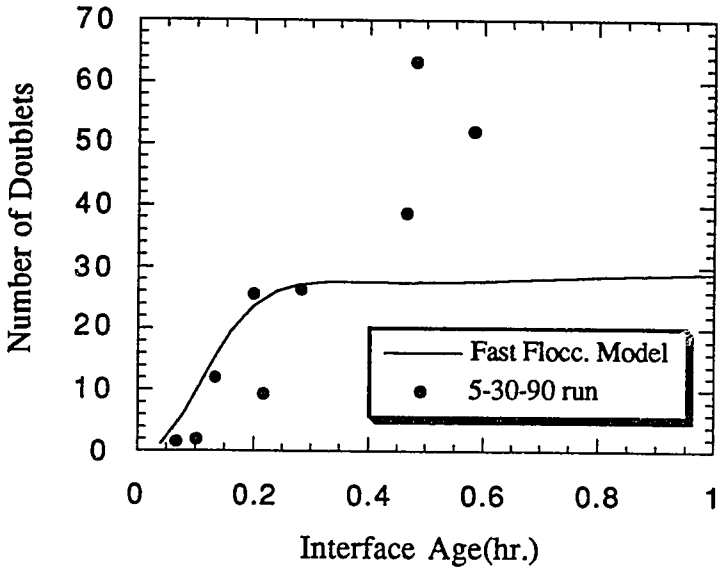

Figure 61. Doublet Evolution (0.1M NaCl, 925 particles/hr.)

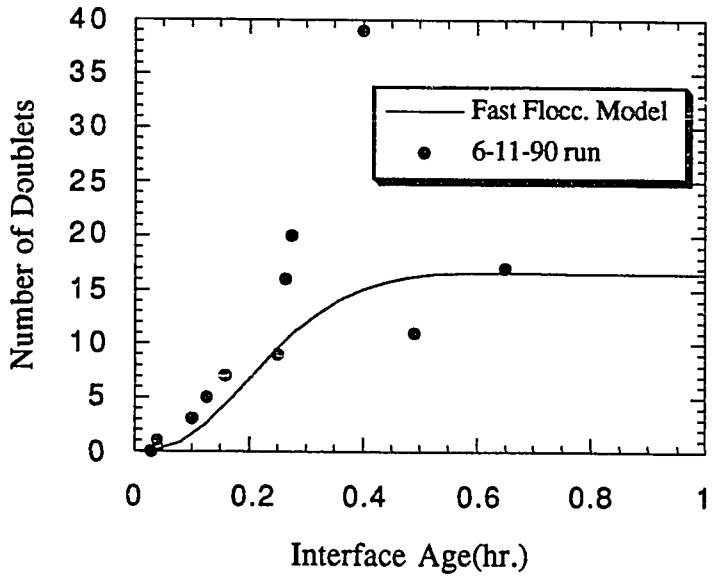

Figure 62. Doublet Evolution (0.2M NaCl, 300 particles/hr.)

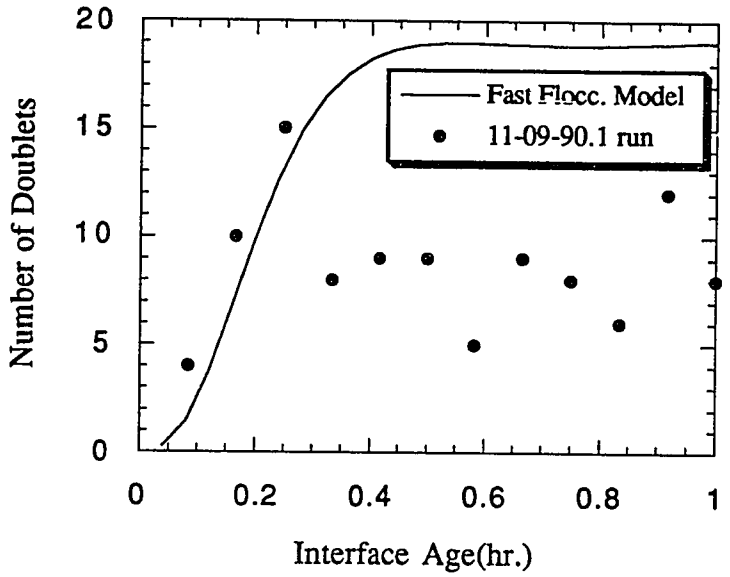

Figure 63. Doublet Evolution (0.2M NaCl, 400 particles/hr.)

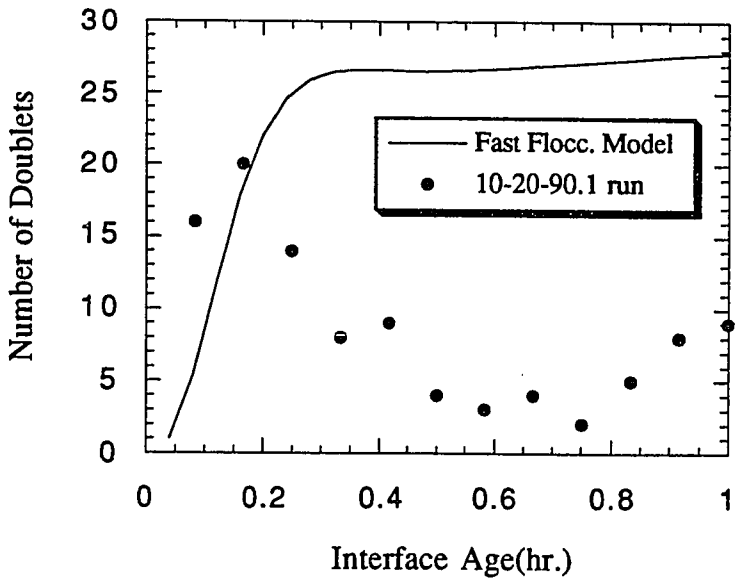

Figure 64. Doublet Evolution (0.2M NaCl, 850 particles/hr.)

The electrolyte content spans the range from distilled water to 0.2M NaCl and adsorption rates vary from 16 particles/hour (distilled water) to 925 particles/hour (0.1M NaCl). Surface doublets in distilled water are almost non-existent, corresponding to substantial stability at the interface. At 0.01M and 0.02M NaCl most of the low adsorption rate (<300 particles/hour) trials show evidence of doublet formation substantially below the fast flocculation limit. For salt concentrations of 0.1M and above the doublet evolution conforms quite closely to fast flocculation predictions. Note that the results are generally more regular and conclusive at the lower adsorption rates, which corresponds to conditions of diminished convection of particles to the surface. The situation of 0.05M NaCl is a borderline case and is difficult to place in either the slow or fast flocculation regime.

At the lower salt concentrations (0.01M and 0.02M NaCl) it is possible to use slow flocculation models to predict the doublet evolution rates based upon calculated collision efficiencies and compare this to fitted values of α in the preceding figures. The fitted and predicted values of α are compared in the following table:

Table 3. Comparison of Collision Efficiencies from Fitted Values and from Potential Energy Calculations at Various Degrees of Immersion

[NaCl] M	Adsorption Rate	$\alpha_{experiment}$	α_{model} (40%)	α_{model} (45%)	α_{model} (50%)	α_{model} (55%)	α_{model} (100%)
0	16	0	0	0	0	0	0
0.01	130,160	.125-.25	1.0	1.0	.975	.93	.175
0.02	475,800	.125-.25	1.0	1.0	1.0	.99	.375
0.10	146-600	1.0	1.0	1.0	1.0	1.0	1.0
0.20	300-850	1.0	1.0	1.0	1.0	1.0	1.0

The experimental α's don't clearly correspond to any particular degree of immersion, but correspond most closely to the 100% immersion case.

Another way to examine the collision efficiency predictions is to see (graphically) if they are consistent with the observed transitions from stability (low salt) to slow flocculation (moderate salt) and from slow to fast flocculation (high salt). Before

proceeding with the graphical comparisons I should introduce another useful benchmark for comparing predicted collision efficiencies. The 100% immersion values shown above are based upon a two-dimensional kinetic theory of aggregation (section 4.3.2), which yield different results than Marmur's kinetic theory for aggregation in the bulk. It is useful to include these bulk stability predictions in our comparisons as an extreme case. Figure 65 demonstrates that the two-dimensional model predicts an enhanced secondary minimum coagulation and a diminished primary maximum coagulation; in accord with the decreased kinetic energy (at the surface) available for surmounting energy barriers or escaping potential wells.

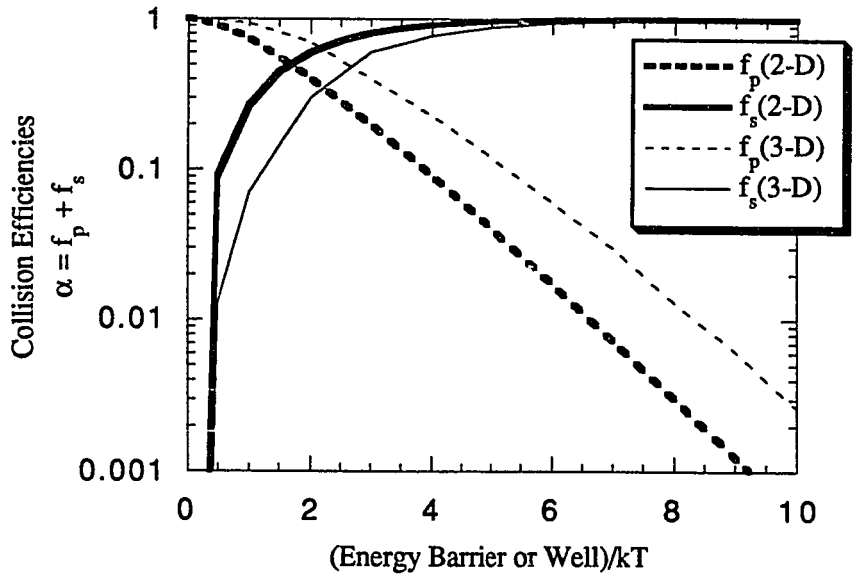

Figure 65. Comparison of Two-Dimensional and Three-Dimensional Kinetic Theories Aggregation

The crucial parameters in any theory of slow flocculation are the heights and depths of potential barriers and wells. The variation of these elements with respect to interfacial position and electrolyte concentration was calculated based upon the models developed in Chapter 4 and is displayed in Figures 66 and 67. As expected, well depths

increase and barrier heights decrease with decreasing particle immersion; both predictions leading to diminished stability at the interface. At low degrees of immersion the barrier height is the controlling factor and the transition from stability to fast flocculation is expected over a narrow range of salt concentrations; while for high degrees of immersion flocculation into a potential well provides for a broader transition from stability to fast flocculation. These effects are quite apparent in the predictions of overall collision efficiency as a function of salt concentration shown in Figure 68.

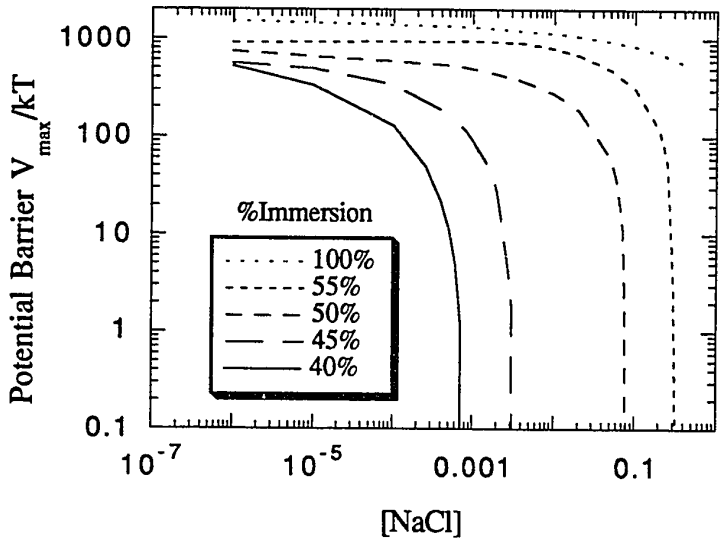

Figure 66. Potential Barrier to Aggregation at the Surface for 1μm standard colloid of this study

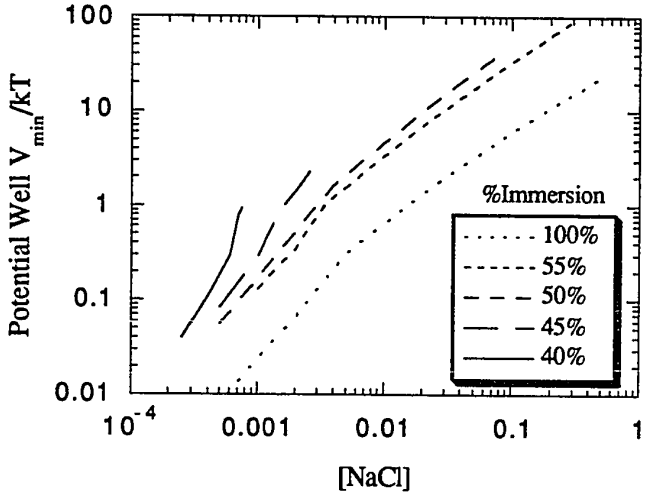

Figure 67 Potential Energy Well Leading to Surface Aggregation for 1μm standard colloid of this study.

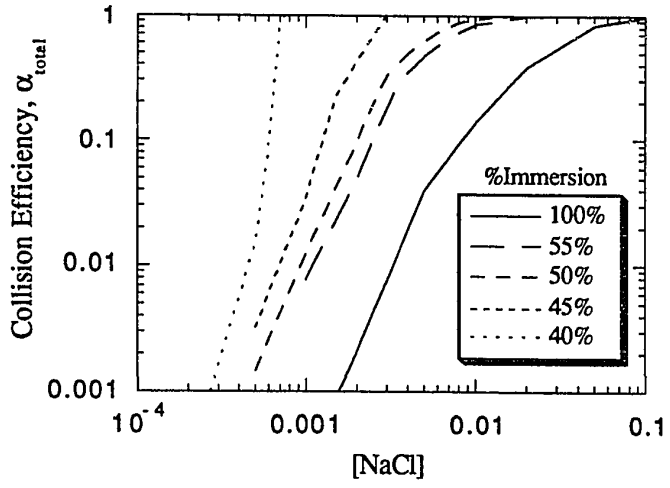

Figure 68. Predicted Overall Collision Efficiencies based upon the 2-D Kinetic Theory Model

It is instructive to narrow the focus a bit by considering only degrees of immersion greater than 50% and overlaying the most reliable data for intermediate values of α ($\alpha \neq 0,1$). For completely immersed colloids (Figure 69.) we see that the two-dimensional kinetic model predicts higher collision efficiencies than the corresponding bulk model. This is indicative of reversible aggregation into a shallow minimum over a wide range of salt concentrations. The data overlay is somewhat ambiguous and does not point directly to a particular mode or precise degree of immersion. This uncertainty derives from both the scatter in the data and the considerable sensitivity of model predictions to the assumed degree of particle immersion. One can also imagine that the particles do not necessarily assume a specific position based upon the average equilibrium contact angle, and a distribution of interfacial positions is quite likely. However it is clear that substantial de-wetting is not necessary to explain the aggregation kinetics observed. It is also worthwhile noting that just the confinement of particles to a two-dimensional geometry can provide for a substantial destabilization.

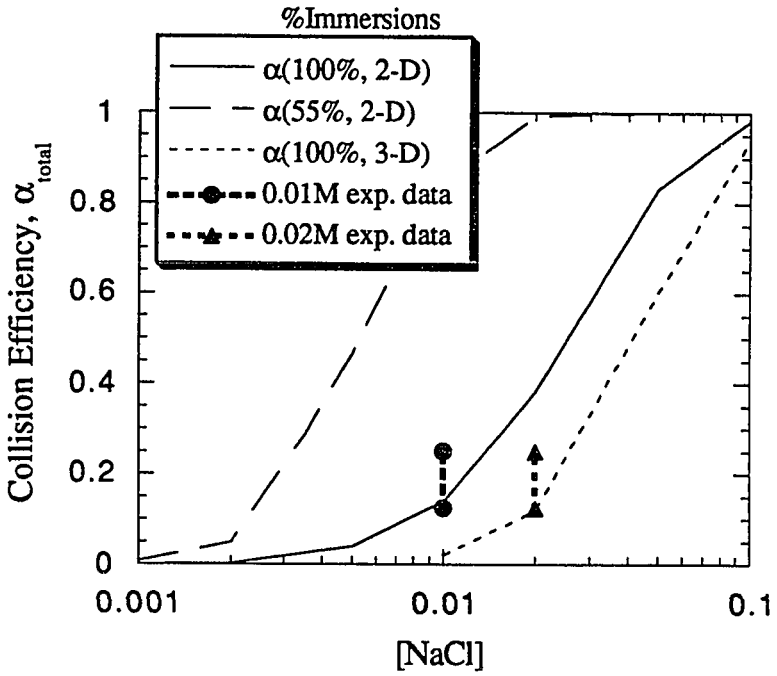

Figure 69. Predicted and Experimental Collision Efficiencies

There is, however, an alternate explanation for the apparent high degree of immersion. Implicit in the previous discussions is the assumption of a contact-line which separates a "wet" (ionized) submerged surface from a dry (unionized) surface. It is also possible, especially for hydrophilic particles(60), that this contact-line is established with a thin wetting-film which adheres to the protruding surface of the particle.

Figure 70. Geometry for Consideration of Thin Wetting-Films on Hydrophilic Particles

These coating films are typically thick enough to allow development of the diffuse double-layer. At extended separations these particles exhibit the enhanced attraction associated with partially immersed spheres (section 4.2), but upon close approach a shared meniscus provides for an interaction which approaches that corresponding to two fully immersed spheres (Figure 70.). Modelling of this effect requires careful solution of the equations of capillary hydrostatics and is beyond the scope of this investigation. It is expected, however, that this effect is not important for the hydrophobic particles used in this study.

The conclusion that we don't require low degrees of particle immersion to explain our surface flocculation observations certainly requires some discussion. This conclusion argues against the basic premise that the interface serves as a locus of instability as a result of a modified interparticle pair potential. The concentration of colloids at the surface due to adsorption and their diminished "kinetic" stability can lead to enhanced surface aggregation for reasons unrelated to pair potential considerations. However this assertion also requires some scrutiny in light of previous observations of both dilute *and* concentrated dispersions. We should expect the disparity between the surface and bulk aggregation modes due to the concentrating effect of adsorption to be most pronounced for dilute dispersions. The majority of experimental studies, including this investigation, have been concerned with the surface aggregation of dilute (< 0.1% by volume) dispersions. Only the study by Lowry focussed upon the surface coagulation of concentrated(35% by volume) colloidal dispersions. In Lowry's study the air-liquid interface was *also* found to be the critical locus of instability. In this instance one cannot

ascribe the marked destabilization due to the renewal of the air-liquid interface to the concentrating effect of adsorption or purely kinetic factors. So while the pair potential models developed in Chapter 4 do not explain the enhanced surface aggregation observed in this particular study; it is likely that these effects are important for other systems which have been studied.

7. Conclusions

The major conclusions of this study address questions about the basic mechanism that controls the aggregation of colloids at the air-water interface. The preceding modelling and experiments support the following points:

1. At high salt concentrations (>0.1M NaCl in this study) colloids exhibit a limiting "fast" flocculation rate which is accurately predicted by our two-dimensional diffusion-limited aggregation model. These predictions serve as an important benchmark for judging the importance of potential barriers and wells in influencing the rate of surface aggregation.

2. At moderate salt concentrations (0.01 - 0.1M NaCl in this study) the "slow" flocculation observed does not require a modified pair potential (i.e. collision efficiency) at the interface in order to explain the population balance predictions. In this case the enhancement in flocculation at the surface with respect to the bulk can be accounted for by the concentration of colloids at the interface by "adsorption" and the subsequent increase in the collision frequency. Other studies with dense dispersions and spread particle monolayers do indicate that an increased "interfacial" collision efficiency, as predicted by the potential energy models, does exist for particles which are substantially de-wet. This seeming conflict reflects the importance of the interfacial particle position in determining the mode of aggregation at the surface.

3. The adsorption of particles to the interface is driven by the hydrophobicity of the colloid surface and can be diminished at low salt concentrations due to a long-ranged electrostatic repulsion.

8. List of References

1. Lowry, V., El-Aasser, M. S., Vanderhoff, J. W., Klein, A. and Silebi, C. A., "Kinetics of Agitation-Induced Coagulation of High-Solid Latexes", *Journal of Colloid and Interface Science* **112**, p. 521 (1986).

2. Pugh, R. J. and Nishkov, I.,"Selective bubble-particle detachment forces and flotation for the galena/quartz system", *in* Processing of Complex Ores, Ed.), p. 87, (1990).

3. Long, J. T., Engineering for Nuclear Fuel Reprocessing, Gordon and Breach Science Publishing Inc., p. 586, New York, (1967).

4. Pickering, S. U., "Emulsions", *Journal of the Chemical Society (London)* **91**, p. 2001 (1907).

5. Kitchener, J. A. and Musselwhite, P. R.,"Theory of Stability of Emulsions", *in* Emulsion Science, (P. Sherman, Ed.), p. 496, Academic Press, London, (1968).

6. Wasan, D. T. and Krantz, W. B. (Ed.), Interfacial Phenomena in the New and Emerging Technologies(Workshop Proceedings, May 29-31, 1986), HITEX Publications, p. 254, New York, (1987).

7. Hunter, R. J., Foundations of Colloid Science (volume 1), Clarendon Press/ Oxfork University Press, p. 512, New York, (1987).

8. Heller, W.,"Mechanical and Surface Coagulation", *in* Colloidal Solutions and Micellar Behavior (ACS Symposium Series #9), (K. Mittal, Ed.), p. 40, (1975).

9. Doroszkowski, A. and Lambourne, L., "Measurement of the Strength of Steric Barriers in Non-Aqueous Polymer Dispersions", *Journal of Polymer Science C* **34**, p. 253 (1971).

10. Doroszkowski, A. and Lambourne, L., "The Measurement of the Dependence of the Strength of Steric Barriers on Their Solvent Environment", *Journal of Colloid and Interface Science* **43**, p. 97 (1973).

11. Garvey, M. J., "Compression Studies on a Monolayer of Polymer Stabilized Latices at the Air/2 Molar Sodium Chloride Sodium Interface", *Colloid and Polymer Science* **257**, p. 70 (1979).

12. Kawaguchi, M., "Monolayer Studies on Adsorbed Layer Thickness of Polyvinylpyrrolidone on Polystyrene Latices and Steric Stabilization Free Energy", *Polymer Journal* **13**, p. 783 (1981).

13. Pieranski, P., "Two-Dimensional Interfacial Colloidal Crystals", *Physical Review Letters* **45**, p. 569 (1980).

14. Goodwin, J. W., Ottewill, R. H. and Parentlich, A., "Optical Examination of Structured Colloidal Dispersions", *Journal of Physical Chemistry* **84**, p. 1580 (1980).

15. Freundlich, H. and Basu, S. K., *Zeitschrift fur Physikalische Chemie (Leipzig)* **115**, p. 203 (1925).

16. Freundlich, H. and Kroch, H., "The Mechanical Coagulation of Copper Oxide Sol", *Zeitschrift fur Physikalische Chemie (Leipzig)* **124**, p. 115 (1926).

17. Freundlich, H. and Loebmann, S., "The Mechanical Coagulation of Goethite Sol", *Kolloid Beihefte* **28**, p. 391 (1931).

18. Freundlich, H. and v. Rechlinghausen, R., "Kinetics of Coagulation at Boundary Surfaces", *Zeitschrift fur Physikalische Chemie (Leipzig)* **A157**, p. 325 (1931).

19. Zsigmondy, R., *Zeitschrift für Elektrochemie* **22**, p. 202 (1916).

20. Heller, W. and Peters, J., "Mechanical and Surface Coagulation: I. Surface Coagulation of α-FeOOH Sols", *Journal of Colloid and Interface Science* **32**, p. 592 (1970).

21. Peters, J. and Heller, W., "Mechanical and Surface Coagulation: II. Coagulation by Stirring of α-FeOOH Sols", *Journal of Colloid and Interface Science* **33**, p. 578 (1970).

22. Heller, W. and deLauder, W. B., "Mechanical and Surface Coagulation: III. Promotion of Mechanical Coagulation by Addition of Destabilizing Electrolyte", *Journal of Colloid and Interface Science* **35**, p. 60 (1971).

23. Heller, W. and Peters, J., "Mechanical and Surface Coagulation: IV. Prevention of Mechanical Coagulation by Surface Active Additives", *Journal of Colloid and Interface Science* **35**, p. 300 (1971).

24. DeLauder, W. B. and Heller, W., "Mechanical and Surface Coagulation: V. The Role of the Solid -Liquid Interface and of Turbulence in Mechanical Coagulation.", *Journal of Colloid and Interface Science* **35**, p. 308 (1971).

25. Diop, S., Heller, W. and Kalousdian, S., "Mechanical and Surface Coagulation: VI. Differential Surface Coagulation in Two-Component Colloidal Solutions", *Journal of Colloid and Interface Science* **70**, p. 328 (1979).

26. Onoda, G. Y., "Direct Observation of Two-Dimensional, Dynamical Clustering and Ordering with Colloids", *Physical Review Letters* **55**, p. 226 (1985).

27. Mahanty, J. and Ninham, B. W., Dispersion Forces, Academic Press, p. 236, New York, (1976).

28. Osmond, D. W. J. and Waite, F. A.,"The Theoretical Basis for the Steric Stabilization of Polymer Dispersions Prepared in Organic Media", *in* Dispersion Polymerization in Organic Media, (K. E. J. Barrett, Ed.), p. 11, (1974).

29. Clayfield, E. J., Lumb, E. C. and Mackey, P. H., "Retarded Dispersion Forces in Colloidal Particles- Exact Integration of the Casimir and Polder Equation", *Journal of Colloid and Interface Science* **37**, p. 382 (1971).

30. Gregory, J., "Approximate Expressions for Retarded van der Waals Interaction", *Journal of Colloid and Interface Science* **83**, p. 138 (1981).

31. Read, A. D. and Kitchener, J. A., "Wetting Films on Silica", *Journal of Colloid and Interface Science* **30**, p. 394 (1969).

32. Langmuir, I., "The Role of Attractive and Repulsive Forces in the Formation of Tactoids, Thixotropic Gels, Protein Crystals and Coacervates", *Journal of Chemical Physics* **6**, p. 873 (1938).

33. Reerink, H. and Overbeek, J. T. G., "The Rate of Coagulation as a Measure of the Stability of Silver Iodide Sols", *Discussions of the Faraday Society* **18**, p. 74 (1954).

34. Deryaguin, B. V. and Churaev, N. V.,"Properties of Water Layers Adjacent to Interfaces", *in* Fluid Interfacial Phenomena, (C. A. Croxton, Ed.), p. 663, (1986).

35. Christenson, H. K., "Non-DLVO Forces between Surfaces-Solvation, Hydration and Capillary Effects", *Journal of Dispersion Science and Technology* **9**, p. 171 (1988).

36. Christenson, H. K. and Claesson, P. M., "Cavitation and the Interaction between Macroscopic Hydrophobic Surfaces", *Science* **239**, p. 390 (1988).

37. Ralston, J., "Thin Films and Froth Flotation", *Advances in Colloid and Interface Science* **19**, p. 21 (1983).

38. Richmond, P., "Some Fundamental Concepts in Flotation", *Chemistry and Industry* **1**, p. 792 (1977).

39. Scheludko, A., Toshev, B. V. and Bojadjiev, D. T., "Attachment of Particles to a Liquid Surface (Capillary Theory of Flotation)", *Journal of the Chemical Society(London) Faraday Transactions I* **72**, p. 2815 (1976).

40. Rapacchietta, A. V. and Neumann, A. W., "Force and Free Energy Analysis at Fluid Interfaces: II. Spheres", *Journal of Colloid and Interface Science* **59**, p. 555 (1977).

41. James, D. F., "The Meniscus on the Outside of a Small Circular Cylinder", *Journal of Fluid Mechanics* **63**, p. 657 (1963).

42. Crank, J., The Mathematics of Diffusion, p. 32, (1975).

43. Hamaker, H. C., "The London-van der Waals Attraction between Spherical Particles", *Physica* **4**, p. 1058 (1937).

44. Clayfield, E. J., Clumb, E. C. and Mackey, P. H., "Retarded Dispersion Forces in Colloidal Particles-Exact Integration of the Casimir-Polder Equation", *Journal of Colloid and Interface Science* **37**, p. 382 (1971).

45. Lyne, M. P., "Electrostatic Interactions between Interfacial Particles." M.S. Thesis, University of British Columbia, 1989.

46. Levine, S. and Lyne, M. P., "Double Layer Interactions of Cylinders and Spheres at an Oil/Water Interface", 63rd ACS Colloid and Surface Science Symposium, (Seattle, Wa., 1989).

47. Gifford, W. A. and Scriven, L. E., "On the Attraction of Floating Particles", *Chemical Engineering Science* **26**, p. 287 (1971).

48. Chan, D. Y. C., Henry, J. D. and White, L. R., "The Interaction of Colloidal Particles at Fluid Interfaces", *Journal of Colloid and Interface Science* **79**, p. 410 (1981).

49. Crank, J., The Mathematics of Diffusion, p. 87, (1975).

50. Overbeek, J. T. G.,"Kinetics of Flocculation (Chapter 15)", *in* Colloid Science, (H. R. Kruyt, Ed.), p. 282, (1952).

51. Fuchs, N., "Über die Stabilität und Aufladung der Aerosole", *Zeitschrift fur Physik* **89**, p. 736 (1934).

52. Marmur, A. J., "A Kinetic Theory Approach to Primary and Secondary Minimum Coagulations and their Combination", *Journal of Colloid and Interface Science* **72**, p. 41 (1979).

53. Getman, F. H., Outlines of Physical Chemistry, p. 640, (1943).

54. Hindmarsh, A. C., "GEARB.. Solution of Ordinary Differential Equations Having Bounded Jacobeans", Lawrence Livermore National Laboratory, UCID-30059, (1975).

55. Smoluchowski, M. v., "Brownian Molecular Movement under the Action of External Forces and its Connection with the Generalized Diffusion Equation (in German)", *Annalen der Physik* **48**, p. 1103 (1916).

56. Finlayson, B. A., Nonlinear Analysis in Chemical Engineering, p. 349, (1980).

57. Chandrasekhar, S., "Stochastic Problems in Astronomy and Physics", *Reviews of Modern Physics* **15**, p. 41 (1943).

58. Levine, S., Bowen, B. D. and Partridge, S. J., "Stabilization of Emulsions by Fine Particles: I. Partitioning of Particles Between Continuous Phase and Oil/Water Interface.", *Colloids and Surfaces* **38**, p. 325 (1989).

59. Levine, S., Bowen, B. D., Partridge and J., S., "Stabilization of Emulsions by Fine Particles: II. Capillary and van der Waals Forces Between Particles", *Colloids and Surfaces* **38**, p. 345 (1989).

60. Zorin, Z., Platikanov, D. and Kolarov, T., "The Transition Region Between Aqueous Wetting Films on Quartz and the Adjacent Mensicus", *Colloids and Surfaces* **22**, p. 147 (1987).

61. Sheppard, E. and Tcheurekdjian, N., "Monolayer Studies: IV. Surface Films of Emulsion Latex Particles", *Journal of Colloid and Interface Science* **28**, p. 481 (1968).

62. Heller, W.,"Ordered and Disordered Aggregation of Colloidal Particles and Macromolecules", *in* Polymer Colloids II, (R. M. Fitch, Ed.), p. 153, Plenum Press, New York, (1979).

63. Finlayson, B. A., Nonlinear Analysis in Chemical Engineering, p. 68, (1980).

64. Finlayson, B. A., Nonlinear Analysis in Chemical Engineering, p. 221, (1980).

Appendix A Deryaguin Integration between Partially Immersed Spheres

It is often the case that models or measurements of the interaction potential between macrobodies are the simplest and most accurate for the case of opposing planar half-spaces (i.e. flat-plate potentials). Deryaguin (1934) introduced an approximate method for deducing the interaction potential between curved surfaces from the corresponding flat-plate potential under the condition that the range of the interaction is small compared with the particle's radius of curvature. The new element in this development is the presence of a "composite" macrobody; that is the interaction potential is not uniform over the surface of the particle.

The basic assumption of the Deryaguin approximation is that the interaction between curved surfaces can be estimated by the sum of the interactions between a series of parallel ring elements (dS_1).

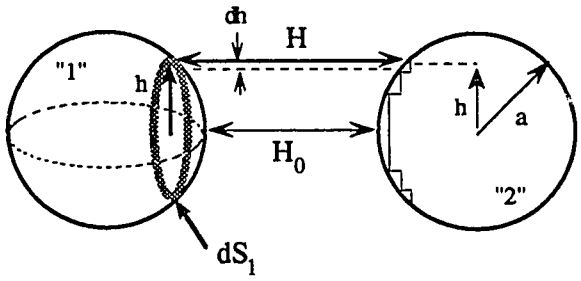

$$V(\text{sphere-sphere}) = \int_{S_1} V(\text{flat-plate})\, dS_1$$

$$V_{s\text{-}s} = \int_0^a 2\pi h\, V_{fp}\, dh \qquad \{A1\}$$

For the case of a partially immersed sphere we must account for the absence of interaction for the "dry" portion:

ϕ = wetted semi-arc
= π – contact angle

$\phi > \pi/2$ $\phi < \pi/2$

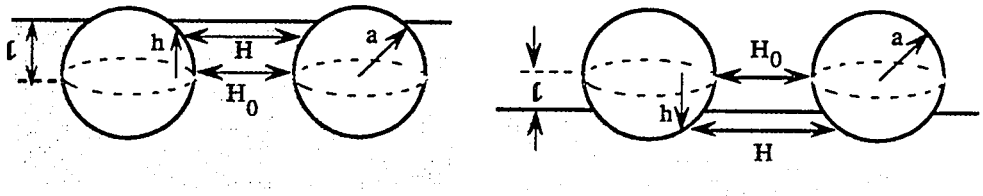

which results in truncated ring elements for h>ℓ and $\phi>\pi/2$, and always for $\phi<\pi/2$:

$\phi > \pi/2$, h > ℓ $\phi < \pi/2$

$$\beta = \pi - 2\sin^{-1}\left(\frac{\ell}{h}\right)$$

$$\beta = \pi - 2\sin^{-1}\left(\frac{\ell}{h}\right)$$

$$\text{"wet" fraction} = 1 - \beta/2\pi = \frac{1}{2} + \frac{\sin^{-1}\left(\frac{\ell}{h}\right)}{\pi}$$

$$\text{"wet" fraction} = \beta/2\pi = \frac{1}{2} \frac{\sin^{-1}\left(\frac{\ell}{h}\right)}{\pi}$$

$$\ell = a\,|\cos\phi|$$

For the case of $\phi>\pi/2$ we have:

$$V_{s\text{-}s} = \int_{S_1} V_{fp}\, dS_1 = \int_0^{\ell} V_{fp}\, 2\pi h\, dh + \int_{\ell}^{a} V_{fp}\, 2\pi h \left(\frac{1}{2} + \frac{\sin^{-1}(\ell/h)}{\pi}\right) dh \qquad \{A2\}$$

Convert variable of integration from h to H since we have $V_{fp}(H)$:

$$h = \sqrt{a^2-(a-\delta)^2} = \sqrt{2a\delta-\delta^2}$$

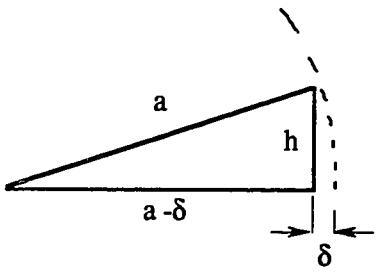

$$h(H) = \sqrt{u} = \sqrt{2a\left(\frac{H-H_0}{2}\right) - \left(\frac{H-H_0}{2}\right)^2}$$

$$dh = \frac{1}{2\sqrt{u}}du = \frac{1}{2\sqrt{u}}a\sqrt{1-h^2/a^2}\,dH$$

$$2hdh = adH\sqrt{1-h^2/a^2},$$

$$= (H - H_0)/2 \quad \text{and for small H} \rightarrow hdh = \frac{a}{2}dH$$

The limits become:

$$h=0 \rightarrow H=H_0$$

$$h=\mathcal{C} \rightarrow H=H_1 = H_0 + 2\left(a - \sqrt{a^2-\mathcal{C}^2}\right)$$

$$h=a \rightarrow H=H_2 = H_0 + 2a$$

$$V_{s\text{-}s}(H) = \pi a\left(\int_{H_0}^{H_1} V_{fp}\,dH + \int_{H_1}^{H_2} V_{fp}\left(\frac{1}{2} + \frac{\sin^{-1}(\mathcal{C}/h)}{\pi}\right)dH\right) \qquad \{A3\}$$

For $\phi<\pi/2$ we arrive at a similar expression:

$$V_{s\text{-}s}(H) = \pi a\left[\int_{H_1}^{H_2} V_{fp}\left(\frac{1}{2} - \frac{\sin^{-1}(\mathcal{C}/h)}{\pi}\right)dH\right] \qquad \{A4\}$$

For a fully immersed sphere we have:

$$V_{s\text{-}s}(100\%) = \pi a\int_{H_0}^{H_2} V_{fp}\,dH \qquad \{A5\}$$

and the diminished interaction between partially immersed particles can be expressed as a fraction of that corresponding to dispersed particles:

$$\text{Fractional Interaction} = V_{s\text{-}s}(H) / V_{s\text{-}s}(100\%) \qquad \{A6\}$$

$$= \frac{\int_{H_0}^{H_1} V_{fp}\, dH + \int_{H_1}^{H_2} V_{fp}\left(\frac{1}{2} + \frac{\sin^{-1}(l/h)}{\pi}\right) dH}{\int_{H_0}^{H_2} V_{fp}\, dH} \quad \text{for } \phi > \pi/2 \qquad \{A7\}$$

$$= \frac{\int_{H_1}^{H_2} V_{fp}\left(\frac{1}{2} - \frac{\sin^{-1}(l/h)}{\pi}\right) dH}{\int_{H_0}^{H_2} V_{fp}\, dH} \quad \text{for } \phi < \pi/2 \qquad \{A8\}$$

For the case of an exponentially decaying potential energy of interaction between two flat plates ($V_{fp} = Ae^{-\kappa H}$ [energy/area]) the preceding integrals cannot be reduced to closed form expressions; so numerical integration was used to generate the following family of curves (Figures 71 and 72).

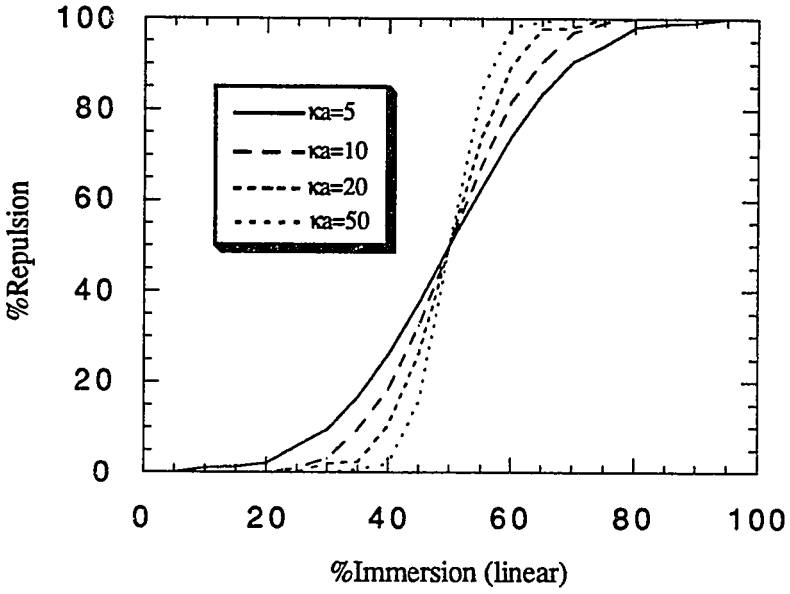

Figure 71. %Repulsion vs. %Immersion for various κa

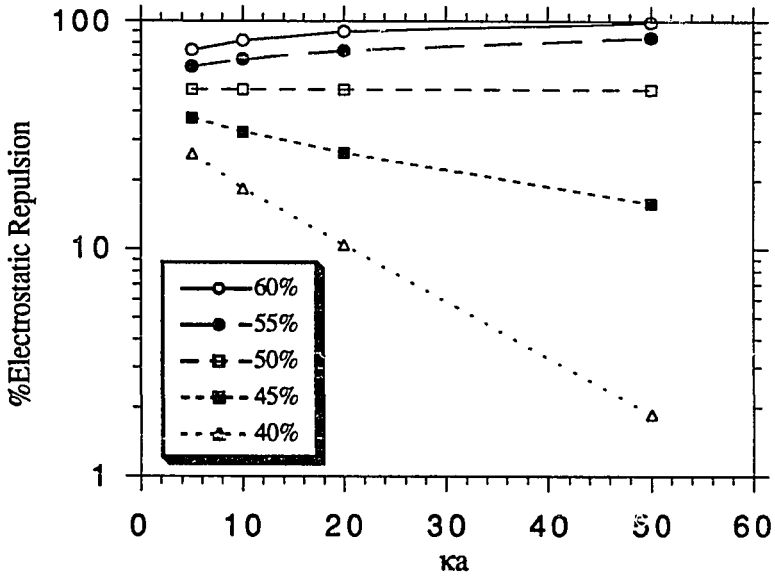

Figure 72. %Repulsion vs.κa for various %Immersions

Appendix B Investigation of Spread Films of Interfacial Colloids

B.1. Interfacial Colloids as Particle Monolayers

Another way to look at interfacial colloids is to consider them as a spread monolayer, rather than adsorbed particles. This approach is drawn from the analogy with the classic experiments of Langmuir and others on the properties of insoluble monolayers of surface active molecules. The experiment consists of spreading the "surfactant" on the subphase(usually water) surface and measuring the surface tension change(Π) produced by contracting and expanding the area(A) (Figure 73.).

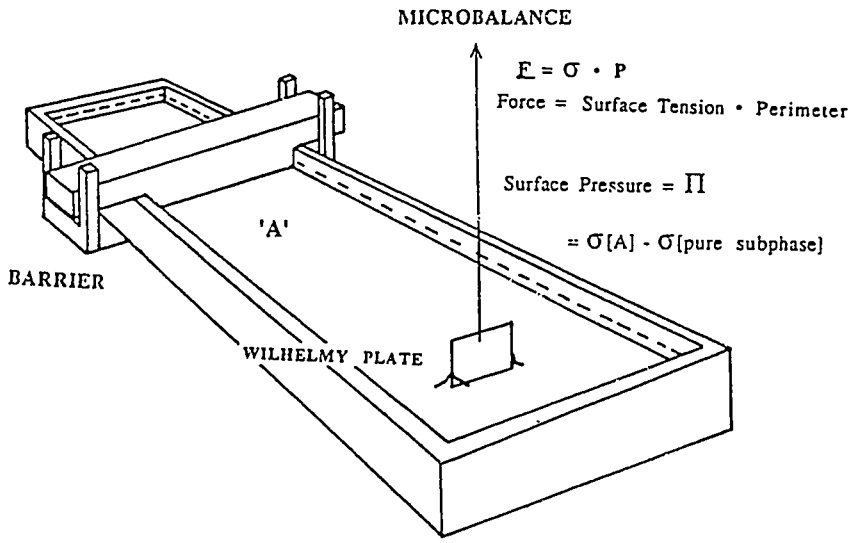

Figure 73. Langmuir-Wilhelmy Film Balance used for Π-A Measurements

The surface tension change has units of dynes/cm. and is interpreted as a two-dimensional pressure(Π). This pressure also corresponds to the change in the Gibbs free energy with respect to interfacial area(dG/dA). By integrating the Π vs. A

curve(Figure 74.) we can arrive at the change in free energy upon compression of the monolayer.

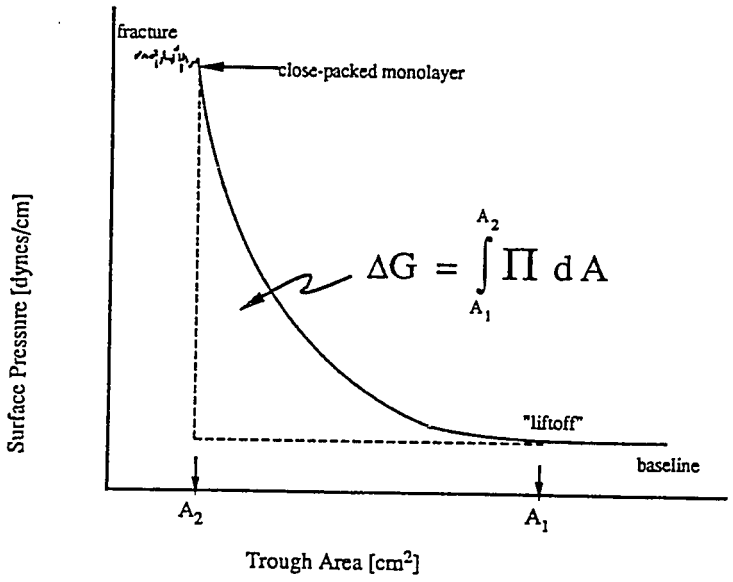

Figure 74. Typical Π vs. A Curve

If we can identify an isotropic unit cell this free energy change can be related to interactions on a molecular/particle level. We can also interpret the surface pressure as arising from the lateral repulsion between surface particles. From this perspective the surface pressure rise measured upon compression corresponds to the increasing force of repulsion experienced by particles as they approach one another. Note that if the particles exhibit a net attraction this method does not measure a negative surface pressure; only repulsive interactions can be probed.

Over the past twenty years there have been a few studies by surface chemists using latex particles as stand-ins for surfactant molecules in surface balance(i.e. Π-A) experiments. The goal of most studies was to uncover the nature of particle-particle interactions in systems with adlayers of solvated polymers. It was hoped that experiments with these particle monolayers would allow critical evaluation of theories of steric stabilization.

The first study of particle monolayers was performed by Sheppard and Tcheurekdjian(61) in 1968. Their goal was much more modest than that put forth above. They worked with latex particles free of any polymer adlayer at the air-water interface. The objective was just to show how these new films could be created and to characterize their behavior. As with fatty-acid molecules, a low surface tension organic spreading liquid(isopropanol /hexane or ethanol/benzene mixtures) was employed to distribute the dispersion at the interface. Upon compression of the particulate monolayer the surface pressure rose steeply over a narrow range of film areas. Sheppard et al found that a limiting area could be identified on the Π-A curve which corresponded(+/- 5%) to hexagonal close-packing of the particles. The authors proposed that film balance experiments provide an alternate means of determining colloid particle size. It should be noted that other investigators have had difficulty using Sheppard's spreading solutions due to rapid destabilization or swelling of the dispersion.

The most extensive study of particulate monolayers was carried out by Doroszkowski and Lambourne(9,10) in the early 1970's. Their investigation was unique in a number of ways. First, they focussed upon particles with adlayers dispersed in various non-aqueous media(heptane, toluene, and cyclohexane). Rather than being suspended at the air/liquid interface, the particles were distributed at the organic/water interface. Apparently these non-aqueous dispersions spread at the interface without spreading aids. Particles were thought to be trapped at the interface due to partial wetting of the colloid surface by the water phase. Finally the polymer adlayers were covalently bound to the latex surface instead of being physically adsorbed.

The Π-A curves gave reasonable values for the range of interaction of polymer adlayers. There was enough uncertainty in the modelling of steric forces to account for the variation of repulsive force(i.e. surface pressure) with particle separation(i.e. monolayer area). The quality of the data however, does not support a detailed theoretical discussion of steric interactions. One of the troubling experimental aspects was the use of a subtractive procedure of dubious validity (described below, see Figure 75.). This procedure was adopted in order to account for the effect of unexplained

surface active impurities thought to be present in the continuous phase of the dispersion. After compression and expansion of the spread particle film an equivalent amount of dispersion supernatant was again added to the surface. As the area was compressed the film now exhibits a higher surface pressure. This elevation of pressure was assigned to the impurity and subtracted from the initial curve in order to negate impurity effects during the first compression. This correction often accounted for more than half of the surface pressure associated with the initial compression. What is even more puzzling is that compression of the dispersion supernatant in the absence of a particulate film showed no evidence of a surface active impurity(i.e. flat Π-A trace). No attempt was made to justify this ad hoc procedure.

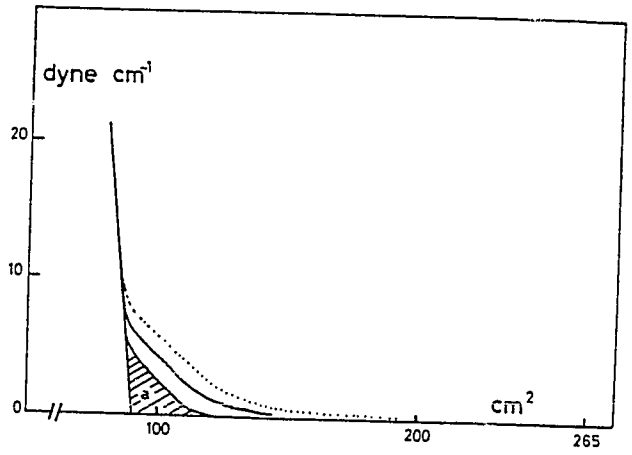

Figure 75. Π-A Trace from Reference 9. Demonstrating Subtractive Correction.

The last significant study to be done on particulate monolayers was performed by Garvey et al(11) during the late 1970's. Again the goal was to measure the repulsive steric force during compression of a particulate monolayer. A water soluble polymer (PVP or polyvinylpyrrolidone, M_W= 40,000) was adsorbed onto 0.33μm polystyrene particles and spread upon a 2M NaCl aqueous subphase. Since salt water has a higher density and surface tension than pure water the dispersion spread on the subphase without the use of organic spreading aids. Garvey detected no surface active impurities in his dispersion and did not invoke any subtractive correction procedure in analyzing his Π-A curves.

The most surprising result of Garvey's work is the report of an extremely long-range steric repulsion(75nm adlayer). The maximum extended chain length of free polymer was reported to be 146nm. Garvey's photon correlation spectroscopy results also indicated a rather extended adlayer(44 +/- 10 nm). Both of these results seem inconsistent with the commonly held view of a more compressed network of polymer segments attached at various intervals to the particle surface. It should be noted that upon repeated compressions of the same film the Π-A curves shifted to lower areas, corresponding to a loss of interfacial particles or adsorbed polymer.

I conclude with mention of the most recent Japanese study in order to demonstrate the confusion that has developed in the investigation of particulate monolayers films. Kawaguchi et al(12) performed experiments similar to those of Garvey. Various molecular weight fractions of PVP(87k M_w, 190k M_w, and 720k M_w) were adsorbed on to 0.56μm diameter polystyrene latex. Measurements of the surface pressure isotherm on 2M NaCl aqueous subphase proceeded along the lines of Garvey's study. However in this study a monolayer of uncoated latex particles was used to provide a baseline Π-A measurement for comparison with the Π-A curves of the coated particles. The investigators claimed that both coated and uncoated particles were stable(no hysteresis in the Π-A curve) at the interface. The assertion that uncoated latex particles are stable in or on a 2M NaCl(aq.) subphase does not agree with my observations(section B.2) or the basic tenets of the DLVO theory. This high electrolyte concentration certainly compresses the double layer thickness such that no significant electrostatic repulsion exists.

It is clear that the study of particulate films has not led to any common understanding of the behavior of interfacial particles. There is not a consensus upon the meaning or usefulness of this method in the scientific community. While one must view the modelling of pair potentials based upon the compression of particulate films skeptically; these experiments do probe the complex nature of particulate film consolidation. It is in this context that they should be viewed. This author's experience with experiments with spread particle films is summarized in the next section.

B.2 Experiments with Interfacial Particles

The original goal of this research was to investigate particle-particle interactions in dispersions which are stabilized by polymer adlayers. It was proposed to measure particle interactions using a Langmuir-Wilhelmy film balance as outlined in the previous section . Because of the difficulty of synthesizing systems for use at the organic/water interface we concentrated on looking at latex particles with adsorbed adlayers of water compatible polymers. Most of the experiments were designed to try to mimic the conditions of Garvey's work (2M NaCl(aq.) subphase, PVP adlayer). The range of experimental conditions studied is summarized below:

Table 4. Π-A Experiments

Polymer Adlayer	Particle Sizes[μm]	Subphase	Spreading Aid
Bare	2.85	u.p. H_2O	Yes
40,000 M_W PVP	2.85,0.57, 0.23, 0.08	2M NaCl	No
40,000 M_W PVP	0.23	0.5M NaCl	Yes
160,000 M_W PVP	2.85, 0.481	2M NaCl	No
160,000 M_W PVP	0.481	0.5M NaCl	No
Pluronic F108(PEO)	2.85	2M NaCl	No

A typical dispersion preparation consists of pre-cleaning, polymer adsorption, removal of excess solution polymer, and concentration by centrifugation. The pre-cleaning step is accomplished by serum replacement and insures that the latex surface is free of contaminants that would inhibit adsorption of the desired polymer. The clean latex is coated with a water soluble polymer adlayer by exposing the particles to concentrations of polymer above plateau adsorption level for 24 hr. In this sequence care must be taken to avoid the complications that can arise from the process of depletion flocculation. The excess polymer that remains in solution is removed by serum replacement or centrifugation. Finally a suitable spreading dispersion is obtained by concentrating the treated sol by centrifugation(2-20 wt.% solids).

Ideally Π-A isotherms reflect the repulsive potential of interaction between interfacial particles. As the compression of a film proceeds from a dilute to a concentrated state the surface pressure will remain constant until particles begin to feel the influence of their neighbors. For coated particles in a salt-water subphase this should occur as the adlayers begin to overlap(at A_1 in Figure 74.). Finally the increase in surface pressure becomes extremely steep as the core-core exclusion dominates the interaction potential(at A_2 in Figure 74).

For a number of reasons these results lead to a more critical interpretation of the Π-A data than previous researchers. These recent tests are probably more extensive than the investigations described in the previous section. Before drawing conclusions, a description of the common features that characterize the particulate films of this study is in order.

The first feature to note concerns the range of adlayer interaction. The initial compression of most films resulted in a steep rise in surface pressure near the area corresponding to a hexagonal close-packed monolayer of particles(Figures 76-79.). This profile corresponds to a much narrower adlayer thickness than reported by previous investigators. For the case of experiments which closely mimic Garvey's work an adlayer thickness of less than 10 nm was measured. This result was confirmed by photon correlation spectroscopy(PCS) measurements. Garvey's study reported an adlayer thickness of 75 nm(from Π-A curve) and 44 nm(from PCS).

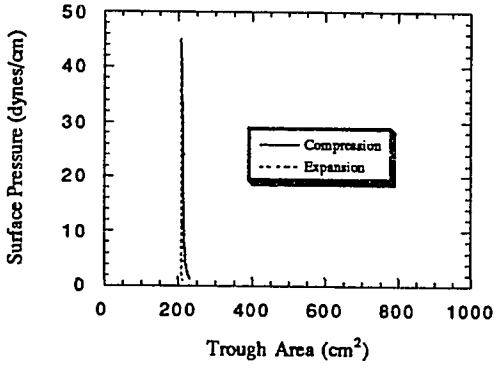

Figure 76. 1st Compression of 2.85μm latex with no adlayer on distilled water

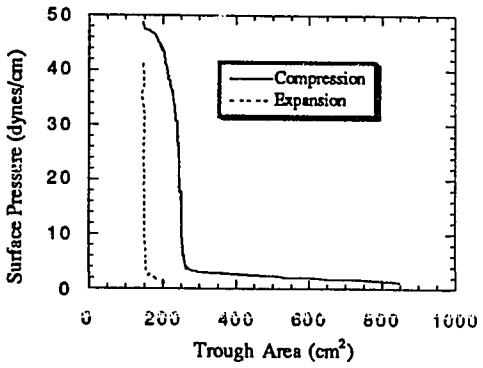

Figure 77. 1st compression of 0.57μm latex with 40,000 M_w PVP on 2M NaCl(aq.) subphase

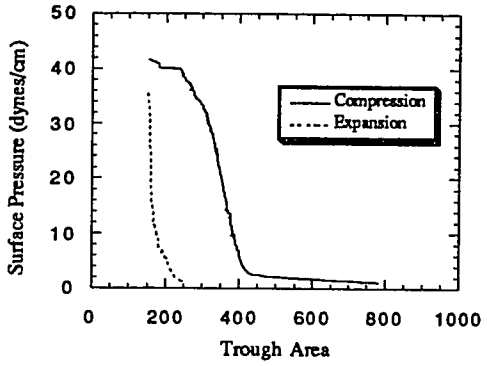

Figure 78. 1st Compression of 0.23μm latex with 40,000 M_w PVP adlayer on 2M NaCl(aq.) subphase

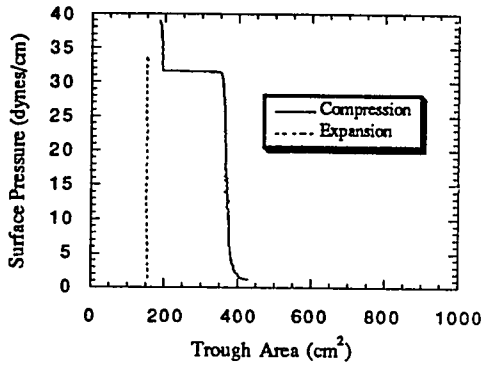

Figure 79. 1st Compression of 2.85μm latex with 160,000 M_w PVP adlayer on 2M NaCl(aq.) subphase

Figures 76-79 Experimental Π-A Curves (1st Compressions)

Another important property of particulate films is their behavior upon repeated compression/expansion cycles. Upon expansion of a film hysteresis was always present; the expansion curve was always below the compression trace. Successive compression cycles also altered the shape and location of the Π-A curves. Repeated compression changed the curve shape from a steep rise to a long gradual increase and shifted the curve to larger areas(Figures 80-83.). This is exactly the opposite of what Garvey reported but is in agreement with Doroszkowski's observations during his second corrective compression.

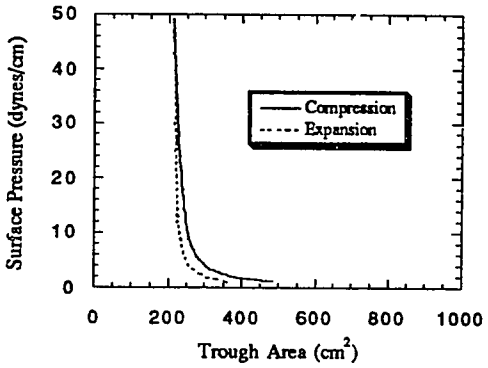

Figure 80. 1st Cycle

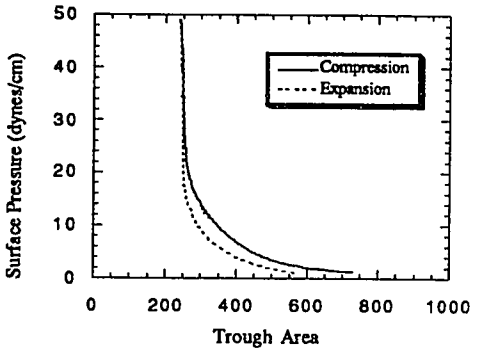

Figure 81. 2nd Cycle

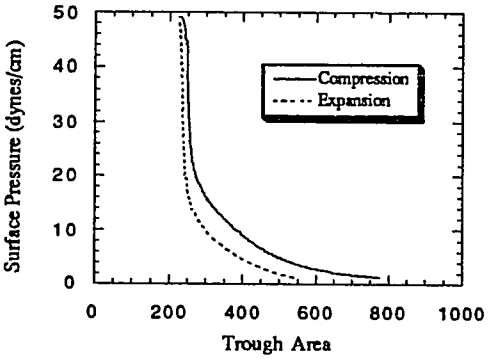

Figure 82. 3rd Cycle

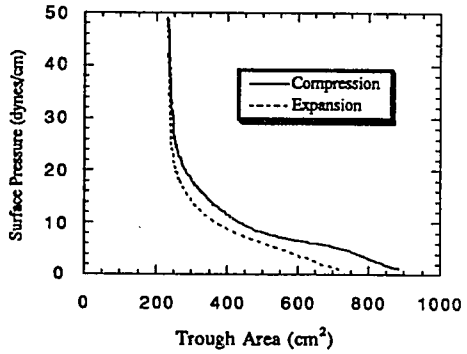

Figure 83. 4th Cycle

Figures 80-83 Behavior of Latex Films upon Repeated Compression(0.23μm latex, 40,000 M_w PVP adlayer,on 2M NaCl(aq.) subphase)

My explanation of these differences is tied to the question of the stability of particle monolayers. Previous investigators assumed that their monolayers were stable with respect to flocculation. The preceding observations and experiments call this into question. Both with the naked eye and the microscope flocculation of particles at the interface is evident. This flocculation was responsible for the broadening of the Π-A curve shape upon repeated compressions(or with elapsed time). It was clear that a more open flocculated network accounted for the more extended Π-A curves. Extensive flocculation of spread films in the absence of film compression was also observed in petri-dishes after only a few hours.

The initial compression of particulate films may seem representative of isolated particle-particle interactions, but even these results may be misleading. If particles exist at the interface with weak or attractive interaction potentials we should expect to see a Π-A curve approximating a square well(i.e. hard-sphere interaction). As the film flocculates the restructuring of the aggregates upon compression will show up as a longer ranged interaction. This softening of the curve can easily be interpreted as a thick adlayer or some other long-range interaction. In order to use film compressions to extract information about particle interactions it is crucial that the monolayers exhibit true, or at least long term, stability. Most of the experiments with particulate films do not provide clear information about particle interaction, but point out the inherent instability of interfacial colloids.

Appendix C Structured Aggregates at the Interface: Surface Tactoids

The early work of Langmuir(32) and others(62) identified the importance of local ordering of colloids in governing dispersion thixotropy and the coacervation of dispersions into an ordered gel-phase and a disordered disperse phase. These regions of local colloidal order are referred to as tactoids and are fundamentally a result of the complex interactions in concentrated (typically > 1% solids) suspensions. Simple pair potential arguments derived from interactions in dilute systems fail to explain this local ordering.

In a few rare instances I have observed structures which appear to be surface analogs to bulk-phase tactoids. While I have not been able to define the reproducible conditions under which these structures appear; I have no reason to believe that they are due to an artifact or contamination. They typically form only after extended surface ages, far beyond the normal period of observation. The fact that these structures are not easily reproducible may reflect some sensitivity to a parameter that we are not aware of (i.e shear at the surface, vibration). I include the following micrographs to document this phenomenon.

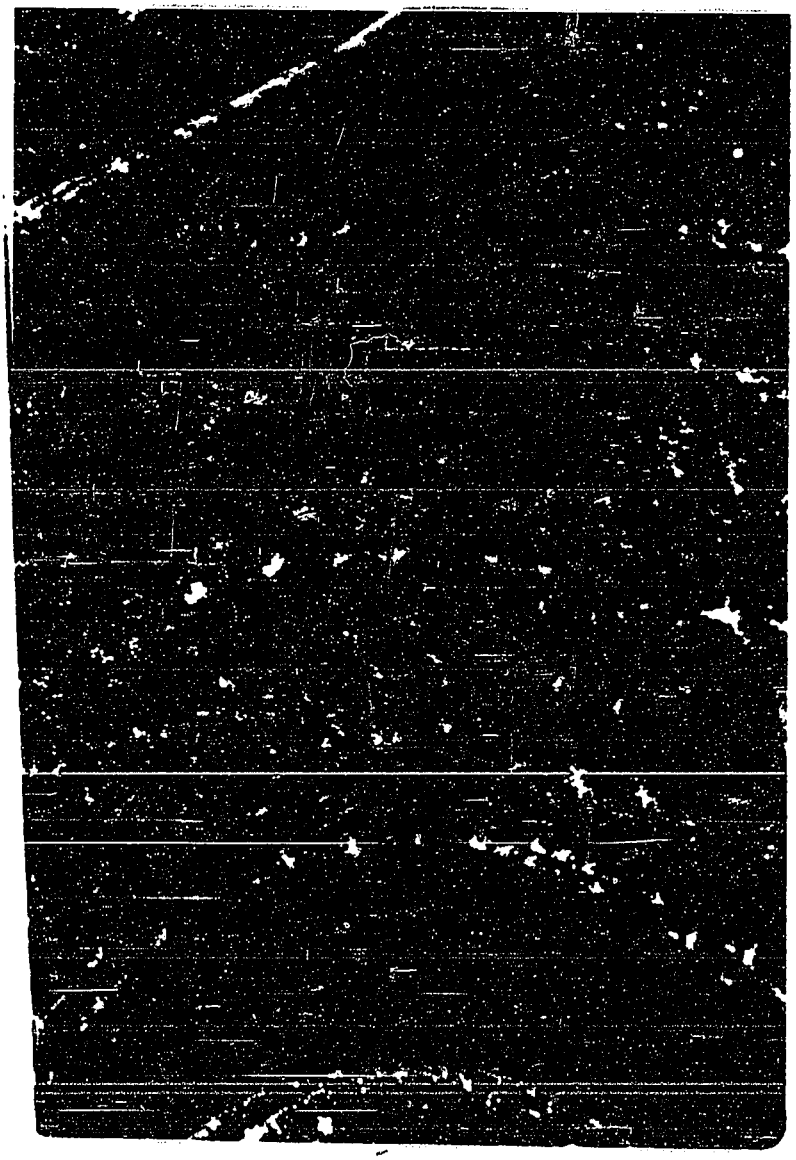

Figure 84. Ordered Surface Aggregates, 0.989μm polystyrene latex (standard colloid),10ppm suspension in 0.05M NaCl viewed in an upright darkfield microscope after about 10 hours, 700X linear magnification (1cm ≈ 14μm)

Figure 85. Ordered Surface Aggregates, 0.989μm polystyrene latex (standard colloid),10ppm suspension in 0.05M NaCl viewed in an upright darkfield

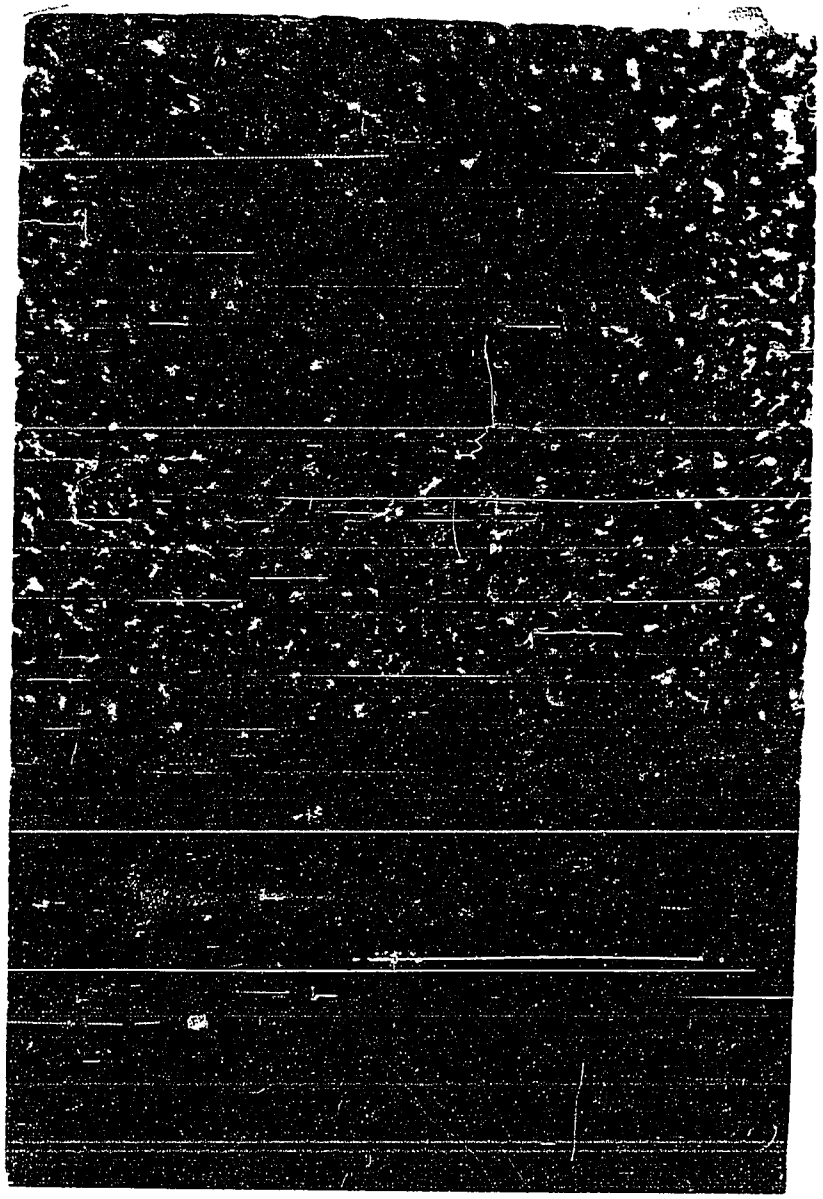

Figure 86. Ordered Surface Aggregates, 0.481μm polystyrene latex (Interfacial Dynamics Corp. # 10-11-33, 112Å^2/COOH), ≈50ppm suspension in 0.1M NaCl viewed in an inverted darkfield microscope after 30 minutes, roughly 700X linear magnification (1cm ≈ 14μm)

Appendix D Numerical Solution of the Smoluchowski Equation
(Diffusion in a Field of Force)

Further discussion of the solution strategy employed in section 4.4 is warranted; since there are a number of details worth documenting. In this appendix I consider: (1) the basic solution strategy, (2) the inherent numerical instability of the Smoluchowski Equation, (3) the necessity and implementation of a non-uniform grid spacing, and finally (4) the procedures necessary to insure the convergence and accuracy of the numerical solutions.

The basic solution strategy was sketched out in section 4.4.1. The transformed PDE.'s were:

$$\frac{\partial C}{\partial \theta} = (1-y)^4\left(\frac{\partial^2 C}{\partial y^2} + \frac{\partial \overline{P}}{\partial y}\frac{\partial C}{\partial y} + C\frac{\partial^2 \overline{P}}{\partial y^2}\right) - n(1-y)^3\left(\frac{\partial C}{\partial y} + C\frac{\partial \overline{P}}{\partial y}\right) \qquad \{D1\}$$

where:

n=2 is for one-dimensional (planar) geometry

n=1 is for two-dimensional (cylindrical) geometry

and the transformed boundary conditions and spatial coordinates were:

transformed B.C.	spatial coordinates (Figures 24, 32)
$C(y=0,\theta>0) = 0$	
$C(y>0,\theta=0) = 1$	$y = z/(z+1),\ z=x/2a$ (1-D)
$C(y=1,\theta>0) = 1$	$y = 1-1/\rho,\ \rho= r/2a$ (2-D)

While this equation is a non-linear parabolic partial differential equation, it can be cast within the framework of a simple initial value problem (IVP):

$$\frac{dC_i}{d\theta} = \mathbf{f}_i\{C_i\} = RHS \qquad \{D2\}$$

where i represents the value at each node on a spatial grid, thus generating a set of simultaneous IVP's. There are a number of straightforward methods for solving this system. Probably the most accurate and stable method uses Gear's implicit integration scheme with self-adjusting integration order and step-size(54). For an evenly spaced grid we can simply estimate the RHS of {D2} using the difference formulas:

$$\frac{dC}{dy} \approx \frac{C_{i+1} - C_{i-1}}{2\Delta y} \qquad \text{and} \qquad \frac{d^2C}{dy^2} \approx \frac{C_{i-1} - 2C_i + C_{i+1}}{(\Delta y)^2} \qquad \{D3\}$$

$$(i = 0,1,2,.....,n \quad \text{or} \quad y = 0 \text{ to } 1 \quad \text{or} \quad z,\rho = 0 \text{ to } \infty)$$

This procedure works quite well for free diffusion (F=0), as is demonstrated by the convergence to the previously determined analytical solutions (Figure 87). In this case the only flux is the diffusive component:

$$J = \text{dimensionless flux} = -\left(\frac{dC}{dz}\right)_{z\to 0} \approx \frac{-(C_1 - C_0)}{\Delta z} \qquad \{D4\}$$

or more accurately by the three point formula(63):

$$\left(\frac{dC}{dz}\right)_{z\to 0} \approx \frac{-3C_0 + 4C_1 - C_2}{2\Delta z} \qquad \{D5\}$$

(replace z by ρ for 2-D cylindrical geometry)

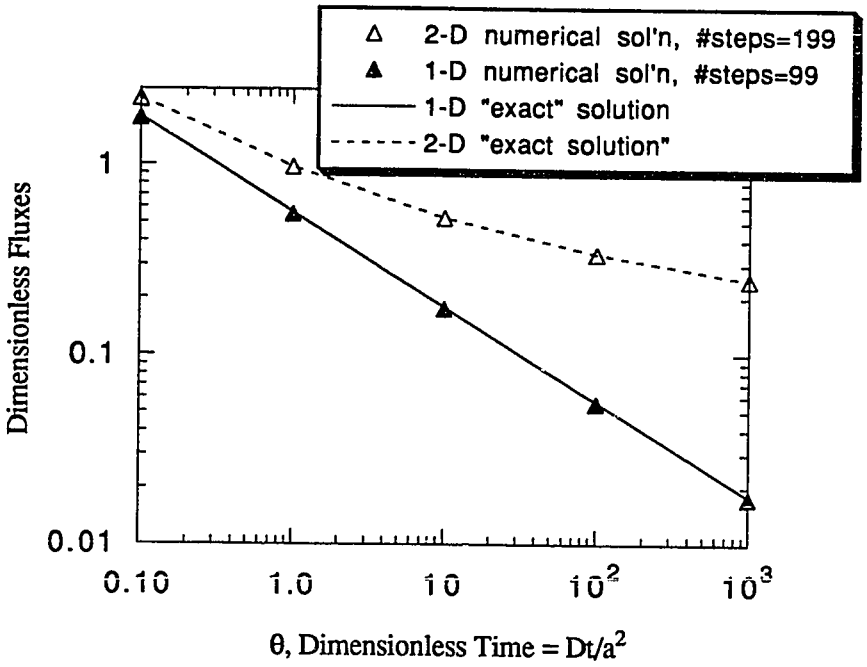

Figure 87. Convergence to "Exact" Analytical Solutions with Uniform Grids

When an external force is present a number of things change. We now have both a diffusive and external flux:

$$\text{Total flux} = -\left(\frac{dC}{dz}\right)_{z\to 0} + (FC)_{z\to 0} = -\left(\frac{dC}{dz}\right)_{z\to 0} - \left(\frac{dP}{dz}C\right)_{z\to 0} \qquad \{D6\}$$

and we must evaluate the external component by appropriate extrapolation back to zero separation (as above, except use simple straight line extrapolation for the external flux, since we have values at the nodes rather than at the node mid-points). There can be further complications introduced by the addition of an external field due to influences on the numerical stability of the PDE[2]. In particular if the external field is a decaying exponential ($P = -A \exp(-\lambda x)$) the untransformed (but dimensionless) 1-D PDE becomes:

[2] I should acknowledge the help of Professor Bruce A. Finlayson in identifying and diagnosing this problem.

$$\frac{\partial C}{\partial \theta}\left(\frac{-e^{\lambda z}}{A\lambda}\right) = \frac{\partial^2 C}{\partial z^2}\left(\frac{-e^{\lambda z}}{A\lambda}\right) + \frac{\partial C}{\partial z} - \lambda C \qquad \{D7\}$$

For the Christenson potential applied to a 1μm sphere approaching the air-water interface $\lambda = 77$, $A = 7270$, and $\lambda A = 560{,}000$. Note that for small z this equation has a boundary layer character, since the highest order derivative is multiplied by a very small parameter (1/560,000). This character is most obvious for the steady-state equation where the LHS = 0.

An even more useful comparison can be made if we recast the equation using the substitutions $\tau = \lambda^2\theta$ and $w = \lambda z$ yielding:

$$\frac{\partial C}{\partial \tau} = \frac{\partial^2 C}{\partial w^2} - Ae^{-w}\left(\frac{\partial C}{\partial w} - C\right) \qquad \{D8\}$$

Note that this equation is very similar in form to the Convective Diffusion Equation [3]:

$$\frac{\partial C}{\partial \theta} = \frac{\partial^2 C}{\partial x^2} - Pe\frac{\partial C}{\partial x} \qquad \text{(Pe = Peclet Number)} \qquad \{D9\}$$

For large Pe (Pe >> 1) we know that the convective term can introduce numerical problems due to the development of sharp moving fronts. In particular Finlayson(64) has reported that the finite difference mesh must meet the following stability criteria:

$$Pe\,\Delta x \leq 2 \qquad \{D10\}$$

or in our case:

$$Ae^{-w}\,\Delta w \leq 2$$

---

[3]This is especially true near the origin since here dc/dw >> c.

Similar stability arguments hold for the two-dimensional case and for calculations involving van der Waals forces.

Rather than generate the huge matrix of IVP's required by a uniform grid and the stability requirement (here $\Delta w \leq 2/7270$) it makes sense to use a non-linear grid which concentrates points near the origin; the source of the numerical instability. Following the conventions outlined by Finlayson(63) for non-uniform grid layout:

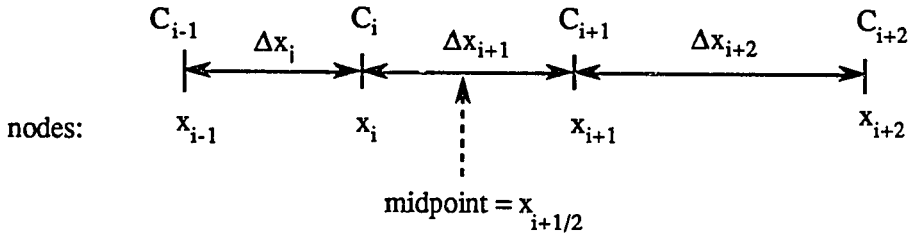

and expanding C_{i+1} and C_{i+2} in Taylor series:

$$C_{i+1} = C_i + C'_i(\Delta x_{i+1}) + \frac{C_i''}{2}(\Delta x_{i+1})^2 + \frac{C_i'''}{6}(\Delta x_{i+1})^3 \qquad \{D11\}$$

$$C_{i+2} = C_i + C'_i(\Delta x_{i+1} + \Delta x_{i+2}) + \frac{C_i''}{2}(\Delta x_{i+1} + \Delta x_{i+2})^2 + \frac{C_i'''}{6}(\Delta x_{i+1} + \Delta x_{i+2})^3 \qquad \{D12\}$$

The goal here is to obtain an expression for C'_i accurate to $O(\Delta x^2)$ by eliminating the C''_i terms. Multiplying the top equation by $((\Delta x_{i+1}+\Delta x_{i+2})/\Delta x_{i+1})^2$ and subtracting gives (to $O(\Delta x^2)$):

$$C'_i = \frac{-[(1+\alpha)^2-1]\,C_i + (1+\alpha)^2\,C_{i+1} - C_{i+2}}{\alpha(\Delta x_{i+1} + \Delta x_{i+2})} \qquad \{D13\}$$

where:

$$\alpha = \text{geometric grid spacing} = \Delta x_{i+1}/\Delta x_i$$

Thus the grid is spaced according to:

$$\left(\sum_{i=1}^{n} \alpha^i\right) \Delta x_1 = \text{ span of spatial coordinate} = 1 \text{ (for our normalized case)} \qquad \{D14\}$$

When employing a non-uniform grid the approach to solving the basic PDE is also somewhat different. It is more convenient to deal with the calculation of the fluxes directly in the formulation of the difference equations:

$$\frac{\partial C}{\partial \theta} = -\nabla \cdot \mathbf{J} = \nabla \cdot \left(-\mathbf{J}^{diff.}\right) + \nabla \cdot \left(-\mathbf{J}^{ext.}\right) \qquad \{D15\}$$

In the 1-D case we have

$$\frac{\partial C}{\partial \theta} = -\frac{\partial}{\partial z}\left(J^{diff.} + J^{ext.}\right) \qquad \{D16\}$$

or in the transformed coordinate (y):

$$\frac{\partial C}{\partial \theta} = \frac{\partial}{\partial y}\left(-J^{diff.} - J^{ext.}\right)\frac{\partial y}{\partial z} = (1-y)^2 \frac{\partial}{\partial y}\left(-J^{diff.} - J^{ext.}\right) \qquad \{D17\}$$

and:

$$-J^{diff.} = \frac{\partial C}{\partial z} = \frac{\partial C}{\partial y}\frac{\partial y}{\partial z} = \frac{\partial C}{\partial y}(1-y)^2 \qquad \{D18\}$$

$$\frac{d}{dy}\left(J^{diff.}\right) = \frac{J^{diff.}_{i+1/2} - J^{diff.}_{i-1/2}}{\left(\Delta y_i + \Delta y_{i+1}\right)/2} \qquad \{D19\}$$

$$-J^{diff.}_{i+1/2} = \frac{C_{i+1} - C_i}{(\Delta y_{i+1})}(1 - y_{i+1/2})^2 \qquad \{D20\}$$

$$-J^{diff.}_{i-1/2} = \frac{C_i - C_{i-1}}{(\Delta y_i)}(1 - y_{i-1/2})^2 \qquad \{D21\}$$

Similarly for J^{ext}:

$$\frac{\partial}{\partial z}(-J^{ext}) = \frac{\partial}{\partial y}(-J^{ext})\frac{\partial y}{\partial z} \qquad \{D22\}$$

$$\frac{d}{dy}(-J^{ext}) = \frac{d}{dy}(-FC) = -\frac{dF}{dy}C - \frac{dC}{dy}F \qquad \{D23\}$$

and only dc/dy need be evaluated by difference formula in the preceding equation:

$$\frac{dC}{dy} \approx \frac{C_{i+1/2} - C_{i-1/2}}{(\Delta y_i + \Delta y_{i+1})/2} = \frac{C_{i+1} - C_{i-1}}{(\Delta y_i + \Delta y_{i+1})} \qquad \{D24\}$$

So the complete difference equation for the 1-D planar geometry takes the form:

$$\frac{\partial C}{\partial \theta} = (1-y_i)^2\left[\frac{\frac{(C_{i+1} - C_i)}{\Delta y_{i+1}}(1-y_{i+1/2})^2 - \frac{(C_i - C_{i-1})}{\Delta y_i}(1-y_{i-1/2})^2}{(\Delta y_{i+1} + \Delta y_i)/2} - \frac{\partial F_i}{\partial y_i}C_i - F_i\frac{(C_{i+1} - C_{i-1})}{(\Delta y_{i+1} + \Delta y_i)}\right] \qquad \{D25\}$$

and the corresponding expression for the 2-D cylindrical geometry is:

$$\frac{\partial C}{\partial \theta} = (1-y_i)^3\left[\frac{\frac{(C_{i+1} - C_i)}{\Delta y_{i+1}}(1-y_{i+1/2}) - \frac{(C_i - C_{i-1})}{\Delta y_i}(1-y_{i-1/2})}{(\Delta y_{i+1} + \Delta y_i)/2} - \frac{\partial F_i}{\partial y_i}\frac{C_i}{(1-y_i)} - \frac{F_i C_i}{(1-y_i)^2} - F_i\frac{(C_{i+1} - C_{i-1})}{(\Delta y_{i+1}+\Delta y_i)(1-y_i)}\right] \qquad \{D26\}$$

Again the flux at the surface can be estimated by simple 2-point or 3-point extrapolation to zero separation.

Before a discussion of convergence and accuracy a few points about the van der Waals potential are in order. Because of the inverse power-law nature of the van der Waals equations an infinite force is predicted at zero surface separation (i.e a singularity). This is obviously not real and is simply a consequence of the extension of continuum modelling a bit too far. However it also means we should choose some small separation at which to cut-off our van der Waals estimates; otherwise we will incur convergence problems and may get "unreal" results. The common practice of cutting off the van der Waals interaction at the diameter of one solvent molecule (in our case 2.5Å) was employed in these calculations.

There are a number of issues to be concerned with when considering convergence of the numerical solution to accurate values. The typical means of verifying convergence is a double extrapolation of the temporal and spatial grids, under appropriate stability constraints, toward zero step-size and identification of the asymptotic convergence as the "answer". Obviously time and memory constraints and the limits of finite precision arithmetic often limit how close we can approach zero step-size. In the problem at hand we actually only have control over the spatial step-size; since the GEARB routine automatically varies the time grid to achieve stable and efficient convergence to within a pre-selected tolerance (ε = relative error bound = root mean square normal $\leq 10^{-7}$ in our case). In the non-uniform spatial grid there are actually two separate parameters to consider: (1) the step-size ratio (α), and (2) the number of steps (N_s). Both α and N_s effect the size of the initial step (Δx_1); while for large N_s the final step size (Δx_n) is solely a function of α ($\Delta x_n \approx 1 - 1/\alpha$). It is important that the initial step be small enough to capture the structure of the concentration profile and potential gradient near the surface (for flux extrapolation); while the refinement of the grid near the "infinite" boundary should be detailed enough for the asymptotic boundary condition to be satisfied. These factors require one to use smaller values of α for large θ's in order to capture the entire concentration profile within the grid.

Finally one can use a variety of measures as the yardstick for convergence. Either the concentration profile, calculated fluxes at the nodes (or nodal mid-points), or the flux

extrapolated to the surface can be chosen as the convergence criteria. Since we are most interested in the flux values I will concentrate on the nodal and extrapolated fluxes. It is worthwhile to look at the distribution of nodal fluxes first. Figure 88 shows the results from a typical calculation. The important point here is that the total flux establishes a relatively constant value, easily extrapolated to zero separation, long before one can make the same claim for the component diffusive and external fluxes. Therefore the value of the total flux extrapolated to zero separation is used as the convergence criteria. A typical convergence of the extrapolated total flux as the step-size is decreased is shown in Figure 89.

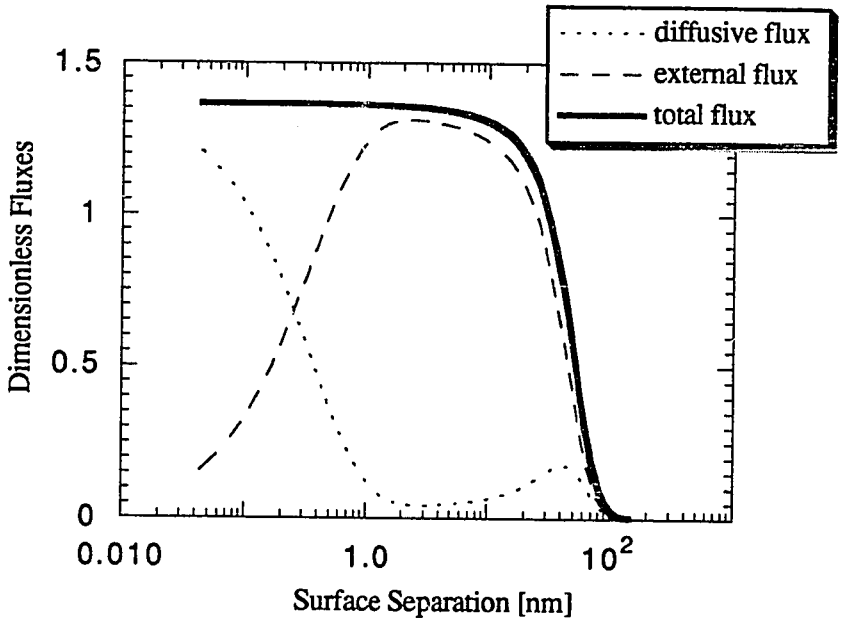

Figure 88. Component and Total Flux Variation with Separation for Enhanced Adsorption to the Interface due to Hydrophobic Attraction
(10nm spheres, 200 steps, α =1.005, θ=1)

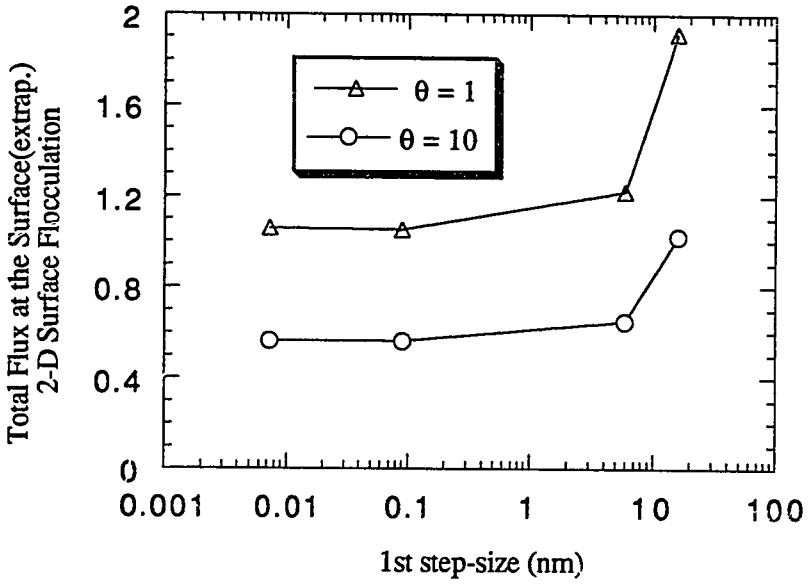

Figure 89. Convergence of Total Surface Flocculation Flux with Initial Step-Size, for Hydrophobic Enhancement (1μm spheres, α =1.01)

VITA

David Francis Williams was born near Tokyo Japan in the Tachikawa United States Air Force Base Hospital on July 3, 1956. His secondary schooling took place in Arlington Virginia; on the outskirts of Washington D.C. Between 1974 and 1978 he pursued an undergraduate degree at Virginia Polytechnic Institute and State University (Virginia Tech") and graduated in March 1978 with a Bachelor of Science degree in Chemical Engineering (Nuclear Engineering minor). In April 1978 he accepted a professional position on the Chemical Technology Division Staff at Oak Ridge National Laboratory (ORNL) and worked on a variety of R&D projects for the following seven years. The first four years at ORNL were devoted to the development and scale-up of the internal gelation process for continuous production of UO_2 and UO_2-PuO_2 advanced nuclear fuel (i.e. Gel-Sphere-Pac Fuel Concept). The final three years were spent in a research capacity during which time programs on the application of dynamic light-scattering to: (a) the measurement of high temperature fluid viscosities, and (b) the study of the early stages of sub-micron particle growth during precipitation, were developed. During the time at Oak Ridge he pursued a Master's degree on a part-time basis at the University of Tennessee (Knoxville) and was awarded his Master of Science degree in Chemical Engineering in March of 1985. The thesis title was " Determination of High Temperature Fluid Viscosity Using Dynamic Light Scattering". He left Oak Ridge National Laboratory in July 1985 to pursue a Ph.D. with a focus on Surface and Colloid Science at the University of Washington.